UNIVERSIDAD DE JAÉN

ESCUELA POLITÉCNICA SUPERIOR DE JAÉN
DEPARTAMENTO DE INFORMÁTICA

TESIS DOCTORAL

SPECTRAL CARACTERIZATION AND SEMANTIC SEGMENTATION OF COMPLEX 3D MODELS IN NATURAL ENVIRONMENTS

PRESENTADA POR:
JUAN MANUEL JURADO RODRÍGUEZ

DIRIGIDA POR:
DR. D. FRANCISCO RAMÓN FEITO HIGUERUELA
DRA. DÑA. LIDIA ORTEGA ALVARADO
DR. D. JUAN JOSÉ CUBILLAS MERCADO

JAÉN, 10 DE DICIEMBRE DE 2020

ISBN 978-84-9159-379-9

SPECTRAL CHARACTERIZATION AND SEMANTIC SEGMENTATION OF COMPLEX 3D MODELS IN NATURAL ENVIRONMENTS

DOCTORAL DISSERTATION

JUAN MANUEL JURADO RODRÍGUEZ

Universidad de Jaén

Juan Manuel Jurado Rodríguez

Spectral characterization and semantic segmentation of complex 3D models in natural environments

Spectral characterization and semantic segmentation of complex 3D models in natural environments

Juan Manuel Jurado Rodríguez

Supervisors:
Francisco Ramón Feito Higueruela
Lidia Ortega Alvarado
Juan José Cubillas Mercado

Universidad de Jaén

Departamento de Informática
Escuela Politécnica Superior de Jaén
Universidad de Jaén

November 2020

Abstract

This doctoral thesis presents main contributions in two fields related to Remote Sensing and Computer Vision: (1) the characterization of 3D scenarios from multispectral images and (2) semantic segmentation of point clouds. As a result of this research, the software GEU, *v.1.0*, (Geospatial and Environmental tools of University of Jaén) has been developed. This PhD thesis is presented in the form of a compendium of publication. Four articles have been published in renowned scientific journals and several contributions have been presented at national and international conferences.

The first part of the thesis focuses on the fusion of spectral and morphological variables of 3D tree structures. This work proposes a method for the enrichment of point clouds from multispectral images. For this purpose, high resolution RGB images are acquired to model the 3D scenario and multispectral images to capture the amount of reflected light at several wavelengths. In order to fuse both datatypes, a new algorithm is provided to map multispectral images on the point cloud. This doctoral dissertation presents different applications of this algorithm to two different surveyed areas: an olive plantation and a forest region. In the first work, a multi-temporal monitoring is carried out to study the evolution presented by an olive plantation. The individual detection of each plant and its morphological and spectral characterization is carried out in two different campaigns. Secondly, an area of Mediterranean forest where different tree species coexist is studied. In this work, the correlation between the canopy reflectance and the 3D structure for each tree is analyzed. Finally, 3D viewer is developed for an interactive visualization of results, thus achieving a free navigation around the 3D model, whose appearance changes depending on the selection of available information layers.

In the second part of this thesis, several advances are proposed for the semantic segmentation of natural materials and the recognition of individual grapevines in point clouds. The first work is related to the segmentation of real-world materials with a similar appearance in the visible spectrum. To this end, a new method based on hierarchical clustering is proposed. This uses spatial and spectral features linked to a 3D model in order to detect key feature patterns related to every material. The second work focuses on using spatial and geometric data for the segmentation of 3D point clouds of vineyards. According to the results of this research, a new method is proposed for the efficient location of each plant based on the recognition of its trunk, as well as the identification of missing plants along the vine row. This method means a significant advance in the detection of individual grapevines and the efficient monitoring in vineyards.

Resumen

Esta tesis doctoral presenta sus principales contribuciones en la caracterización de escenarios 3D a partir de imágenes multiespectrales y la segmentación semántica de nubes de puntos. Como resultado de esta investigación, se ha desarrollado el software GEU (Geospatial and Environmental tools of University of Jaén) que integra el conjunto de métodos desarrollados. Dicha tesis doctoral es presentada por compendio de cuatro publicaciones en revistas científicas de alto impacto y varias conferencias nacionales e internacionales.

La primera parte de la tesis se centra en la fusión de variables espectrales y morfológicas de estructuras arbóreas en escenarios naturales de nuestro entorno. Se ha propuesto un método para el enriquecimiento de modelos 3D a partir de imágenes multiespectrales. Por un lado, se han capturado imágenes RGB de alta resolución, que son utilizadas para la reconstrucción tridimensional del modelo. Por otro lado, se han tomado imágenes multiespectrales para medir la reflectancia espectral en distintas longitudes de onda. El desarrollo de esta investigación se ha llevado a cabo sobre dos áreas de estudio: una plantación de olivar y una zona forestal. En el primer trabajo, se ha analizado la evolución temporal que presenta una plantación de olivar mediante la detección individual de cada árbol y la caracterización morfológica y espectral de su modelo 3D. En el segundo trabajo, se ha estudiado un área de bosque Mediterráneo en donde coexisten varias especies arbóreas. El objetivo es analizar la correlación existente entre la reflectancia medida en cada árbol y su estructura 3D. En ambos casos, se ha trabajado para lograr una visualización interactiva y realista de los resultados en un entorno 3D, cuya apariencia varía según la capa de información activada.

La segunda parte de la tesis se centra en la explotación del conjunto de características intrínsecas a los modelos 3D con el fin de proponer avances en la segmentación semántica de distintos tipos de materiales y el reconocimiento de patrones geométricos específicos de la estructura 3D de una planta. El primer trabajo consiste en hacer uso de nuestro método para caracterizar espectralmente un escenario en el que coexisten distintos tipos de materiales. El objetivo es aplicar técnicas de clasificación no supervisada para reconocer automáticamente distintos tipos de materiales a partir de variables espectral y espaciales asociadas al modelo 3D. El segundo trabajo se centra en el uso de datos espaciales y geométricos para la segmentación de viñedos que han sido reconstruidos en 3D. En este caso, se ha propuesto un nuevo método para localización eficiente de cada planta a partir del reconocimiento de su tronco, así como la localización de faltas a lo largo de cada fila. Este método supone un avance significativo para la detección individual de vides y monitorización eficiente en viñedos.

Acknowledgments

Previo al desarrollo de los contenidos presentes en esta tesis doctoral, quisiera agradecer a un conjunto de personas que en lo académico y personal me han brindado su ayuda, comprensión y compartido su tiempo a lo largo de estos años.

En primer lugar, quiero expresar mi mas sincero agradecimiento a mis directores de tesis Francisco Feito, Lidia Ortega y Juan José Cubillas. Gracias Francisco por ser mi compañero de viaje en lo profesional y personal, por ayudarme a superar momentos complicados y enseñarme tantas cosas que no podría resumir en estas lineas. Gracias Lidia por haber confiado en mí desde el principio, acompañarme en cada momento y darme paso a un nuevo horizonte repleto de oportunidades. Gracias Juan José por mostrarme siempre tu perspectiva transversal y guiarme durante estos años. En general, gracias por haber sido mis directores y confiar en mí de la manera que lo habéis hecho.

El carácter multidisciplinar de esta investigación me ha conducido a la colaboración activa con otros investigadores que han sido coautores de algunos trabajos realizados y a los que les agradezco su inestimable ayuda. De forma especial, quisiera agradecer la labor de María Isabel Ramos, Carlos Enríquez, Carlos Ogayar, José Luís Cárdenas y Luís Pádua por su implicación en los trabajo realizados. También agradecer a todos los miembros del Grupo de Informática Gráfica y Geomática de Jaén (GGGJ) por hacerme sentir uno más desde el principio y compartir tantos momentos amenos que han sido muy gratificantes.

De igual manera quisiera mostrar mi agradecimiento a Joaquim J. Sousa por darme la oportunidad de realizar la estancia de investigación en la Universidad de Trás-os-Montes e Alto Douro y transmitirme su ilusión y visión de equipo que me ha servido de motivación y gran ayuda.

Gracias familia, por ayudarme a tomar las decisiones más importantes de mi vida. En especial a mis padres, gracias por transmitirme siempre vuestros valores y confianza en mí y a María del Carmen, eres el motor que impulsa mi día a día.

Por último, quisiera transmitir mi agradecimiento a la Universidad de Jaén y a su escuela de doctorado por la ayuda que me concedió para la realización de la estancia de investigación a fin de obtener la mención de Doctor Internacional. Del mismo modo, mi agradecimiento al proyecto TIN2017-84968-R que ha servido de apoyo en esta investigación.

Comenzaba esta sección agradeciendo a personas, la finalizo diciendo que todos ellos ya son amigos, que juntos, formamos un equipo de trabajo de gran valor desde el punto de vista profesional y humano.

Contents

List of Figures

List of Tables

List of Algorithms

Acronyms

GEU	Geospatial and Environmental Tools of UJA
UAV	Unmanned Aerial Vehicle
LiDAR	Light Detection and Ranging
SAR	Synthetic Aperture Radar
GIS	Geographical Information System
PA	Precision Agriculture
PV	Precision Viticulture
SfM	Structure from Motion
GPU	Graphics Processing Unit
DL	Deep Learning
VNIR	Visible and Near Infrared
REG	Red-Edge band
CHM	Canopy Height Model
GSD	Ground Sampling Distance
VI	Vegetation Index
NIR	Near Infrared
NDVI	Normalized Difference Vegetation Index
GRVI	Green-Red Vegetation Index
RVI	Ratio Vegetation Index
NDRE	Normalized Difference Red-edge Index
LAI	Leaf Area Index

ICP	Iterative Closest Point method
NDRE	Normalized Difference Red-edge Index
LAI	Leaf Area Index
ICP	Iterative Closest Point method
FOV	Field of View
HFOV	Horizontal Field of View
VFOV	Vertical Field of View
UTM	Universal Transverse Mercator
KNN	K-Nearest Neighbors
GNSS	Global Navigation Satellite System
DBH	Diameter Breast Height
PCL	Point Cloud Library
RTK	Real Time Kenematic
SOR	Statistical Outlier Removal
BRDF	Bidirectional Reflectance Distribution Function
DSM	Digital Surface Model
DEM	Digital Elevation Model
GPS	Global Positioning System
CRP	Close-Range Photogrammetry
IMU	Inertial Measurement Unit
RMSE	Root-Mean-Square Error
OBIA	Object-Based Image Analysis

Part I

Introduction and Overview

This part introduces a big picture of this doctoral dissertation, as well as the main aims and objectives of this research. Then, a summary of measurable contributions are presented.

1 Introduction

The generation of 3D models to represent real-world scenarios has become increasingly prevalent for many applications of subfields of Computer Vision, Computer Graphics and Remote Sensing related to their acquisition, analysis and visualization. Over the last few years, the proliferation of image-based sensors has led to collecting huge datasets of urban or natural environments for multiple purposes. This thesis addresses several open problems related to multi-source data fusion (to integrate data captured from different sensors), computer vision (to derive key information from images and 3D models) and 3D mapping (to generate 3D models enriched from multispectral images). As a result of this research, we have developed GEU (Geospatial and Environmental tools of University of Jaén). This is a research-oriented tool to create, process and visualize 3D point clouds labeled with multispectral data.

This thesis presents contributions in two different areas within the field of Remote Sensing and Computer Vision: (1) the multispectral characterization of 3D models (Part II) and (2) the semantic segmentation of point clouds (Part III). This chapter provides a brief introduction into these two areas, and main contributions to each of them.

1.1 Multispectral characterization of 3D models

The first part of this doctoral dissertation focuses on the multispectral characterization of 3D models, with the goal of exploring novel monitoring and analysis methods based on enriched 3D point clouds. Nowadays, the use of Unmanned Aerial Vehicles (UAV) sensors allows us to capture a high geometric and spectral resolution of real-world scenarios. In fact, more and more studies are being carried out using different types of sensors for monitoring multiple environmental variables [1, 2]. The use of drone-based technologies facilitates a more detailed observation of natural environments instead of traditional acquisition methods based on satellites or aircraft. As a result, the volume of data related to the territory is growing exponentially. In this field, it is increasingly common to use several types of sensors together in order to monitor a wide variety of features in natural scenarios. However, the exploitation of these huge datasets requires the development of novel methods for fusing multi-source information. According to the studies presented in this thesis, 3D data and multispectral information are fused in order to reveal occluded features which cannot be directly detected by a bidimensional-based ap-

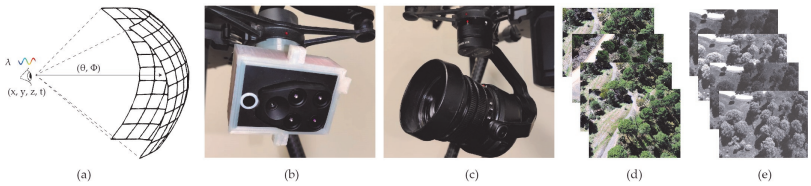

Figure 1 – Materials and data used in this research: (**a**) scheme of an image capture determined by the camera position (x,y,z), camera direction (θ, Φ), wavelength (λ) and time of capture (t), (**b**) the multispectral sensor, (**c**) the digital camera, (**d**) high-resolution RGB images and (**e**) multispectral images.

proach. First, the surveyed scenario is modeled and then, multispectral images are mapped on a 3D point cloud. Figure 1 shows materials and input data used in this research. Thus, the GEU software presents a disruption in relation to the existing methods to efficiently generate, process and visualize enriched 3D models with reflectance values beyond the visible range.

The 3D reconstruction of natural scenarios is challenging since the vegetation structure is irregular, there are many overlapping entities and the dynamic lighting changes the appearance of existing materials. However, drone systems are able to take high-resolution images from many points of view in order to capture the environment as fully as possible. To generate dense 3D point clouds of real-world scenarios, there are four main techniques: (1) Light Detection and Ranging (LiDAR) systems [3, 4], (2) Red Green Blue -Depth (RGB-D) cameras [5], (3) Synthetic Aperture Radar (SAR) systems [6], and (4) image-derived methods [7, 8]. According to these acquisition techniques, RGB-D cameras present limitations due to the insufficient image resolution to model vegetation structures. SAR point clouds are commonly used to generate maps of surface deformation or digital elevation as well as providing four-dimensional imaging. Regarding LiDAR technology, this can be used achieving high quality 3D models, but it is quite expensive and on many occasions it involves time-consuming acquisition tasks. In contrast to above-mentioned techniques, image-based methods are gaining in popularity for modeling real-world scenarios. The well-known structure-from-motion (SfM) algorithm is widely used to generate 3D point clouds only using overlapping images. Both the increase of image resolution and the available points of view using a drone result in 3D models with an accurate geometry of the captured objects. The point cloud is the most commonly data type used for the 3D representation of real-world scenarios. The generation of volumetric models in this type of environment is based on applying inverse procedural methods considering the point cloud as a guide for the procedural modeling of the plant geometry [9]. However, this thesis

focuses directly on point clouds to avoid adding extra complexity and to provide a general use of the proposed algorithms.

The observation of physical phenomena beyond the visible spectrum is generally the most applied technique for the detection of significant features in natural environments. In fact, the spectral reflectance of real-world objects is a key feature which influences the appearance of materials, the plant health and the 3D shape of vegetation structures. Reflectance can be measured using multispectral or hyperspectral sensors [10]. Traditionally, multispectral data have been studied on two-dimensional maps losing an enormous amount of information of lateral and partially occluded parts of observed entities. To overcome this limitation, the integration of 3D models and multispectral data enables a new way to study and assess the development of natural entities under real environmental effects, considering the relationship of their 3D structures and spectral behaviors. Moreover, we have worked to provide an interactive visualization of resulting 3D models managing several information layers which represent different model features. This means an important advance in studying in multispectral data in a 3D environment and achieving an accurate analysis of changing entities in nature. Finally, these models may be automatically characterized by temporal data in order to monitor the development of surveyed scenario.

In particular, this thesis presents contributions to (i) multi-source data fusion, (ii) efficient multispectral image mapping on point clouds, (iii) occlusion detection from multiple view points in a 3D scenario, (iv) multi-temporal monitoring of individual plants, and (v) spectral and morphological characterization of tree species.

1.2 Semantic segmentation of point clouds

The environment understanding in real-world scenarios has become increasingly prevalent due to the development of novel methods for semantic segmentation in Computer Vision. In the last few years, many studies based on Deep Learning (DL) have been proposed to identify different objects in spectral or RGB images [11, 12]. More recently, the fast-forward acquisition of 3D data from different sensors based on stereo- or multi-view imagery involves the development of new approaches which exploit spatial and geometric features [13]. In this thesis, the multi-source data fusion and the development of spatial-based methods is the key idea to propose several advances in the material segmentation in natural environments and the geometric pattern recognition in 3D point clouds.

The characterization of natural spaces by the accurate observation of their material properties is highly demanded in both Remote Sensing and Computer Vision. The proliferation of novel sensors enables the collection of heterogeneous data to acquire a comprehensive knowledge of living and non-living entities in the ecosystem. The high resolution of consumer-grade RGB cameras is frequently used for the geometric reconstruction of many types of environments. Nevertheless, the understanding of natural spaces is still challenging. The automatic segmentation of real-world materials in nature is a complex task because there are many overlapping structures and dynamic lighting. Our research in this area is targeted towards (i) material segmentation of natural environments which present a homogeneous appearance in the visible spectrum and (ii) the trunk recognition of grapevines to determine the 3D location by removing the ground, leaves and noisy points in the point cloud.

Firstly, we have developed a method based on fusing spatial and multispectral features for the unsupervised classification of natural materials in a 3D point cloud. A high-resolution camera and a multispectral sensor are mounted on a manufactured device in order to simultaneously capture RGB and multispectral images. Our method is tested in a controlled scenario, where different natural objects coexist. Initially, the input RGB images are processed to generate a point cloud by applying the SfM algorithm. Then, the multispectral images are mapped on the three-dimensional model to characterize the geometry with the reflectance captured from four narrow bands (green, red, red-edge and near-infrared). The reflectance, the visible color and the spatial component are combined to extract key differences among all existing materials. For this purpose, a hierarchical cluster analysis is applied to identify the feature pattern for every material and to segment the point cloud into sets of points, each one corresponding to a different material. As a result, the tree trunk, the leaves, different species of low plants, the ground and rocks can be clearly recognized in the scene. These results demonstrate the feasibility of our method to distinguish between similar natural materials and to identify them in a 3D scenario considering multispectral and spatial features.

Secondly, we have presented a novel method for the trunk recognition of grapevines using UAV-based point cloud data. The optimization of vineyard management requires efficient and automated methods in order to identify individual plants. In the last few years, UAVs have become one of the main sources of remote sensing information for Precision Viticulture (PV) applications. In fact, high resolution UAV-based imagery offers a unique capability for modeling plant's structure enabling possible the recognition of significant geometrical features in photogrammetric

point clouds. Despite the proliferation of innovative technologies in viticulture, the identification of individual grapevines relies on image-based segmentation techniques [14]. In that way, grapevine and non-grapevine features are separated and individual plants are estimated considering a fixed distance between them. Our method focuses on the recognition of key geometrical parameters to ensure the existence of every plant in the 3D model. This solution represents an important advance in order to monitor individual plants, locating each one in the vineyard based on the processing and analysis of a 3D point cloud.

In summary, the main contributions in this field are: (i) the automatic segmentation of similar materials applying unsupervised classification, (ii) an efficient methodology for semantic material labeling in 3D point clouds, (iii) the automatic recognition of individual grapevines from geometrical parameters, not requiring any prior knowledge, and (iv) the estimation of missing plants in vineyard for the optimization of the harvest production.

1.3 Aims and Objectives

The overall goal of this thesis is to propose several advances in the characterization and processing of 3D models based on the idea that the generation of enriched 3D models from multispectral data can help us to overcome inherent limitations of using bidimensional data with a partial viewing experience of results. In addition, this objective leads us to the second part of this research focused on segmentation of 3D models considering spectral and geometric features. This dissertation is characterized by a multidisciplinary approach since novel methodologies and algorithms have been proposed in the fields of image acquisition and processing, heterogeneous data fusion, 3D mapping, multi-temporal analysis and semantic segmentation. Throughout this thesis we push further in this direction, providing the GEU framework, which integrates every method developed. Currently, more applications are being developed using GEU to address several open problems. This work is described as future research in Chapter 6.

Figure 2 presents an overview of results related to the twofold objectives of this research: (1) the study of multispectral features of 3D models from natural environments and (2) the semantic segmentation of point clouds using multispectral and spatial features to classify natural materials and detect individual grapevines. According to the most significant advances in these fields, main objectives of this thesis are listed below:

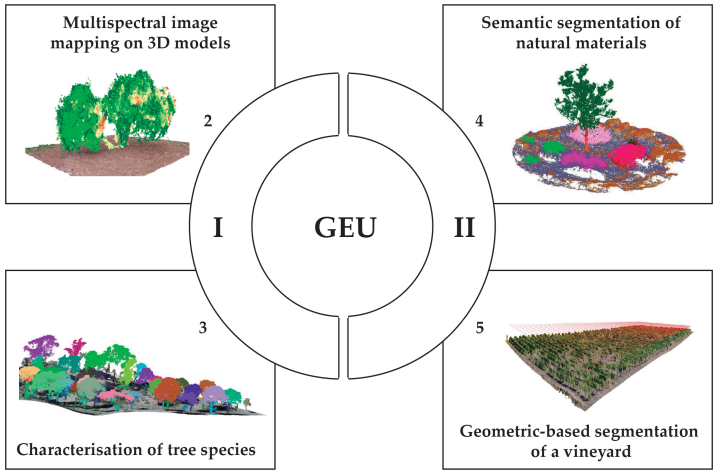

Figure 2 – Overview of main objectives addressed in this research.

- The development of a new method for multispectral image mapping on point clouds which represent real-world scenarios. This method enables (1) obtaining the reflectance maps for each capture, (2) testing the occlusion in the 3D environment, (3) mapping every 3D point on visible pixels in the multispectral images, and (4) integrating multi-temporal data. The results should be enriched 3D models with several information layers, which can be inspected through an efficient and interactive visualization in a 3D environment.

- The use of proposed method to characterize several tree species in a Mediterranean forest and to study the relationship between morphological and multispectral features for each one. To this end, the detection of individual trees is required to obtain several features of the 3D structure and to analyze the impact of canopy reflectance.

- A new method for the semantic segmentation of 3D models for the recognition of real-world materials based on unsupervised classification. The proposed algorithm uses point cloud data and multispectral traits to identify similar natural materials.

- The development of a novel method for grapevine trunk detection, using 3D point cloud data. It focuses on the recognition of key geometrical parameters to ensure the existence of every plant in the 3D model. This method helps to identify individual trunks, posts and missing plants, thus enabling an accurate 3D location for each plant and the possibility of developing multi-temporal studies.

1.4 Dissertation Structure

This dissertation is divided in four parts organized in a set of chapters:

- Part I includes the current chapter to present a big picture of the research topic and main contributions and goals of this work. Furthermore, measurable results obtained are mentioned.

- Part II is devoted to multispectral characterization of 3D models. In Chapter 2, we tackle the problem of fusing multispectral data and point clouds. To this end, a novel method is developed for mapping 3D points on their corresponding pixels for each multispectral image. Moreover, in this process, an occlusion test is developed to avoid mapping occluded points on incorrect pixels. Thus, an enriched point cloud is generated in such a way that each 3D point stores its reflectance, observed at different wavelength. Currently, this method is being improved using the graphics processing unit (GPU) to accelerate the performance, thus enabling the use of 3D models from large scenarios. This last work is presented as further research since it is not completely finished. In Chapter 3, we address a novel study focused on the relationship between morphological and spectral features of different tree species in a Mediterranean Forest. This advance enables the characterization of tree species in order to study the biodiversity in a real ecosystem, considering the plant geometry and the canopy reflectance.

- Part III tackles the long-standing problem of semantic segmentation of real-world scenarios. The topic of Chapter 4 is based on natural material segmentation using the spatial distribution of spectral attributes of the 3D model. As a result, a labeled model is provided to be used by supervised learning algorithms. In Chapter 5, several advances are proposed, using geometric-based segmentation in order to detect individual plants in vineyards by the the trunk detection using point cloud data. Furthermore, the proposed method helps us to recognize human-made posts, missing plants and to determine the location for each one. The results of this study might influence on individual monitoring of every grapevine, multi-temporal studies and making accurate support decision systems for an optimal vineyard management.

- Part IV concludes this dissertation by highlighting the main contributions and pointing out open problems to be addressed as future work.

This research and its contributions would not have been possible if it had not been carried out in collaboration with different colleagues. To improve understanding, the presented work is described and contextualized at the beginning of each chapter.

1.5 Contributions and measurable results

1.5.1 Publications

The work presented in this thesis has been published in four JCR indexed journals and several peer-reviewed conference publications:

- Multispectral Mapping on 3D Models and Multi-Temporal Monitoring for Individual Characterization of Olive Trees (Chapter 2, Part II)
  - This work was accepted to Remote Sensing [15]. This journal has an impact factor of 4.509 in the category of Remote Sensing (data from 2019).
  - Previous results were published in the national conference Congreso Español de Informática Gráfica (CEIG), 2018 [16].
- The Impact of Canopy Reflectance on the 3D Structure of Individual Trees in a Mediterranean Forest (Chapter 3, Part II)
  - This work was accepted to Remote Sensing [17]. This journal has an impact factor of 4.509 in the category of Remote Sensing (data from 2019).
- Semantic Segmentation of Natural Materials on a Point Cloud Using Spatial and Multispectral Features (Chapter 4, Part III)
  - This work was accepted to Sensors [18]. This journal has an impact factor of 3.275 in the category of Instruments and Instrumentation (data from 2019).
  - Preliminary results were published in the the 14th International Joint Conference on Computer Vision, Imaging and Computer Graphics Theory and Applications (GRAPP), 2019 [19].
- Automatic Grapevine Trunk Detection on UAV-Based Point Cloud (Chapter 5, Part III)
  - This work was accepted to Remote Sensing [20]. This journal has an impact factor of 4.509 in the category of Remote Sensing (data from 2019).

In addition to these previous publications, during my PhD I have participated in other research projects not directly related with the topic of this thesis:

- *Topological Data Models for Virtual Management of Hidden Facilities Through Digital Reality.* This work by Lidia Ortega was published in IEEE Access, 2020, [21].

- *The UAS-Based 3D Image Characterization of Mozarabic Church Ruins in Bobastro (Málaga), Spain.* This work by Carlos Enríquez was published in Remote Sensing, 2020, [22].

- *Prediction of the increase in health services demand based on the analysis of reasons of calls received by a customer relationship man-agement.* This work by Juan José Cubillas was published in The International journal of health planning and management, 2019,[23].

- *High Precision Geomatic Tools for Improving Harvest of Olive Grove in Advance.* This work by M.ª Isabel Ramos was published in the International Congress on Engineering and Sustainability in the XXI Century, 2019, [24].

- *3D Farm Management Information System for Precision Agriculture.* This work by J.L. Cárdenas was published in the International Congress on Engineering and Sustainability in the XXI Century, 2019, [25].

- *3D Environment Understanding in Real-time Using Input CAD Models for AR Applications.* This work by David Jurado was published Spanish Computer Graphics Conference (CEIG), 2019, [26].

- *Multispectral Registration, Undistortion and Tree Detection for Pre-cision Agriculture.* This work by Alfonso Lopez was published Spanish Computer Graphics Conference (CEIG), 2019, [27].

- *Spatio-temporal data fusion for monitoring terrain of olive plantations in the South of Spain.* This work done by myself was published in the COST Action on Environmental Monitoring with UAS - HARMONIOUS, 2018.

- *3D underground reconstruction for real-time and collaborative vir-tual reality environment.* This work done by myself was pub-lished in the 26th International Conference in Central Europe on Computer Graphics, Visualization and Computer Vision (WSCG), 2018, [28].

- *Advances for 3D printing: Remote control system and multi-material solutions.* This work done by myself was published in the 26th In-ternational Conference in Central Europe on Computer Graphics, Visualization and Computer Vision, 2018, [28].

- *Web-based GIS application for real-time interaction of underground infrastructure through virtual reality.* This work done by myself was published in the 25th ACM International Conference on Advances in Geographic Information Systems, 2017, [28].

Finally, the following publications have been already submitted pending to be accepted:

- J.M. Jurado, L. Pádua, J.R. Jiménez, F.R. Feito and J.J. Sousa. A Similarity Measure for Efficient Material Recognition Using Hyperspectral Imaging. *Submitted to Eurographics (EG) 2021.*

- A. López, J.M. Jurado, C.J. Ogayar and F.R. Feito. A framework for registering UAV-based imagery for crop-tracking in Precision Agriculture. *Submitted to International Journal of Applied Earth Observations and Geoinformation.*

- M.I. Ramos, J.J. Cubillas, Jurado, J.M. Jurado and F.R. Feito. Improvement of the prediction of harvest in olive grove. *Submitted to Computers & Electronics in Agriculture.*

- D. Jurado, J.M. Jurado, L. Ortega and F.R. Feito. Interactive facility management through mixed reality: A new approach to geometrical markerless positioning indoors. *Submitted to Graphics & Visual Computing.*

1.5.2 Research stay

The research stay was carried out during this PhD, founded by the Doctoral School of University of Jaén. Based on it, a fruitful collaboration started between the Computer Graphics and Geomatics Group of Jaén and the Joaquim Sousa's group at the University of Trás-os-Montes and Alto Douro (UTAD), which continues today and from which a promising research has spawned.

- June 2020 - October 2020 (four months): Visiting student at the University of Trás-os-Montes and Alto Douro (UTAD). Supervisor: Prof. Dr. Joaquim João Sousa.

1.5.3 Supervised students

Throughout this thesis, I have supervised the following final degree projects and master thesis:

- 2020: Tamara Morales. *TFM: Herramienta gráfica para la reconstrucción de fragmentos en arqueología.* Grade: 9/10.
- 2020: Andressa de Sousa Cardoso. *TFG: Avances en la gestión del olivar mediante herramientas geomáticas.* Grade: 10/10.
- 2019: David Jurado Rodríguez. *TFM: Realidad aumentada y mixta para reconocimiento y gestión de infraestructuras en edificios.* Grade: 10/10.
- 2019: José Luis Cárdenas Donoso. *TFM: Gestión avanzada de información procedente de drones.* Grade: 9/10.
- 2019: Javier Serrano Casas. *TFG: Sistema de realidad aumentada para supervisión de instalaciones de edificios v.II.* Grade: 10/10.
- 2018: David Jurado Rodríguez. *TFG: Sistema de realidad aumentada para supervisión de instalaciones de edificios.* Grade: 9.5/10.
- 2018: Daniel de la Rosa de la Rosa. *TFG: Gestión de información procedente de drones.* Grade: 9/10.

1.5.4 Research projects

During my PhD, I have been involved in the following research projects:

- GIS3D4D: Herramientas de Informática Gráfica para la gestión de datos 3D y 4D. Aplicando técnicas de RV & RA a Infraestructuras Urbanas y Arqueología. Project N.º: TIN2017-84968-R. IP: Francisco R. Feito and Lidia Ortega.
- GIS3D: Aportaciones para las ciudades inteligentes. Hacia un SIG 3D del subsuelo. Project N.º: TIN2014-58218-R. PI: IP: Francisco R. Feito and Lidia Ortega.

Part II

Multispectral characterization of 3D models

This part is divided into two chapters. The first one presents the algorithm for the multispectral image mapping on 3D point clouds. The second chapter concerns the impact of reflectance on the 3D structure of different tree species.

2 Multispectral Mapping on 3D Models and Multi-Temporal Monitoring for Individual Characterization of Olive Trees

About this chapter

The work presented in this chapter has been published in two venues: some preliminary results were presented at a national conference, the *Congreso Español de Informática Gráfica (CEIG) 2018,* and the whole work was later published in the journal *Remote Sensing.* This research means the start point of this thesis, in which a novel method for multispectral image mapping on 3D models is proposed under the supervision of Francisco R. Feito, Lidia Ortega and Juan J. Cubillas.

J.M. Jurado, L. Ortega, and F.R. Feito.
3D Mapping Approach to Analyze the Evolution of Vegetation Using Multispectral Imagery
Proc. of the Spanish Conference on Computer Graphics (CEIG), p. 129, Jun. 2018.

J.M. Jurado, L. Ortega, J.J. Cubillas, and F.R. Feito.
Multispectral Mapping on 3D Models and Multi-Temporal Monitoring for Individual Characterization of Olive Trees
Remote Sensing, Vol. 12, no. 7, p. 1106, Mar. 2020.

2.1 Introduction

Olive plants are among the most ancient cultivated fruit trees. For many centuries, the production of olive trees has had an important impact on the Spanish economy. Specifically, Jaén, a southern region of Spain, is considered one of the most relevant producers of virgin olive oil around the world [29]. This province contains 550 thousand hectares of olive groves and produces around 50% (600 thousand tons per year) of the total national olive oil production, and more than 20% of the world's total production of olive oil. Therefore, advances to increase the final production and farming sustainability of olive trees have a high impact on the local economy.

Remote sensing techniques are effective solutions for data acquisition with different spatio-temporal resolutions [30]. Early approaches proposed methods to analyze the evolution of olive trees using satellite images and Geographic Information Systems (GIS) [31, 32, 33]. According to the emergence of novel sensors for plant phenotyping, some studies

were presented to assess plant sustainability using heterogeneous data (spectral indices and temperature) [34, 35]. More recently, Zarco et al. [36] used a hyperspectral sensor (visible and near-infrared (VNIR) model; Headwall Photonics) and a thermal camera (FLIR SC655; FLIR System) to study the Xylella fastidiosa propagation in olive trees through the analysis of some physiological traits over orthomosaic maps. In general, previous works include interesting methods for monitoring and feature extraction of olive trees. However, these are based on bi-dimensional information using a multilayered plant-trait scheme. Therefore, many values from the image-based observations have to be interpolated in the same pixel of the orthomosaic map. Thus, the overall measurements of the plant traits are computed by a coarse estimation. The novelty of our approach lies in focusing on automatically mapping meaningful plant traits on a 3D model of an olive orchard. Our study object is the point cloud of every olive tree, which is enriched by the leaf reflectance response to plant stress. Undoubtedly, the contribution of drone technology in this field is highly positive to get a higher spatial resolution of 3D models and detailed observations of plant reflectance by a more efficient approach [37, 38].

Among the available aerial remote sensing platforms, Unmanned Aerial Vehicles (UAVs) are considered to be cost-effective and they can capture high-resolution imagery from multiple viewpoints [39, 40]. In contrast to satellite images, UAV-based cameras provide a higher spatial resolution and a more detailed observation of individual plants [41]. These solutions are an increasingly used trend for several monitoring tasks using various types of sensors [42]. As a result, the use of drone provides a high versatility during the acquisition process, by planning custom flights at different heights or angles to capture images. Regarding some UAV-based applications in Precision Agriculture (PA), Vanegas et al. [43] used hyperspatial and hyperspectral data for improving the plant pest surveillance in vineyards. Other approaches focused on using drones either for the classification of tree species [44] or the acquisition of thermographic and multispectral features to inspect the plant status [45, 46]. In this paper, the input images are collected by two UAV-based systems (a high-resolution RGB camera and a multispectral sensor), which provide accurate data of plant shape and reflectance response. Moreover, a multi-temporal approach is considered to monitor the variation of observed plant features.

According to the study of plant morphology, the 3D reconstruction of the branching structure can be modeled by photogrammetric techniques as well as Light Detection and Ranging (LiDAR) sensors. Nevertheless, the modeling of 3D plant structures is still challenging because olive

trees contain many overlapping branches in the crown and a high leaf density, which make the generation of plant geometry quite complicated. Some studies proposed different methods for the assessment of geometric features such as the height, area or volume of fruit trees [47, 48, 49] and for the detection of potential phytosanitary problems at the canopy level [50, 51]. Undoubtedly, the complete plant geometry provides a real perception of many morphological traits, which cannot be directly identified in the image. Zarco-Tejada et al. [52] measured the height of olive trees through the photogrammetric process based on UAV-based imagery using a consumer-grade camera onboard a low-cost unmanned platform. The generated 3D scenes had a sufficient resolution to quantify a single-tree height with a similar accuracy to more complex and costly LiDAR systems. However, the resulting point cloud mainly represents the ground and higher branches of olive trees with a significant lack of lateral and internal structures. Our method provides a more accurate reconstruction of plant structure with a higher density of 3D points for each olive tree. Consequently, the trunk, main branches, and many leaves are modeled on a dense point cloud. The efficient managing of these heavy geometric models to merge with spectral layers is also discussed in this work.

Research in ecology studies the evolution of plants through a detailed plant inventory by monitoring at different canopy scales and image-based remote sensing [53]. Unlike a direct visual disease detection on-site, UAV-based sensors are commonly used to measure plant reflectance in several narrow-bands [54]. Leaf reflectance can be observed at different wavelengths, in which the reflected light depends on some biochemical components of the leaf internal structure (chlorophylls and carotenoids) [55]. Multispectral sensors capture several significant bands to detect many properties for diagnosing the plant physiological status such as the drought and heat stress, nutrient content, and plant biomass. Several approaches provide advances for the vegetation assessment using different spectral traits of plants [56, 45]. Thus, vegetation monitoring is possible through feature extraction to promote sustainable farming [57]. Other approaches used multispectral data to propose a 2D-based analysis for disease detection [58] and segmentation of vegetation areas [59]. In addition, recent contributions are provided by the fusion of LiDAR and hyperspectral remotely sensed data [60]. Regarding the novelty of our methodology to previous works, we propose the generation of a reflectance map for each multispectral image to project all pixel values on the point cloud. The plant reflectance is observed from multiple viewpoints to detect the light interactions with top, lateral and lower branches of the tree.

Recently, several studies have presented novel methods by fusing heterogeneous image datasets to extract key feature patterns of the monitored plantation. Nevalainen et al. [61] used hyperspectral imaging for individual tree detection with UAV-based photogrammetric point clouds. Degerickx et al. [3] provided an urban tree health assessment using airborne hyperspectral and LiDAR imagery. In addition, other studies focus on multi-temporal plant diagnosing from very high-resolution satellite images [62] and individual crop measurements based on the clustering of terrestrial LiDAR data [63]. Specifically, UAV-based approaches use drone sensors for an accurate reconstruction of photogrammetric point clouds [64] and even forest inventory [65]. The resulting 3D models of the plant structure can be used for feature extraction of tree height and volume, which provides information about the morphology of olive trees. By applying the proposed methodology, many input feature layers can be mapped on the 3D model of plants without any human intervention. A fully automated method is proposed to enrich the point cloud with spectral data relating to plant health. Our results can be inspected in a 3D virtual environment for visual-based assessments by an expert.

The individual tree detection plays an increasingly significant role in an automated plant-monitoring process. Mohan et al. [66] used UAV-based imagery for individual tree detection using a local-maxima based algorithm on Canopy Height Models (CHMs). Individual Tree Crown Detection and Delineation (ITCD) algorithms have advanced through novel approaches by the integration of heterogeneous data sources [67, 68]. Marques et al. [69] proposed a fully automated process to monitor chestnuts plantations. This method is based on RGB and multispectral imagery for tree identification and counting as well as feature plant extraction. However, it is based on an image segmentation instead of a 3D classification. Previous works mainly describe an image-based segmentation by using orthomosaics. In our research, the multispectral and geometric data are used to identify every olive tree as a single entity on the point cloud. In this way, a multi-temporal inventory is developed to study the evolution of morphological and spectral features of olive trees.

Regarding the focus of our study, it is based on the fusion of multispectral imagery and photogrammetric 3D point clouds and multitemporal analysis of individual olive trees. UAV image sets have been acquired using a high-resolution camera and a multispectral sensor. Multispectral image mapping on the 3D model of an olive plantation is the core of this paper. The capability of multi-temporal analysis of plant development by multispectral monitoring is also approached. The presented methodology provides a novel framework for a fully automated fusion of UAV-based heterogeneous data over high detailed 3D tree mod-

els. This paper is organized as follows: Section 2.2 describes the materials and methods used in this research; Section 2.3 shows the results of the proposed methodology; Section 2.4 analyzes the results and the novelty of our approach; Section 2.5 presents the main conclusions.

2.2 Materials and Methods

The study area characterization, the description of the used UAV and sensors and the methods applied to acquire, process, and analyze the data models are presented in this section. The methodology is based on four main stages: multispectral image mapping on the point cloud, individual tree segmentation, feature extraction, and multi-temporal analysis.

2.2.1 Study Area and Data Acquisition

Our method takes input data from the monitoring of an olive plantation, which is located in Jaén. The study area covers 2 hectares of olive trees in which the proposed methodology has been tested and optimized. This is also characterized by some buildings, human objects, a road and other types of vegetation. Figure 3 presents a general overview of the study area. In this paper, the geometry and leaf reflectance of olive trees are the target features, which are acquired and analyzed for individual tree.

The use of UAV in remote sensing provides the collection of heterogeneous data through optimal trajectories and a high detail level of the plant shape. Instead of satellite images, UAV-based acquisition process has a high versatility and provides multiple observations of target crops from different viewpoints. The morphological structure of the olive tree is very complex, with many self-hidden branches, which makes the plant monitoring more difficult. In this research, a professional drone (model: DJI Matrice 210) is used to collect heterogeneous-aerial imagery. On board the drone a high-resolution digital camera (model: Sony Alpha 7 RIII) and a multispectral sensor (model: Parrot Sequoia) are mounted. These devices are very different from each other. On the one side, a full-frame RGB camera takes photos with 48 megapixels (MP), thereby observing the study area with a great spatial resolution. On the other side, the multispectral sensor captures reflectance in four spectral bands: the near-infrared (NIR) from 770 nm to 810 nm, the red from 640 nm to 680 nm, the green from 530 nm to 570 nm, and the red-edge (REG) from 730 nm tp 740 nm. This device has a wide-angle lens with a focal length of 4mm to cover more ground area in a single capture. However, a

high visual deformation is presented in the image. In this way, the development of plant reflectance is monitored from every wavelength range, which captures meaningful changes in plants related to their health status. A detailed explanation of feature extraction for each multispectral band is described in Section 2.3.4.

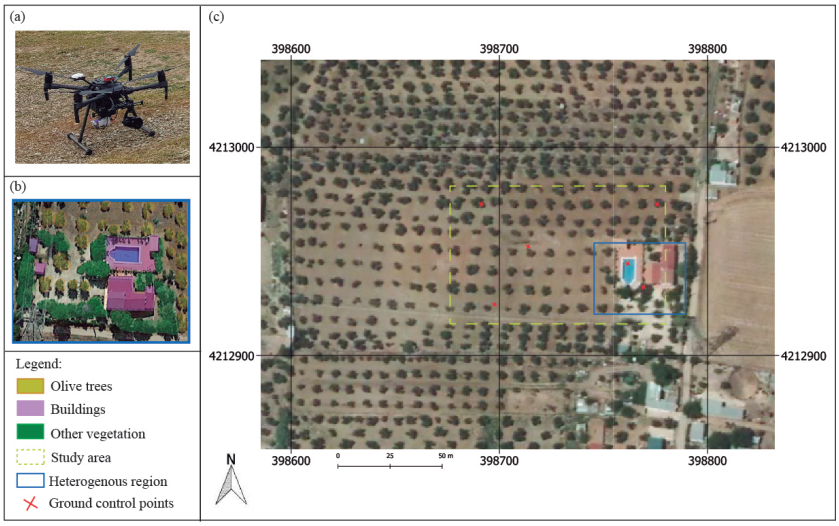

Figure 3 – General overview of the surveyed area: (**a**) unmanned aerial vehicles (UAV)-based acquisition system, (**b**) a complex area where olive trees, buildings and other vegetation coexist, and (**c**) the area of the study in the olive plantation, coordinates in ETRS89 (UTM Zone 30N).

This work includes the temporal domain to detect crucial changes of olive trees at different time frames. Two campaigns have been carried out in the same season to avoid some pruning effects for the estimation of morphological properties. Table 1 summarizes the main parameters for each one. The flights were conducted above all the olive trees in the plantations capturing multiple overlapping images (90%) with both cameras simultaneously. As mentioned above, the lateral and lower branches and shoots of these trees are very important to evaluate some key traits directly related to plant vigorousness, stunted growth, nutritional deficiency, viral infection, etc. For this reason, our approach uses 3D plant models, which were generated by a high-resolution camera and the capturing angle was determined between 65 and 70 degrees. Then, open-source software (Pix4Dcapture) was used to plan the flights, in which the user determines the area of interest, flight direction, longitudinal and lateral overlapping, flight height and the Ground Sampling Distance (GSD). These were conducted close to the solar noon time to minimize the plant shadows and specular lighting. The height of flight

was the same for all acquisition processes, 30 meters by considering an adequate GSD in RGB (1 cm) and multispectral (2.8 cm) images.

Date	Drone	Sensor	Overlap	Images
15/08/2018	DJI Matrice 210	Multispectral: Parrot Sequoia	frontal: 90% side: 80%	264 RGB 179 (×4) Multi
25/08/2019		RGB: Sony Alpha 7RIII		280 RGB 210 (×4) Multi

Table 1 – Flight programming and key features of the resulting models.

2.2.2 Data Processing

The methodology described in this article consists of a fully automated multi-temporal monitoring of olive plantations through the multispectral image mapping on a comprehensive 3D model of individual olive trees. Moreover, the K-means [70] algorithm is used to classify individual olive trees on the point cloud according to their spatial, geometric and spectral features. The proposed framework also supports a multi-temporal analysis and can assume input data at different time frames without any human intervention for the data fusion process. Hence, an individual tree inventory is carried out to evaluate the spectral response for a period of time as well as its relationship with morphological properties such as the tree height and volume.

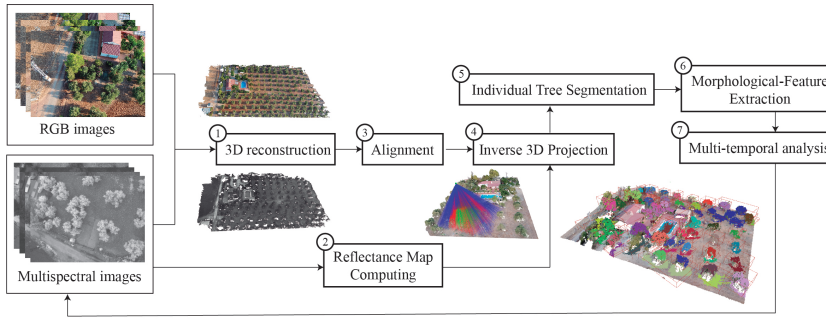

Figure 4 – Overview of the proposed methodology for fusing multispectral images and RGB point clouds and multi-temporal monitoring of olive trees.

In summary, the main contributions are (1) multispectral image mapping on comprehensive 3D models of olive trees, (2) multi-temporal monitoring and analysis of the spectral reflectance for individual olive trees. The flow diagram of our framework is shown in Figure 4. This scheme illustrates the main steps, which have been performed. As the first step, input RGB and multispectral images are used for the 3D reconstruction

of the olive plantation. Once the position and orientation of the high-resolution model are corrected by some tie points, both point clouds are aligned to be set in the same coordinate system. Before the multispectral image mapping, the reflectance maps are calculated for every multispectral image. Then, the 3D model is enriched by reflectance values, which are weighted considering the viewpoint of the multispectral camera. The next step in the process is the method for the classification of individual olive trees. Finally, according to the data acquired from the two flight campaigns, the variability of morphological and spectral traits is extracted and multi-temporal analysis of these results is presented.

This section presents all the methods developed to create this framework. The evolution of olive trees has been analyzed by fusing multispectral and morphological traits over the 3D models. The 3D reconstruction of the olive plantation, the multispectral image processing, the mathematical model applied for image mapping on the 3D models and the feature-based extraction of individual olive trees are the main techniques.

2.2.2.1 Point Cloud Reconstruction

The precise modeling of olive trees requires a high spatial resolution to generate most of their thin branches and tiny leaves. Geometry-based methods may reconstruct botanically correct skeletal structures of existing plants. In this article, we mainly focus on image-based modeling as an efficient technique for plant reconstruction in natural environments with acceptable results. In this regard, UAV-based cameras serve as cost-effective solutions to acquire a higher spatial resolution rather than satellite imagery or airborne LiDAR. The use of drone systems provides the capability to plan custom flights with different heights, thereby enabling a more detailed and full observation of each olive tree.

In this paper, the first step of the proposed methodology, Figure 4, is the 3D reconstruction of the olive plantation. According to image sequences captured by the RGB camera and multispectral sensor, two point clouds are generated where multiple olive trees, the ground, buildings, and some human objects appear. The RGB high-resolution point cloud contains a high detail of the plant geometry and is used to measure the height and volume of every olive tree. The multispectral point cloud has a lower spatial resolution and it is only used for the alignment process.

The photogrammetric processing is applied through Pix4Dmapper Pro software (Pix4D SA, Lausanne, Switzerland), which is based on the

structure-from-motion (SfM) algorithm [71]. This method can detect the same regions of overlapping images, determine their geometric relationships and infer the rigid scene structure (point set) with the pose (position and orientation) of all cameras. Table 2 shows the main features of the resulting point clouds. The densification of the 3D models is studied by considering the size of the point clouds and the ground-sampling distance (GSD). Due to the lower resolution of multispectral images, the mean GSD is 3.53 cm, which means a larger ground area per pixel than RGB images. Consequently, the densification of the point cloud is more sparse. Unlike previous datasets, the RGB-based camera provides a higher image resolution, resulting in the mean GSD is 0.78 cm and the point cloud being much higher. Therefore, the pixel size is under 1 cm, which implies a high resolution of olive tree modeling.

Campaign	Sensor	3D Densified Points	GSD(cm)
1	RGB	101.846.488	0.84
	Multispectral	3.513.641	3.53
2	RGB	153.441.547	0.78
	Multispectral	3.776.247	3.37

Table 2 – Point cloud densification details.

2.2.2.2 Reflectance Map Computing

The plant status is greatly influenced by many environmental effects in the surrounding area. In terms of the assessment of vegetation health, the multi-temporal monitoring of the spectral response of crops plays a key role. Our method uses multispectral images to observe the reflectance of olive trees for two flight campaigns. This section focuses on multispectral image processing from each viewpoint and the extraction of some Vegetation Indices (VIs). The used multispectral system is composed of a multispectral camera, which captures four narrow bands, and a sunshine sensor to measure the incident sunlight. The input images are processed to calculate a reflectance map for each one by applying Algorithm 1.

The reflectance of any object is its effectiveness to reflect the radiant energy, which means the fraction of incident electromagnetic power reflected. In our study, the spectral reflectance is calculated by measuring the incoming sunlight irradiance and reflected irradiance by the surface of the object captured. Equation (2.1) is used to estimate the reflectance value (R) for each pixel of every multispectral image.

$$R = k_i \left(\frac{\Phi_e^r}{\Phi_e^i} \right) \cos(\theta) \tag{2.1}$$

Algorithm 1: Reflectance Map Computing.

```
Input: Multispectral image (i);
Result: Reflectance maps;
for Every image i do
    Sun irradiance calculation;
    Radiometric calibration;
    for Every pixel of i do
        Reflectance estimation;
```

where K_i is the calibration coefficient of every band i, Φ_e^r is the radiant flux reflected by the object captured, Φ_e^i is the radiant flux incidence by the sun and θ is the angle between the direction vector of sun rays and direction vector of the sunshine sensor.

The incoming sunlight irradiance (Φ_e^i) is measured by the sunshine sensor, which is mounted on top of the UAV. This device is continuously capturing the lighting conditions during the flight time. Moreover, the angle between the sunshine sensor and the sunlight direction must be considered to compensate for the light reflection. The mathematical formulation of this magnitude is defined in Equation (2.2).

$$\Phi_e^i = \frac{\nu}{g\tau} \tag{2.2}$$

where ν is a sensor count value, g is the relative gain factor and τ is the exposure time in seconds.

The next step is to calculate the reflected irradiance (Φ_e^r) by using metadata (Exif) stored in the image. Every pixel $\mathbf{p}$ in the image $\mathbf{I}$ provides a reflected irradiance value, which is calculated by applying the Equation (2.3).

$$\Phi_e^r = f^2 \frac{\rho - B}{A\gamma\varepsilon + C} \tag{2.3}$$

where g is the f-number = 2.2, p is defined by pixel intensity, ε is the exposure time, γ is the ISO parameter = 100 and A, B and C are the calibration coefficients measured per camera in production.

Finally, the plant reflectance must be radiometrically calibrated using a panel, which provides known reflectance values of the target surface. Three images are captured over this panel for each multispectral band with different exposure levels. This process is made at the beginning and

at the end of each flight. In this way, multi-temporal data, which are taken at different time frames and weather conditions, can be compared to each other. To calculate this calibration coefficient K, Equation (2.4) is applied.

$$K_i = R_i \left(\frac{\Phi_e^i}{\Phi_e^r} \right) \tag{2.4}$$

where R_i is the known reflectance for each band i, Φ_e^i is the radiant flux incidence from the sunlight and Φ_e^r is the radiant flux reflected by the calibration panel.

Regarding previous approaches to calculate the plant reflectance, these usually generate either a single orthomosaic or reflectance map by every flight campaign of the study area [72]. Nevertheless, this approach implies the interpolation of many values, which are overlapped on the same pixel coordinates. Consequently, just the mean value may be stored for each pixel. In this regard, the novelty of our approach is the calculation of a reflectance map for each multispectral image, which provides significant values about the spectral response of olive trees from a singular viewpoint. Then, the reflectance maps are going to be mapped on the RGB point cloud by considering the occlusion detection and the viewpoint of the multispectral camera (Section 2.2.2.3).

In addition, some spectral bands have been combined to estimate some VIs [73, 74]. Firstly, the sharp contrast between soil and leaf reflectance in the NIR and red bands is typically used to calculate the Normalized Difference Vegetation Index (NDVI) [75]. It is a well-known spectral index applied in remote sensing. In general, NDVI evaluates the green biomass, leaf cover or chlorophyll per unit ground area. Secondly, green and NIR bands are also used together to estimate the Green-Red Vegetation Index (GRVI), which is strongly influenced by changes in leaf pigments. Thirdly, Ratio Vegetation Index (RVI) [76] is used for the estimation of biomass and Leaf Area Index (LAI). Finally, the Normalized Difference Red-Edge Index (NDRE) is also calculated by combining red-edge and near-infrared bands7. It is more suitable than NDVI for monitoring the growing season when plants accumulate a critical level of leaf cover and chlorophyll content [77]. In the following Table 3, the mathematical formula for the calculation of each vegetation index [78].

2.2.2.3 Multispectral Image Mapping

The ratio of plant absorption and reflection is highly influenced by morphological characteristics of plants such as branching structure, leaf density, canopy volume, etc. The relationship between plant geometry

Index	Formula
Normalized Difference Vegetation Index	$NDVI = \frac{NIR-RED}{NIR+RED}$
Green Ratio Vegetation Index	$GRVI = \frac{NIR}{GREEN}$
Ratio Vegetaion Index	$RVI = \frac{NIR}{RED}$
Normalized Difference Red-Edge Index	$NDRE = \frac{NIR-REG}{NIR+REG}$

Table 3 – The calculation of vegetation indices (VIs).

and the reflectance response of plants is one of the main contributions of this paper. We provide an automatic method to enrich the high-resolution point cloud with meaningful traits of the plant status. Therefore, the comprehensive 3D model contains geometric and spectral features by mapping the multispectral images on the high-resolution point cloud. In this section, the third and fourth methods in Figure 4 are described: the data alignment and the inverse 3D projection.

The alignment of multispectral images and a high-resolution RGB point cloud is carried out by the development of an automatic method to set the same coordinate system for both datasets. A possible solution might be the use of ground control points (GCPs) in the multispectral point cloud to correct its position and scale. However, it implies the human intervention by a time-consuming task. Moreover, the multispectral images have a lower resolution than RGB images and being in a grayscale palette makes the tie points recognition difficult. To ensure a fully automated multispectral image mapping we have applied the iterative-closest-point (ICP) algorithm [79] for the geometry-based alignment of multispectral and RGB cloud for every campaign. This method assesses the corresponding point pairs based on a weighting calculation from distance computing and compatibility of normal vectors. A normal vector defines how a surface responds to lighting. The amount of light reflected by a surface is proportional to the angle between its normal vector and the lighting direction. In this work, normals are computed through the reconstruction method (SfM). As a result, a rigid transformation is obtained minimizing the sum of the squared error in Equation (2.5).

$$E(R,t) = \frac{1}{N_p} \sum_{i=1}^{N_p} ||x_i - Rp_i - t||^2 \tag{2.5}$$

where: x_i and p_i are corresponding points, t is the translation vector and R is the rotation matrix.

Once both 3D models are aligned, the multispectral point cloud is discarded and the resulting transformation matrix is applied for all mul-

tispectral images. In this way, the position of these images is corrected and can be correctly projected to the high-resolution RGB point cloud.

The following step, once output data are in the same coordinate system, is the multispectral image mapping on the 3D model. In general, UAV-based multispectral sensors use fisheye lenses to capture extensive areas at a low altitude. The monitoring of large plantations requires devices with a wide field of view (FOV) to get a high overlapping rate of all images. However, the quality and image resolution of the resulting data-set are highly reduced comparing to digital cameras. Moreover, multispectral images do not comply with the central perspective projection and present a high geometric deformation. As a result, the distortion model of the camera has been considered for the image mapping on the high-resolution 3D model.

For this purpose, an inverse 3D projection is developed to assign each 3D point of the point cloud the corresponding pixel of the multispectral image, in which it is visible. Every 3D point (with coordinates: *X, Y, Z*) is mapped to image coordinates (x_d, y_d) by considering the fisheye camera model. This distortion model is determined by the parameters C, D, E, F, which describe an affine deformation of the circular image in pixel coordinates. The polynomial fisheye, with the coefficients p_2, p_3, p_4, is defined in Equation (2.6).

$$\rho = \theta + p_2\theta^2 + p_3\theta^3 + p_4\theta^4 \tag{2.6}$$

where:

$$\theta = \frac{2}{\pi}\arctan\left(\frac{\sqrt{X^2+Y^2}}{Z}\right); \theta\epsilon[0,1]$$

where: X, Y and Z are the coordinates of 3D point.

By applying the previous distortion model of the multispectral camera, the pixel coordinates (x_d, y_d) of the 3D point projection is calculated by the Equation (2.7):

$$\begin{bmatrix} x_d \\ y_d \end{bmatrix} = \begin{bmatrix} C & D \\ E & F \end{bmatrix} \begin{bmatrix} x_{hbt} \\ y_{hbt} \end{bmatrix} + \begin{bmatrix} c_x \\ c_y \end{bmatrix} \tag{2.7}$$

where:

$$\begin{bmatrix} x_{hbt} \\ y_{hbt} \end{bmatrix} = \begin{bmatrix} \frac{\rho X}{\sqrt{X^2+Y^2}} \\ \frac{\rho Y}{\sqrt{X^2+Y^2}} \end{bmatrix}$$

and (c_x, cy) is the principal point in pixel coordinates.

As mentioned before in Section 2.2.1, the oblique angle of drone images provides a full observation for every olive tree. Lateral and lower branches can be modeled as well as the plant reflectance is measured from multiple viewpoints. However, occlusion problems and inaccurate measurements of the reflectance has to be solved to get a correct mapping.

A weighting procedure is developed to assess the reliability of reflectance from each viewpoint. The multispectral camera captures a more reliable reflectance of an object's surface if its direction vector is similar to the normal vector of such an object. If the angle of both vectors is very high, the reflectance detected is more irregular and less reliable. Our method focuses on the comparison between the vector direction of each multispectral view and the normal vector of every 3D point. If its value is close to 0°, the 3D point is observed from almost a perpendicular view in the multispectral image. In this way, reflectance maps are calculated considering 3 ranges: a perpendicular view (0° to 25°), an oblique view 25° to 60° and an indirect view (greater than 60°). The left image in Figure 5 presents a theoretical example of the previous explanation. The green arrow is the normal vector of a 3D point and the purple arrow is the direction vector of the camera. The angle between both vectors is showed as alpha.

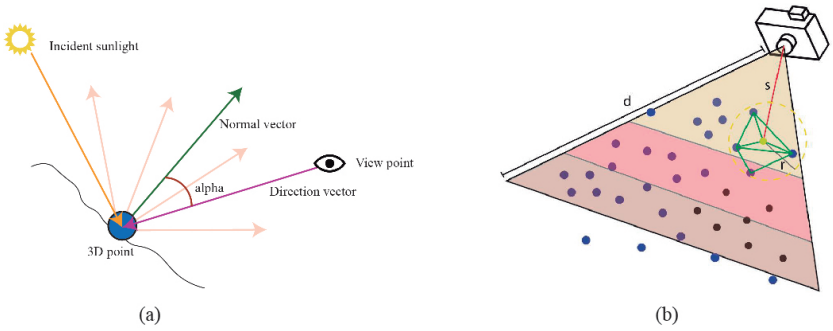

Figure 5 – Operations on 3D points: (**a**) the lighting interactions where the alpha angle is used as a reference for the weighting process, and (**b**) the visibility test on the point cloud.

Then, an occlusion test is carried out to get an accurate image mapping on the point cloud. Although a 3D point is located in the visibility range of multispectral imaging, it may be occluded by a closer geometry to the viewpoint of the camera. In this regard, we propose a method to check the point visibility from every multispectral camera. The right image in Figure 5 presents the scheme for this approach. Firstly, 3D points

(blue points) inside the view frustum of the camera are candidates to be projected in the image plane. Secondly, these candidate points are ordered by measuring the Euclidean distance between the camera and the 3D point position. Thirdly, from the nearest-to-farthest points, a minimal triangulated surface is formed by considering the target point (the yellow point) and their neighbors. The nearest neighbor search is based on the radius and the angle between normal vectors. These parameters are set to ensure one thousand points at least. The resulting minimal surfaces are used to detect occluded points (black points) which are discarded to be projected in that image. This algorithm is repeated until all points are checked. As a result, the geometry of the olive plantation is correlated to its multispectral response and thus, a meaningful feature pattern can be detected for the segmentation of individual olive trees in the point cloud.

2.2.2.4 Individual Tree Segmentation

Our approach supports the multi-temporal monitoring at individual tree level. To this end, a point cloud classification method is carried out to identify every olive tree in the surveyed area. 3D geometry and multispectral data are the input data for the segmentation of individual trees. Unlike previous works based on image segmentation for individual tree registration [80], which does not work properly in areas with high overlapping of trees or hard shadows, we propose an efficient 3D-based segmentation of individual olive trees.

Initially, a coarse segmentation of the point cloud is developed to classify the vegetation areas and the soil surface. At the canopy level, the sharp contrast between the soil and leaf reflectance is used for the automated identification of vegetation areas in the ratio from the NIR to the red band. For this reason, the NDVI is the most adequate index for olive tree recognition and also it is not highly affected by the shadow cast of trees.

Nevertheless, some outliers of the NDVI cause errors in the point-based classification. To overcome this problem, an optimization method is carried out by applying k-nearest neighbors (KNN) [81]. The category of every 3D point is compared to their neighbors and it changes if most of these points have been classified in other classes. The density of the point cloud is very high, so a higher radius for the neighbor selection might affect the final performance negatively. The radius for the neighbor selection is set as 50 cm by considering the GSD of the point cloud and the impact on performance. According to the k-dimensional tree (k-d tree) [82], which organizes the point cloud in a space with k

dimensions, an efficient range search is performed. This data structure is three-dimensional and each level splits all subdivisions along a specific dimension using a perpendicular hyper-plane to the corresponding axis.

The following step is to identify each olive tree as an individual entity. For this purpose, 3D points belonging to the vegetation class are partitioned into different clusters by the application of the K-means algorithm. The number of possible clusters is not explicit, thus it depends on the heterogeneity of the scene. Through this method, a search for nearest-neighbor points is developed regarding these constraints: the distance between the 3D points, the minimum cluster size, and the direction of normal vectors. In this work, we have defined the maximum distance lower than 15 centimeters, the maximum degree between normal vectors from 0 to 180 degrees and the cluster size must be greater than one thousand points.

Once each olive tree is identified as a unique entity on the point cloud, multi-temporal monitoring and analysis may be performed. According to the previous method for fusing multispectral data and 3D reconstruction of the olive trees, several semantic layers may be overlapped to study different environmental variables. Moreover, an individual inventory for each olive tree can be performed to study its evolution, considering multitemporal data series.

2.2.2.5 Morphological-Feature Extraction

According to the sixth step in Figure 4, the morphological development of olive trees is studied by monitoring the changes in height and volume. These parameters are necessary to determine adequate plant growth. In this regard, pruning activity has a high influence on these properties. This issue has been considered and the collected data in the same season of two different olive harvesting.

The plant height has been used to measure crop growth [52]. This feature provides additional information that complements spectral vegetation indices for predicting growth and yields. In this study, the plant space is decomposed by a 3D octree with a spatial resolution of 20 cm. This value is enough to estimate an accurate overall tree volume and assure the efficient performance of the method. This data structure is based on a tree topology in which every internal node has exactly eight children [83]. Firstly, a bounding box is defined to calculate the maximum dimensions of the tree. In this way, the height can be directly obtained from this geometric shape. Then, the whole space is decomposed into multiple voxels and a voxel-based inclusion test is applied. In

this phase, we have to check if any voxel contains one 3D point at least. Finally, the total volume is calculated by the sum of each voxel volume, which partially contains some parts of the olive tree.

The proposed framework allows the processing of multi-temporal data to analyze the evolution of plant morphology and leaf spectral reflectance over time. In this regard, the variability of studied features (Table 4) is carried out by statistical analysis to detect key changes for two flight campaigns.

Feature	Description
Spectra	
Green	It has the highest plant reflection of the visible range.
NIR	It is the least sensitive band to chlorophyll.
Red	Healthy plants present a high absorption of red light.
REG	This band is used for the assessment of plant stress.
VIs	
NDVI	It is used for vegetation recognition and plant assessment.
RVI	It can be used for biomass and leaf area index estimation.
GRVI	This index is used for the leaf density or vigor of vegetation.
NDRE	It is sensitive to chlorophyll and soil background effects.
3D Plant	
Height	The vertical distance from the soil to the highest branch
Volume	The space occupied by the 3D structure of olive trees

Table 4 – A summary of all characteristics under study.

In this study, multispectral and morphological features are considered for the analysis process. The evolution of olive trees is analyzed by a qualitative and quantitative approach. On the one hand, the measurement of spectral traits is meaningful to assess the plant health, thereby the crucial changes of the reflectance between both campaigns are studied. In this regard, the leaf pigments play a key role in the reflected light in the observed narrow bands. Moreover, NDVI, RVI, GRVI, and NDRE are also compared by analyzing the significant variability of each one on graphics and colorized 3D models. On the other hand, the development of the plant shape is also included in the analysis stage. The height and volume are calculated for each olive tree. These values are fundamental to get a comprehensive knowledge of the plant growth. Our approach provides a fully automated procedure to study the multispectral information and high detailed geometry of an olive plantation. The results of our analysis are presented in Section 2.3.

2.2.3 Validation Procedure

In this study, the extraction of morphological and multispectral features of olive trees has to be validated for each flight campaign. Both flights were performed in the same season, corresponding to the olive fruit final ripening stage. At this time, olive trees are not affected by pruning factors, which are performed after harvesting olive fruit. Firstly, to ensure the calibration of the measured reflectance in two acquisition processes, a calibration panel is used. A calibration coefficient (K) is calculated for each narrow band as mentioned in Section 2.2.2.2.

Moreover, the geometry of the RGB point cloud has to be measurable to obtain accurate morphological features of the olive trees (the height and volume). Although the UAV includes a Global Navigation Satellite System (GNSS) receiver, it has a random error so the resulting scale and position of the point cloud are not correctly determined. To overcome the previous problem, six GCPs are distributed throughout the surveyed area. These points are acquired using a Real Time Kinematic (RTK) GNSS (Topcon GR5) with a centimeter accuracy linked to the Andalusian Positioning Network. The overall accuracy is studied by the RMSE for n observed checkpoints, as the below Equation (2.8) and (2.9). For a 3D point with coordinates (X, Y, Z), the residuals are calculated by subtracting the coordinates that were measured by GNSS and the interpolated corresponding 3D reference point on the point cloud. The resulting model has been corrected using previous GCPs, which have been clearly identified in the point cloud.

$$RMSE_{X,Y} = \sqrt{\frac{1}{n}\Sigma_{i=1}^{n}\Big(X_{i,ref} - X_{i,GNSS}\Big)^2 + \Big(Y_{i,ref} - Y_{i,GNSS}\Big)^2} \tag{2.8}$$

$$RMSE_Z = \sqrt{\frac{1}{n}\Sigma_{i=1}^{n}\Big(Z_{i,ref} - Z_{i,GNSS}\Big)^2} \tag{2.9}$$

Regarding the use of fixed marks to measure the GPS points on the ground, it is not adequate because many tillage techniques are carried out in the olive plantation. Moreover, one of our goals is the automated flow, which is why significant objects in the surveyed area are used to determine the location of GCPs (Figure 6). In this way, the GPS measurements are required for the first time.

Once GCPs are set, a vertical and horizontal adjustment is applied to the point cloud. Therefore, the 3D model is translated, rotated and scaled to improve the accuracy of the point cloud. According to the validation of the height and volume of olive trees, the great size of the

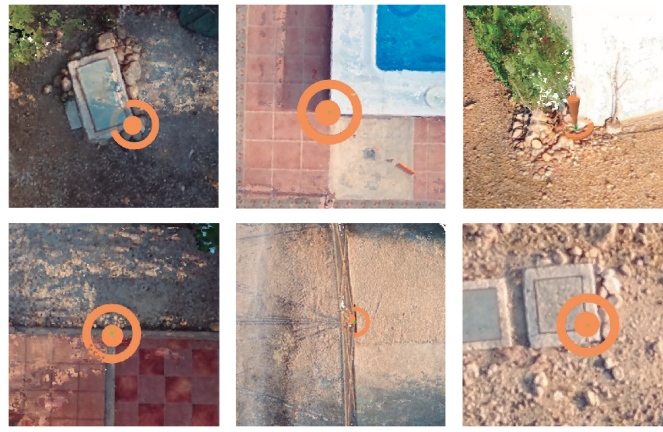

Figure 6 – Meaningful objects used as marks for an accurate georeferencing.

tree crown, as well as the irregular shape of the canopy makes it difficult for field data extraction [84]. In this study, these parameters have been checked by the measurements of physical objects in the olive plantation, which are visible from the aerial images. Specifically, the height and volume of ten reference objects are measured (Figure 7). These human-made objects can be measured much easier than olive trees and their correct dimensions validate the geometric precision of olive tree models. In this way, due to the shape of these physical objects being fixed, the manual field data acquisition only was made for the first time.

Figure 7 – Measurements of the height and volume of several objects in the surveyed area, which are taken as reference to validate the model scale.

2.3 Results

According to the application of previous algorithms, the olive plantations can potentially benefit from monitoring and analytic operations.

The proposed framework provides the capability to study the evolution of olive trees by considering some morphological and spectral features in a 3D space where lateral and lower regions are observed from multiple viewpoints. The following results prove the novelty of this method.

2.3.1 Characterization of Study Area

The researched olive plantation is characterized by a high-resolution point cloud with 0.78 cm GSD in the first flight campaign and 0.84 cm in the second one. This 3D model contains a high detail level of the plant geometry. Figure 8 presents the result of the photogrammetric process.

Figure 8 – The 3D reconstruction of study area and detailed views of some tree models.

The overall shape of the plant canopy has been accurately generated. The trunk, main branches and multiple leaves of olive trees can be correctly identified in the 3D model. More detailed views of some olive trees are shown in the bottom images of Figure 8, which have high point-based densification around 250 thousand of 3D points as average. Some holes appear in the ground because these regions were occluded by the plant structure.

Likewise, multispectral images have been captured to characterize the surveyed area with the spectral response of olive trees in two flight campaigns. Figure 9 shows all observed bands from the multispectral camera. Each one measures the reflectance from a different wavelength

range, and these measurements provide meaningful information to determine key features of the plant status. According to these images, a point cloud is generated for each flight campaign. These are just used as input data for the automated alignment process between the RGB point cloud and multispectral imagery.

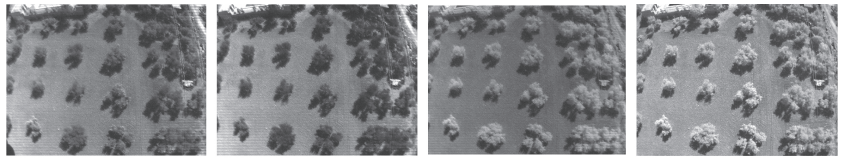

(a) (b) (c) (d)

Figure 9 – Reflectance maps for a single capture: (**a**) green, (**b**) red, (**c**) red-edge, and (**d**) near-infrared.

2.3.2 Accuracy Assessment

Regarding the accuracy of the previous photogrammetric process for each flight campaign, Table 5 presents the absolute and relative errors of the reconstructed point cloud. The error in the GCP is the distance between the initial position of computed points in the 3D model and the position in their corresponding GCPs. It means the accuracy of drone GPS. A Higher deviation was found in the Z-axis (the height) whereas the error rate was much lower in both, the X and Y axes. According to the theoretical error for each direction (X: easting, Y: northing, and Z: height), it indicates the relative accuracy using the error ellipsoid axes of GCPs. The relative accuracy is quite great under 5 cm in X and Y and 33 cm on the Z-axis. A summary of the RMSE for both acquisition stages is presented in Table 6. In general, the absolute error on the second point cloud is higher than on the first and the relative error is slightly more accurate for the second reconstruction.

Our methodology provides a fully automatic process for the analysis of the evolution of olive trees in two time frames by considering some morphological and physiological features. One of our goals is to avoid human intervention to acquire UAV-based data and measurements taken in the field. Therefore, the validation of the estimated height and volume is carried out using fixed physical objects in the olive plantation. In this regard, ten reference objects are considered to be measured in the field for the first time. The estimated measurement is very similar to the field data. The mean error in height is 5 cm and the mean error to estimate the volume is 0.4 m^3. These results demonstrate the adequate georeferencing of the point cloud and the precise geometry of the 3D model.

ID	Campaign	Error Distance to GCP (m)			Theoretical Error (m)		
		X	Y	Z	X	Y	Z
1	1	0.49	−1.00	−6.66	0.047	0.020	0.216
	2	−1.00	−2.36	11.53	0.004	0.004	0.015
2	1	0.45	−0.96	−6.53	0.002	0.002	0.028
	2	−0.98	−2.43	11.42	0.006	0.005	0.021
3	1	1.39	−1.77	−6.35	0.021	0.037	0.328
	2	−0.28	−1.99	11.59	0.001	0.001	0.002
4	1	0.52	−1.107	−6.41	0.049	0.048	0.115
	2	−1.01	−2.28	11.62	0.002	0.002	0.009
5	1	0.814	−0.657	−6.52	0.036	0.063	0.103
	2	−0.65	−1.91	11.68	0.008	0.011	0.029
6	1	0.591	−0.965	−6.71	0.017	0.008	0.098
	2	−0.93	−2.35	11.49	0.003	0.004	0.020

Table 5 – Error of computed point to ground control points (GCP) and theoretical error in each direction (X, Y, Z) on the six (GCPs) for each campaign.

Flight Campaign	RMSE/Global (m)		RMSE/Relative (m)	
	(X,Y)	(Z)	(X,Y)	(Z)
1	1.313	6.53	0.042	0.148
2	2.877	11.555	0.005	0.016

Table 6 – Root mean square error (RMSE) of global and relative accuracy in each direction (X, Y, Z) for each flight campaign.

2.3.3 Heterogeneous Data Fusion

In this section, we present the results by the fusion between the high-resolution point cloud and multispectral images. The position of multispectral images is corrected by the alignment of the multispectral and RGB point cloud (Figure 10). This last one is taken as reference, which has been previously georeferenced by multiple GCPs. Regarding the accuracy of this method, a global RMSE is used to measure the differences between the aligned point clouds. In the first campaign, the error is 2.80 cm and 2.20 cm in the second campaign. These values are considered because both are lower than the GSD of the multispectral point cloud (3.53 cm). Then, by applying the proposed method for multispectral image mapping on the point cloud, the RGB point cloud is also enriched with meaningful semantic layers, which describe the spectral development of plants. The merge of both data types is useful for multiple monitoring tasks and assists with the automated identification of vegetation in the 3D model.

(a) (b)

Figure 10 – 3D alignment: (**a**) initial position of point clouds, and (**b**) aligned point clouds.

According to the method for the automated recognition of olive trees (Figure 4), these are classified by considering some key features. The left image of Figure 11 shows the segmentation of existing vegetation and the right image depicts the recognition of individual olive trees. Firstly, the NDVI is used to identify the vegetation areas. Then, meaningful spectral traits are studied to differentiate the olive trees to the rest of the existing vegetation. The right image of Figure 11 presents the individual segmentation of every olive tree. According to the leaf densification of this plant specie, the olive trees can be identified with a reflectance in NIR as 0.30 and REG as 0.20. Other existing plants use to have a more leafy canopy than olive trees, so the mean reflectance slightly increases in previous bands. Moreover, the spatial component helps to K-means to identify every olive tree. This method works properly because all the olive trees in the plantation (72) have been detected as unique 3D models.

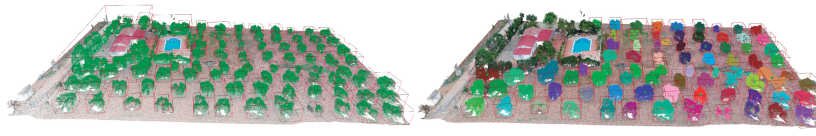

(a) (b)

Figure 11 – Individual tree classification: (**a**) detection of vegetation area, and (**b**) segmentation of olive trees.

2.3.4 Morphological and Spectral Features

Once olive trees have been identified in the olive orchard, the height and volume are measured for each 3D model. A part of the point cloud is shown in Figure 12 to explain the results of this process. The bounding box of every olive tree is calculated to determine the height and the initial volume for the plant space decomposition. The volume is estimated by

a voxel-based partitioning of the plant space. The voxels, which have been partially occupied by some 3D points of the plant geometry, are colored red.

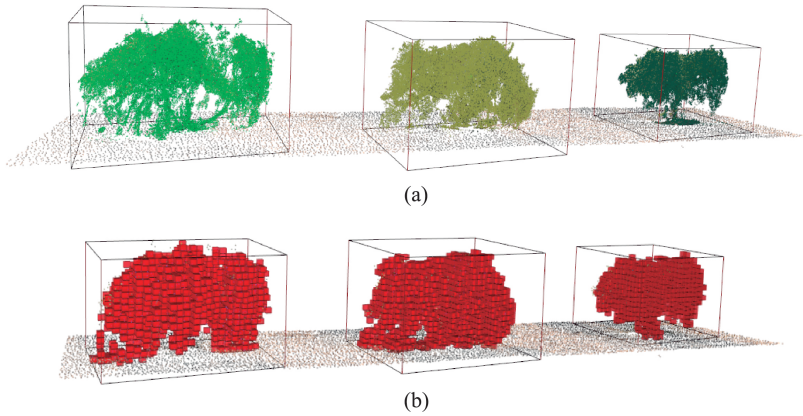

Figure 12 – The height and volume estimation of individual olive trees: (**a**) the generation of bounding boxes, and (**b**) the voxel-based decomposition of the plant model.

Regarding estimated height and volume of olive trees, Figure 13 presents the resulting measurements of 72 olive trees, which have been recognized in the surveyed area. The X-axis represents different ranges of height (m) or volume (m^3) and the Y-axis shows the number of olive trees for each group. In general, the mean volume of olive trees is close to 16.7 m^3 in the first campaign. For the second one, the volume measurements slightly increase, it is 17.28 m^3 on average. According to the height variability, the mean value for both time frames is 2.9 m. These results are discussed in more detail in Section 2.4.

According to multispectral features, which are studied for each olive tree, Figure 14 presents the distribution of reflectance values in every wavelength (left image) and the vegetation indices (right image) for the two campaigns.

Considering the reflected light captured by every narrow band, the higher values are detected in NIR. The vegetation spectrum typically absorbs in the red, slightly reflects at the green wavelength and strongly reflects in the NIR and REG bands. In both flight campaigns, the NIR values are the highest close to 0.35 on average. In the REG band, the mean reflectance is close to a 20% of incident light. The lowest values are measured in the visible range, the green and red bands, where leaves

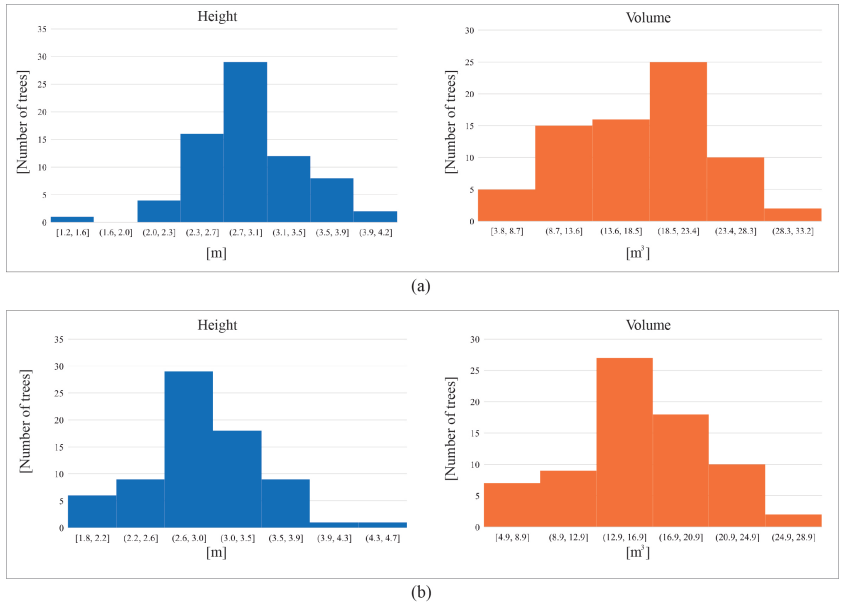

Figure 13 – Height and volume measured in: (**a**) the first campaign, and (**b**) the second campaign.

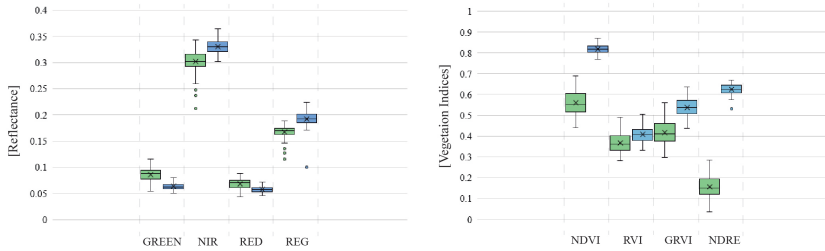

Figure 14 – Plant reflectance and vegetation indices in the first (green color) and second campaigns (blue color).

absorb most of the sunlight. Regarding the results of VIs, a positive trend is detected if we compare the resulting values between the first and second campaigns. The overall value of the NDVI in olive trees changes from 0.55 to 0.81, which means a significant improvement in the plant vigor. Relating to RVI values, these are much higher in vegetation areas in which a strong contrast is observed between the red and NIR bands. The GRVI measures the relationship between the NIR and green bands. In general, the reflected light in the green band is higher than the red band, thus GRVI values are usually upper than RVI. Finally, the NDRE

presents the lowest values in the first campaign and these significantly increase for the second one. It is due to the higher leaf reflectance, which is observed by the REG band in the second flight campaign. A more detailed discussion of the plant development is described in the following Section 2.3.5.

2.3.5 Multi-temporal Analysis

The evolution of plant traits has been studied in two flight campaigns. Multispectral and morphological features are extracted for each olive tree by observing the top, lateral, and low branches. These characteristics are analyzed by the variability of data through different graphics and by a visual-based inspection in the 3D model of the olive plantation. Figure 15 presents a summary of the morphological and spectral changes in the olive plantation.

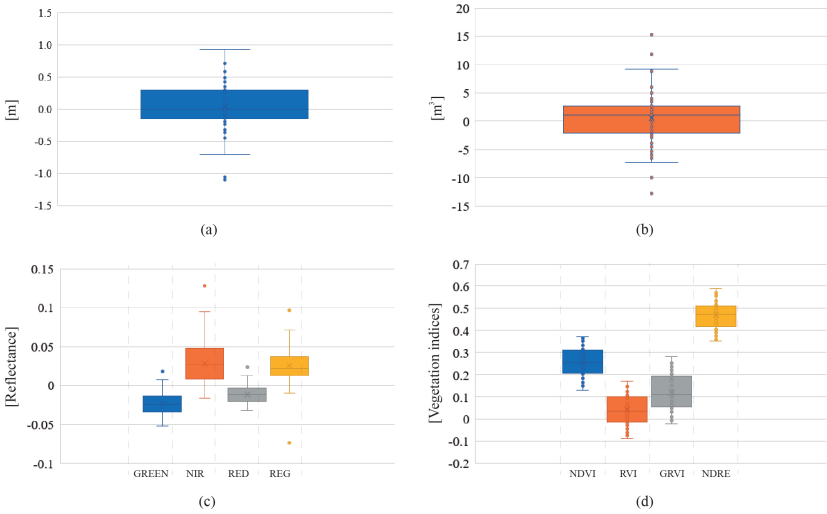

Figure 15 – Variability of morphological and spectral features: (**a**) the height, (**b**) the volume, (**c**) the multispectral bands, and (**d**) the vegetation indices.

According to the variability of data in general, the trend in the crop sustainability is positive. Firstly, the height presents minimal changes close to 0.04 m on average. It is due to the fact that during the pruning stage, farmers remove the highest branches to facilitate the olive fruit harvest. Secondly, the mean volume of olive trees has increased 0.53 m^3, and the overall volume of the olive plantation has increased to 113.17%. Regarding the main changes of the spectral traits in olive

trees, a greater difference is detected in the infrared domain rather than in visible bands. Most of the incident light is absorbed by plant leaves so a lower reflectance is detected in green and red bands. In the second campaign, the visible light is absorbed by 2% more than the first one. In contrast to the red and green bands, the plant reflectance increases in the NIR and REG bands for the second campaign. Finally, the variability of the vegetation indices demonstrates the healthy evolution of olive trees. The estimated VIs are higher in the second campaign. Specifically, the NVDI increases from 0.55 to 0.81, the mean NDRE values in the plant canopy changes from 0.15 to 0.62, which means better health in the studied crops.

Figure 16 presents the evolution of studied vegetation indices on the point cloud for two different campaigns. The color scale is defined by the highest values in the green color and the lowest values in the black color. By the visual inspection of the enriched 3D model for each campaign, an initial assessment of the crop health can be made. The interactive visualization of every plant regions from different viewpoints is very useful to study the plant status. In the first campaign, high contrast of olive trees and ground can be detected for each VI model. According to the NDVI point cloud, a high contrast is visible between the ground and olive trees. Nevertheless, in the second campaign, the emergence of low vegetation around the olive trees supposes higher values on ground level. The RVI point cloud provides a saturated color for the ground reflectance. The variability of this index in the plant canopy is not very significant. The visualization of the GRVI 3D model shows a greener color for olive trees and a higher value on the ground level due to the increase of reflectance detected in the green band. Finally, the NDRE is the most sensitive index to the leaf area and orientation. This index can provide a better measurement of the reflectance variability in areas where the NDVI measures uniform values. In the second campaign, the reflectance of the REG band significantly increases on plant and ground level for the second campaign. Consequently, the resulting NDRE point cloud shows higher values for the ground and olive trees. In general, the overall development of olive trees can be considered to be quite healthy. The variability of studied indices demonstrates that in the second campaign, olive trees have more vigorous branches with a higher leaf and canopy reflectance in the near-infrared domain.

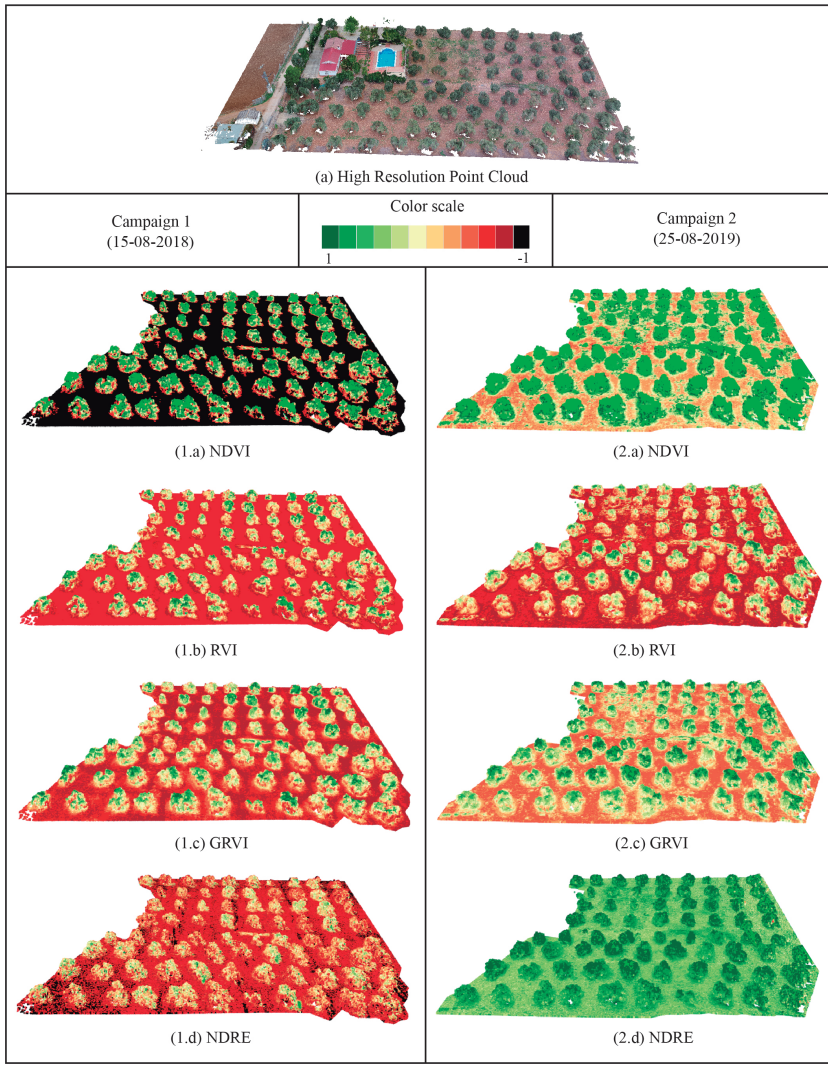

Figure 16 – Multi-temporal monitoring of surveyed olive orchard in two campaigns. For each one, four enriched 3D models are showed considering different vegetation indices.

2.4 Discussion

The results provided by the application of our methodology demonstrate its utility to extract meaningful traits on the plant structure of olive trees. In this farming sector, the use of novel remote sensing techniques during every tillage stage is not still sufficient for monitoring the plant status and early detection of some diseases, which cause a negative effect of the olive production. Therefore, the use of emerging platforms like UAVs and the development of efficient methods are becoming increasingly important gather and combine heterogeneous data, which provide meaningful features of an olive tree health [37, 38]. This paper proposes a novel approach focused on fusing geometric and spectral traits of an olive orchard. The extraction of morphological and multispectral features of comprehensive 3D models, as well as the multi-temporal monitoring of these features to assess the plant development of olive trees, are the core of our method.

Remote sensing methods for the estimation of plant height and volume increase in importance for PA, using either LiDAR or photogrammetry. In this study, image-based sensors are used to observe the structure and reflectance for each olive. Consequently, olive trees were characterized by the spectral reflectance and some morphological properties such as the height and volume. Yan et al. [85] proposed the use of a concave hull operation for the extraction of structural plant parameters. In contrast, our solution is based on a voxel-based decomposition of the plant space using a 3D octree, which is widely used for the partition of three-dimensional space by recursive subdivision [83, 86]. An advantage of our method is that it is not affected by the irregular shape and disperse branching of the tree canopy whereas the calculation of the concave hull is not the most adequate solution in this case. Moreover, the triangulation of the concave hull requires the correction of non-manifold geometry in the photogrammetric model and the generation of the 3D mesh, which negatively affects the final performance.

One of the goals of our approach is to ensure the automatic process for each step of the proposed methodology. Unlike other approaches [72] based on field data acquisition and GCPs measurement in every flight campaign, the validation of the morphological features was made by measuring the dimensions of fixed physical objects in the olive plantation. It supposes a higher efficient technique to acquire validated data for further flight campaigns without repeated time-consuming acquisitions of field data. Regarding the result of this study, the creation of a spatio-temporal inventory of individual olive trees by the 3D plant structures, spectral reflectance and VIs, as well as the vegetation evolution

are discussed in the following sections.

2.4.1 Inventory of Individual Olive Trees

One of the main contributions of our approach is the automatic fusion between the photogrammetric point cloud of olive trees and multispectral images. The resulting geometry of olive trees has been modeled with a high spatial density (20 thousand of points by a cubic meter on average). The managing of the high detailed model of the olive plantation has been accelerated by a spatial data structure, the k-d tree. Therefore, an interactive visualization of the point cloud can be performed in real-time, using the canvas of the proposed application. It is an important novelty of our method in contrast to other approaches based on bidimensional and fixed observations [34, 35, 36]

In this study, the high-resolution RGB point cloud is enriched with a reflectance response at various multispectral bands. The RMSE of data alignment is lower than 3 cm, which is considered valid because the mean GSD of multispectral images is greater than 3.38 cm. As a result, every 3D point contains many reflectance values at visible bands (green and red), REG and NIR bands and some vegetation indices (NDVI, RVI, GRVI, and NDRE). By the previous characterization of the point cloud, different semantic layers can be analyzed using the proposed framework. It means a novel advance in PA in order to review the spectral response of target crops from any viewpoint in a 3D scenario. Previous works, which use the VIs for the plant assessment [87], can benefit from our approach by using our methods to study the spatial distribution of reflectance on the point cloud.

Moreover, the characterization of the point cloud with multispectral features is meaningful for the recognition of individual olive trees. By applying our method, all olive trees are correctly identified, 72 plants in total. Therefore, the overall reflectance and the height and volumes can be obtained for each tree. In contrast to previous work based on satellite or air-bone to acquire images for monitoring of olive trees [31], we can characterize an olive plantation with a higher spatial resolution of plant structures and their multispectral responses from a 3D perspective. This work focuses on the automation of every method to reduce the time-consuming tasks for heterogeneous data fusion and field data acquisition. Consequently, an efficient multi-temporal approach is provided to assess the evolution of plant health by visualizing the enriched 3D models and the analysis of data variability.

2.4.2 Vegetation Evolution

The use of several sources of remotely-sensed data and field data, which may differ in spatial resolution, spatial–temporal coverage and sensor origins, is becoming increasingly popular due to the recent rapid development in remote sensing techniques [61, 3]. In this work, we address the evolution of olive trees by considering morphological and multispectral traits of olive trees. During both flight campaigns, the vegetative cycle of olive trees was the same when the final stage of olive ripening was underway. In terms of a qualitative and quantitative analysis of the plant development, which is observed in Figures 15 and 16, some meaningful conclusions can be extracted.

In the first campaign, olive trees present 16 m^3 and 2.9 m like mean volume and height values. The reflectance in the visible range is quite low, 8% in green and 6% in red. Otherwise, NIR and REG wavelengths present a higher reflected light close to 30% and 17%, respectively. This ratio of values is greatly determined by leaf pigments of the plant. The most visible light, red light is whereas infrared light is least sensitive to chlorophyll and is more reflected. According to the studied VIs by combining previous multispectral bands, the mean NDVI of olive trees has a low value (0.55). It means that plants might present nutritional stress, a low vigor, or a mid-low canopy cover. By visualizing the enriched 3D model, a high contrast is presented between the soil and trees. Focusing on olive trees, healthier regions of the plants are easily detected by the green color, in contrast to stressed parts that become more brown. In the middle of the surveyed area, a high number of olive trees were detected with lower values of VIs. These key observations were taken into account for the next monitoring.

In the second campaign, the evolution of olive trees shows a positive trend in comparison to the first one. The mean volume of every tree is 17.28 m^3, which means 3% of the volume growth. No significant differences in the tree height measurements have been detected. In the studied multispectral bands, the reflectance in visible bands has decreased to 5% in green and 6% in red. Regarding NIR and REG values, these have increased to 35% and 20% respectively. These changes are interpreted as a significant improvement in plant health. It is justified by the fact that VIs provide better results about the plant sustainability. The NDVI increases to 0.81 and the mean NDRE is 0.59. These differences are caused by the higher reflectance in the infrared domain. Moreover, GRVI and RVI present a slight increase to 0.35 and 0.47 respectively. The visual-based analysis, by using our 3D scenario, demonstrates the adequate evolution of olive trees in the studied plantation. A high dif-

ference is detected in the NDRE model, where the soil and plants show higher values. It is due to the emergence of low vegetation around olive trees in this time frame. Finally, regarding the area in which the lowest reflectance values were obtained in the first campaign, only three olives maintain a similar behaviour. In these cases, the NIR values are lower than the rest close to 20%. Nevertheless, the surrounding olive trees have increased the NDVI by 10%. This approach enables a more complete characterization of olive trees parameters as well as the development of a fully automatic process to analyze the plant evolution by a visual and statistical analysis of the individual crop's profile.

2.5 Conclusions

The potential of novel sensors in precision farming creates a great opportunity to advance in the development of efficient methods and techniques for UAV data processing. The huge quantity of data, which this technology provides in a non-intrusive way, and the high number of available sensors to monitor the vegetation status require advanced applications for fusing heterogeneous information.

The proposed innovative tool has a high utility in PA for using heterogeneous and multi-temporal data series. Our approach proposes novel advances in morphological and spectral feature extraction, 3D segmentation of vegetation and the fusion of the plant geometry and multispectral traits to characterize the comprehensive plant structure. In addition, a visual-based analysis is carried out by using the interactive canvas of our framework. An intuitive interaction with the point cloud, as well as the fluent visualization of every 3D model, becomes a potential scenario to monitor and find out interesting variables in the target crop. Likewise, the variability of data is studied by a statistical approach to detect meaningful changes of morphological and multispectral features in two flight campaigns. Our method is based on mapping many multispectral images on the plant geometry, thereby obtaining spectral information about every region in the 3D plant space. One of our goals was the generation of an efficient and fully automated process for fusing multispectral data with the plant geometry. Thus, experts can directly inspect the plant health on a detailed 3D model with multispectral traits of the tree structure.

Although this solution focuses on olive trees, it can be also applied to other fruit trees. In this study, the surveyed area contains 72 olive trees. High-resolution RGB and multispectral images were captured by UAV-based cameras to reconstruct a 3D model of the olive plantation and to measure the reflected light in some specific spectral bands. The result-

ing geometry was highly detailed with accurate modeling of branches, the trunk, and the tree crown. The 3D model of each olive tree was characterized by the height and volume as well as the mean spectral reflectance and VIs by combining some narrow bands. To compare these features in different time frames, the position, orientation and scale of the RGB point clouds were corrected by the use of GCPs. As a result, an enriched point cloud was obtained with a comprehensive 3D model and accurate reflectance measurements of the plant structure. According to the variability of the studied features, some conclusions were drawn. In general, the target olive plantation shows significant symptoms, which indicate a positive trend. According to our analysis, the mean volume of each olive tree slightly increases in the second campaign. The NDVI value and infrared light increase significantly in the plant space. Most olive trees present more greenery in the second campaign and adequate plant growth is observed. This trend is visible by reviewing the enriched models of olive tree structure in the 3D environment.

Several open problems can be subject to further research. Regarding the gathered features about the morphology and spectral response for each tree, we will focus on the study of disease detection. Moreover, we want to use the proposed method for soil monitoring. Finally, the application of this framework for the plant species classification is an interesting topic to approach in the future.

3 The Impact of Canopy Reflectance on the 3D Structure of Individual Trees in a Mediterranean Forest

About this chapter

The work presented in this chapter has been published in the journal *Remote Sensing*. In this research, a novel methodology is presented to study the impact of the canopy reflectance on 3D tree structures in a Mediterranean forest. While I led the line of work (under the supervision of Francisco R. Feito), M.ª Isabel Ramos and Carlos Enríquez collaborated with this publication in data acquisition and processing.

J.M. Jurado, M.I. Ramos, C. Enríquez, and F.R. Feito.
The Impact of Canopy Reflectance on the 3D Structure of Individual Trees in a Mediterranean Forest
Remote Sensing, Vol. 12, no. 9, p. 1430, May. 2020.

3.1 Introduction

Forests play a key role in the conservation of biological diversity and suppression of climate change effects. The observation of its comprehensive three-dimensional (3D) structure has been the focus of recent advances in remote sensing [88]. Moreover, the observation of reflectance on the 3D tree structure is useful to detect the relationship between the shape of trees and their spectral behaviours. Collection of spectral and structural parameters of trees in the field has often been a time-consuming process with limited spatial resolution [89].

In recent years, a great variety of technologies and methods have been used to measure and observe 3D vegetation structures, such as RaDAR [90], Light Detection and Ranging (LiDAR) [91] or photogrammetric techniques like the structure-from-motion (SfM) [92]. Regarding the improvement in image quality, photogrammetry has been widely used for the 3D reconstruction of single-tree architecture. Unlike LiDAR technology, SfM-based methods are a more cost-effective solution and the accuracy of the results is quite acceptable [19]. Grant et al. [93] made a comparison of LiDAR and satellite photogrammetry for forest inventory and the results clearly showed that point cloud data obtained from stereo satellite imagery were useful for the acquisition of forest inventory attributes. Furthermore, Unmanned Aerial Vehicles (UAVs) provide a great opportunity to capture multi-source remote sensing data of the

forest structure [94, 95]. The imaging sensors can capture heterogeneous data in order to observe particular ecosystem functions. Regarding some UAV-based applications in forestry, Tomaštík et al. [96] studied the accuracy of photogrammetric UAV-based point clouds under conditions of a partially-open forest canopy and Tian et al. [97] proposed a novel tree-height extraction approach for individual trees by combining terrestrial laser scanners (TLS) and UAV.

While a 3D forest structure can easily be assessed in a holistic way using terrestrial LiDAR [98, 99], single-tree information is often needed. Therefore, a comprehensive inventory of 3D forest requires a proper segmentation of individual trees and an accurate delineation of the canopy structure. One of the most popular clustering methods for the segmentation of the point cloud is the k-means algorithm [100, 101]. This method needs some seed points, whose location strongly influence the correct recognition of each tree. In this scenario, some approaches based on the Canopy Height Model (CHM) were proposed to detect treetops and determine the initial seed points [102]. However, the most important drawback of this method is that an inappropriate choice of k, the number of clusters, might yield poor clustering results. In this study, a spatial segmentation of the tree crown is proposed for the individual segmentation in the study area. According to the study of tree structure, Chen et al. [103] proposed a novel methodology for the trunk and crown segmentation using LiDAR data. In this study, we propose a novel approach for the tree segmentation and the crown and trunk recognition on photogrammetric point clouds. Regarding the extraction of structural attributes, the tree height, the crown volume and the diameter breast height (DBH) are meaningful traits in order to observe tree growth and tree species characterization. Generally, previous works used various novel platforms to create and characterize the 3D structure of a forest but the study and modeling of forest dynamics are still challenging.

Recent research has proposed solutions based on fusing hyperspectral, multispectral or thermal images for the environmental understanding [45, 104, 10]. Nevertheless, most of these observations are fundamentally two-dimensional (2D) and the tree structure is measured by using orthomosaics of the study area. In reality, forests are complex 3D systems, so the extraction of a comprehensive knowledge of trees has to be carried out in the 3D space. Moreover, the use of multispectral images can be used to observe the light absorption of the tree canopy from meaningful spectral bands [105] as well as to measure the canopy structure [106]. The spectral reflectance and 3D tree structure can be used together to study the light propagation in a forest and to classify the tree species. In this regard, several studies were proposed for the recognition

of spectral reflectance patterns in forests and the competition for light in forest gaps [107, 108].

The aim of this study was to measure the incident sunlight on the tree canopy and to analyze the impact on the structural tree parameters such as the tree height, trunk diameter and the crown volume. The main contributions of the proposed methodology are: (1) the reflectance-based characterization of the 3D forest structure, (2) the fully automatic segmentation of individual trees, (3) the analysis of dependency between structural and spectral parameters by considering different tree species. This article is structured as follows: Section 3.2 describes the study area and sensors used for data collection. Section 3.3 shows the proposed methods for data acquisition, 3D reconstruction, multispectral map computing, point cloud characterization, segmentation of individual trees, reflectance-based analysis and validation. In Section 3.4, the results are presented and main issues are discussed in Section 3.5. Finally, Section 3.6 presents the main conclusions and further research.

3.2 Materials

3.2.1 Study Area

The study was conducted in a Mediterranean forest, situated in Sierra Morena Nature Reserve (38 06' N, 4 10' W) in Jaén, a southern province of Spain located about 500 m above sea level. Figure 17 shows the study area in which this research was conducted.

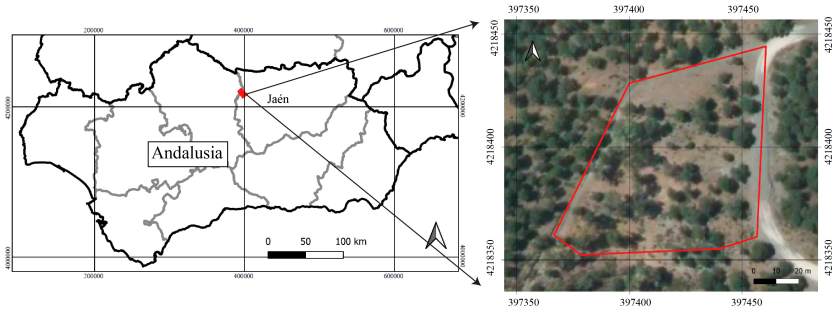

Figure 17 – Research area. The left image represents the south of Spain (Andalusia). The right image is the map of the observed forest in Jaén. The coordinates are UTM (zone 30) referred to ETRS89.

This region has a semi-continental climate with a mean annual temperature of 25.1, a mean relative humidity of 70% and a mean annual

precipitation of 1341 mm [109]. The study area is characterized by different tree species such as the oak, pine and eucalyptus as well as other Mediterranean shrubs. Moreover, the ground in this area has a concave shape with a slight slope. For the purpose of our research, we covered an area of 0.6 ha.

3.2.2 UAV-based and Field Data

The use of UAV in remote sensing provides the collection of heterogeneous data through optimal trajectories and a high detail level of the plant shape. In contrast to satellite images, the UAV-based acquisition process has a high versatility and provides multiple observations of target crops from different viewpoints. The morphological structure of trees is complex, with many self-hidden branches, which makes the observation of 3D structure more difficult.

In this research, a professional drone (model: DJI Matrice 210) was used to collect aerial imagery. On board the drone a high-resolution digital camera (model: X5s) and a multispectral sensor (model: Parrot Sequoia) were mounted. These devices were very different from each other. On the one side, a full-frame RGB camera took photos with 20.8 megapixels (MP), thereby observing the study area with a great spatial resolution. On the other side, the multispectral sensor captured the reflectance in four spectral bands: the near-infrared (NIR) from 770 nm to 810 nm, the red from 640 nm to 680 nm, the green from 530 nm to 570 nm and the red-edge (REG) from 730 nm to 740 nm. This device has a wide-angle lens with a focal length of 4 mm to cover more ground area in a single capture. However, a high visual deformation was presented in the image. In this way, the development of the canopy reflectance was monitored from every wavelength range in order to characterize the spectral behavior for each single tree. In addition, the Red and NIR bands were combined to calculate the Normalized Difference Vegetation Index (NDVI). It is a well-known spectral index applied in remote sensing to assess the green biomass, leaf cover and chlorophyll per unit ground area [75, 110].

An important aspect of the data collection process was to ensure an accurate geolocation and geometric quality. Therefore, it was necessary to design the distribution of Ground Control Points (GCPs). These are marked points on the ground that have a known geographic location of the whole area into a national grid and height datum. This network of points was used to georeference the images, and thus the point clouds were unified into the same reference system.

GCPs were measured on the center point of circular targets of 25 mm. These were covered with an aluminum foil to ensure a high contrast in RGB images and a full reflectance in multispectral images. The coordinates of GCPs network were obtained from a couple of Global Navigation Satellite System (GNSS) receivers (model: Topcon GR5) using Real-Time-Kinematic (RTK) technique. One receiver was set in a fixed point and a second one was used to measure every point in the field. The fixed point was located in a high place of the study area in order to avoid any possible interference. The reference frame was ETRS89 and the projection was Universal Transverse Mercator (UTM) zone 30, and the altitude was referred to the mean sea level data at Alicante (Spain).

Regarding the field data to measure the tree height and trunk diameter, these were taken using a Total Station (TS) (Model: Leica TCR 805 reflectorless). The TS is a surveying instrument which measures angles and distances using an electronic distance measurement (EDM). The angles and distances were measured by the TS, and the coordinates (X, Y, and Z; or east, north, and elevation) of surveyed points are relative to the TS. To get an absolute location it is necessary to know the absolute coordinates of the TS position (base station) and another reference point. A direct line of sight between the TS and the reference point is also required. For the first time, the TS have to be orientated, so we pointed to the reference point and then, to the target point. Moreover, the resulting coordinates were automatically transformed to our reference system. In this way, the coordinates of the 3D tree structure were measured.

3.3 Methods

In this research, some steps were developed from the acquisition of aerial images to the reflectance-based analysis of the 3D structures on individual trees. Figure 18 shows a diagram which summarizes the main sections of the proposed methodology. Initially, the RGB images were used to generate a dense point cloud which was geometrically corrected by the use of GCPs. Then, this 3D model was enriched using reflectance data, which described the plant response to incident sunlight. According to spatial and spectral features of the point cloud, a method for individual tree detection was proposed. Moreover, once every tree was segmented, the crown and trunk were identified and some structure-based features were extracted. Finally, our analysis was based on the study of the impact of the mean canopy reflectance on the 3D structure of trees. The proposed methodology for the extraction, processing and analyzing the studied tree parameters was implemented in C++ using Point Cloud Library (PCL) [111] and OpenCV [112].

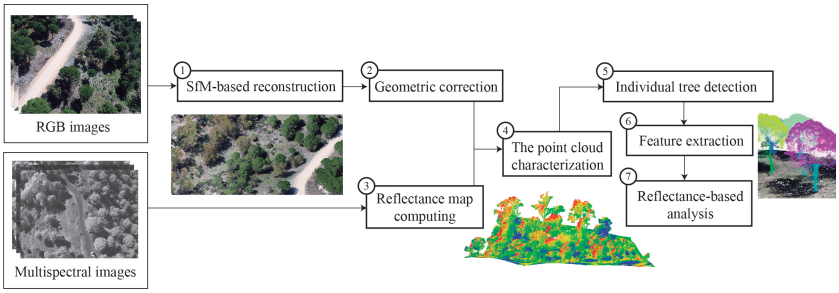

Figure 18 – The flow diagram of the proposed methodology.

3.3.1 UAV-based Acquisition

The use of UAVs for the observation of the 3D forest structure is a great opportunity to capture more detailed images with a higher spatial resolution than satellite images. Regarding the lighting conditions, the camera settings need to be determined by fixed values in order to avoid over- or under- exposed images. The photogrammetric results are highly influenced by the quality of input images. Therefore, sensors, settings and acquisition plans have to be considered to ensure optimal image data. Regarding the parameters of digital camera, the ISO was 100, the aperture was set to f/6.3 and exposition time was 1/500 s. This camera setting ensures the capture of sharp images without motion blur, which has negative impacts on the quality of photogrammetric reproduction. According to the multispectral sensor, these parameters were set by default (ISO: 100, f-number: 2.2 and exposure time: 1/5417).

In this research, one flight was performed in order to acquire a comprehensive observation of the tree geometry and reflectance. It was conducted close to the solar noon time in order to minimize the plant shadows and specular lighting. The time flight was 25 minutes. As mentioned before, a digital high-resolution camera and a multispectral sensor were mounted together on board the UAV during the flight. The spatial resolution of each sensor is different, so the flight plan must ensure that the the ground sampling distance (GSD) of both image sets is under 3 cm. Thus, the tree structure can be observed through a high spectral resolution. According to the specification of the multispectral sensor, which has the lowest image resolution, the flight height was set to 30 m. Regarding the flight path, a double grid was carried out to capture the tree structure from multiple viewpoints with a side and front overlap of 90%. Moreover, the capturing angle is another factor to take into account in any photogrammetric acquisition. In this case, the high-resolution RGB camera was mounted with an inclination of 60 Therefore, the lateral and

low branches of trees could be detected in the image and these were reconstructed on the 3D model. The multispectral sensor was oriented perpendicular to the ground (90 to ensure accurate measurements of canopy reflectance.

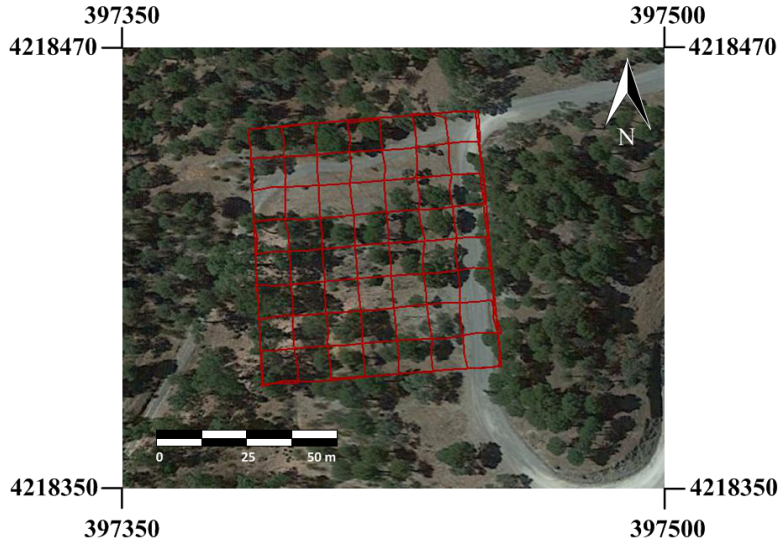

Figure 19 – The flight path in the study area (coordinates: UTM zone 30N referred to ETRS89).

3.3.2 Point Cloud Reconstruction

The observation of 3D forest structure by high-resolution cameras has been recently improved by the optimization of image-based methods. In this regard, the adoption of Structure from Motion (SfM) [8] is changing the acquisition of remote sensing data in forestry [7]. In contrast to other approaches based on LiDAR data [88], the application of SfM enables to collect the fit-for-purpose data to assess the single-tree architecture from multiple viewpoints. The potential of using UAVs and consumer-grade cameras for the 3D reconstruction is a great opportunity to observe the comprehensive development of a forest. In fact, there is increasing interest in UAV forest surveys which can arguably be attributed to photogrammetric processing [113].

SfM photogrammetry employs an automated process to identify and match key points between overlapping images. Therefore, the complex geometry of plants poses an important challenge to detect similarities in the image. To apply SfM photogrammetry in forestry, some relevant

aspects to obtain an accurate survey are as follows: (1) any feature to be reconstructed should be visible in at least three images, (2) the study area should be sufficiently illuminated, (3) the image scale should be 1/2 or 1/4 to recognize more key points. We have used Pix4D software to generate the dense point cloud and make the geometric corrections in the resulting 3D model.

Regarding the results of the SfM, the point cloud have to be corrected in order to ensure a correct position and scale. For this purpose, twenty-three GCPs were measured but only seven points were used for the georeferencing; the rest were used to validate the results. All these points were located on visible areas from the viewpoint of the aerial images captured. Therefore, we could achieve a centimeter accuracy in the study area, and the parameters of the tree structure were correctly measured. Finally, the dense point cloud was submitted to a noise filtering process in order to remove points around the tree shape, which were generated by the SfM method. In this case, we applied the Statistical Outlier Removal (SOR) algorithm, in which 100 neighbours were considered to calculate the distance between them and to remove the points that were farther than the average distance and the standard deviation. The left image in Figure 20 shows an example of an observed tree on the point cloud, which presents a high noise around the tree trunk. By applying the noise filter, these points are automatically removed as shown on the right in Figure 20.

Figure 20 – The point-based filter of a cutout of the point cloud. (**a**) The original dense point cloud, and (**b**) The filtered point cloud.

3.3.3 Reflectance Map Computing

Multispectral imaging provides image information in spectral as well as spatial domains. The surface bidirectional reflectance distribution

function (BRDF) measures the distribution of the reflected light by leaves, which is directly related to the tree growth. In this study, a multispectral sensor was used to measure the canopy reflectance of the observed forest area from multiple viewpoints. As mentioned before, this sensor is composed by four lenses to capture the reflected irradiance and a sunshine sensor to measure the incident irradiance. The resulting multispectral images provided an accurate measurement of reflectance in some specific narrow-bands of the electromagnetic spectrum. Firstly, in the near-infrared (NIR), the vegetation can easily be recognized due to the fact that this band is less sensitive to chlorophyll. Secondly, the Green and Red bands are very useful to study the reflected light by the tree canopy in the visible range. Finally, the REG band captures the reflectance between the Red and NIR and plays a key role detecting a key contrast from the visible to infrared light.

The capture of spectral reflectance can be influenced by several parameters such as changes of ambient light, the shutter speed, etc. Therefore, the multispectral images have to be radiometrically corrected by a calibration target. In our study, the spectral reflectance was calculated by measuring the incoming sunlight irradiance and reflected irradiance by the surface of the object captured. Equation 3.1 was used to estimate the reflectance value (R) for each pixel of every multispectral image.

$$R = K \left(\frac{\Phi_e^r}{\Phi_e^i} \right) \cos(\theta) \tag{3.1}$$

where K_i is the calibration coefficient of every band i, Φ_e^r is the radiant flux reflected by the object captured, Φ_e^i is the radiant flux incidence by the sun and θ is the angle between the direction vector of sun rays and direction vector of the sunshine sensor.

The incoming sunlight irradiance (Φ_e^i) was measured by the sunshine sensor, which was mounted on top of the acquisition system. This device was continuously capturing the lighting conditions during the acquisition process. Moreover, the angle between the sunshine sensor and the sunlight direction have to be taken into account to compensate the light reflection. A mean value of the incident light was estimated for each multispectral image. The mathematical formulation of this magnitude is defined in Equation 3.2.

$$\Phi_e^i = \frac{\nu}{g\tau} \tag{3.2}$$

where ν is a sensor count value, g is the relative gain factor and τ is the exposure time in seconds.

The next step was the calculation of the reflected irradiance (Φ_e^r) by using metadata (Exif) stored in the image. Every pixel $\mathbf{p}$ in the image $\mathbf{I}$ provided a reflected irradiance value, which was calculated by applying the Equation 3.3.

$$\Phi_e^r = f^2 \frac{\rho - B}{A\gamma\varepsilon + C} \tag{3.3}$$

where g is the f-number = 2.2, p is defined by pixel intensity, ε is the exposure time, γ is the ISO parameter = 100 and A, B and C are the calibration coefficients measured per camera in production.

Finally, the plant reflectance has to be radiometrically calibrated. Therefore, a calibration panel was used to calculate the calibration coefficient (K) regarding a known reflectance for every multispectral band. Three images were captured over this panel at different exposure levels. This process was carried out at the beginning and at the end of the acquisition process. Then, the Equation 3.4 was applied to calculate a calibration coefficient K for each observed band.

$$K_i = R_i \left(\frac{\Phi_e^i}{\Phi_e^r} \right) \tag{3.4}$$

where R_i is the known reflectance for each band i, Φ_e^i is the radiant flux incidence from the sunlight and Φ_e^r is the radiant flux reflected by the calibration panel.

Moreover, the reflectance values in the Red and NIR bands were combined to estimate the NDVI. This spectral index is widely used in remote sensing for the assessment of a plant health. Although this study is out of the scope of this work, the use of the NDVI is very interesting to identify the vegetation on the ground and study the tree vigor. As a result, reflectance and NDVI maps were obtained for each multispectral image and these were mapped on the point cloud to characterize it with meaningful spectral traits.

3.3.4 Point Cloud Characterization

In this section, we propose a variation of the method developed by Jurado et al. [15], which focuses on multispectral image mapping on 3D point clouds. Thus, the geometry can be enriched by spectral features in order to describe physiological properties of vegetation. The core of this method is the inverse 3D projection in order to calculate the pixels of multispectral images, in which 3D points of the cloud are directly visible. In this research, a variation of this method was applied, so the point cloud of our study area was characterized by the spectral reflectance from every observed narrow-band. Therefore, the reflected light by every single tree was measured and the key geometric changes on the 3D structure were detected.

Regarding the proposed optimization in this work, firstly, the point cloud was spatially indexed using an octree [82] in order to ensure a more efficient neighbour search in the visibility test. Secondly, the view frustum for each multispectral camera was calculated by considering four cutting-planes. The vertical field of view (VFOV) and the horizontal field of view (HFOV) were determined by the parameters of the multispectral sensor (VFOV: 48.5nd HFOV: 61.9. Consequently, only the points inside the volume of view frustum were considered to be projected in the image (Figure 21). Finally, a new approach was proposed to improve the efficiency of visibility test. In contrast to the occlusion detection on the point cloud by the creation of minimal triangulated surfaces, a distance-based matrix was used for each multispectral capture. Our method only enables one-to-one relationships so only one 3D point can be projected on one pixel. The size of this matrix was determined by the multispectral image resolution. For each pixel a distance from the projected 3D point and the camera position was saved. This matrix was updated in order to obtain for each cell the 3D point to be projected, which had the minimum distance to the position camera. As a result, the resolution of the point cloud was higher than multispectral images, so multiple 3D points were not characterized by any reflectance values. To overcome this problem, a k-nearest neighbour search (KNN) [81] was developed in order to assign the mean reflectance of the neighbours to unprojected points.

This process was an important step in the proposed methodology in order to characterize the geometry with meaningful data about the light competition in the study area. For each 3D point, we could determine the light which was reflected or absorbed in four multispectral bands. Undoubtedly, the mean canopy reflectance is a key factor which determines the development of a tree structure. Therefore, the next step was

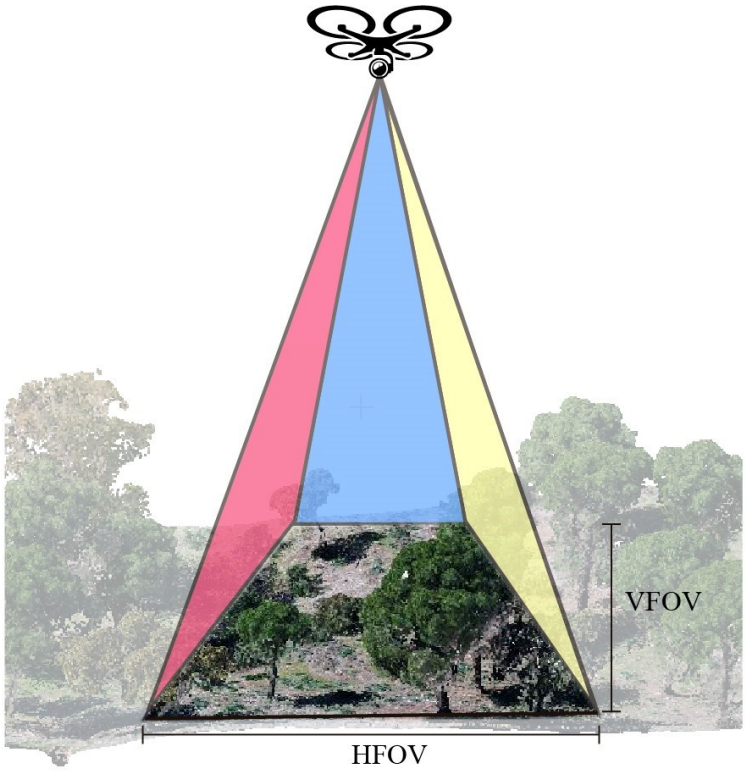

Figure 21 – The 3D space of the point cloud which is covered from a multispectral image.

to focus on the individual detection of single trees in the study area.

3.3.5 Individual Tree Detection

The segmentation of individual trees is a critical process for the assessment of the single-tree architecture. A variety of methods have been proposed to identify individual tree crowns based on raster images [114, 115]. However, our point-based approach directly uses spatial constraints on the point cloud rather than the raster images. The proposed method for the individual tree detection was divided in two steps: (1) the segmentation of individual tree crowns and (2) the tree trunk recognition.

The first step was the segmentation of the tree crown on the point cloud. The study scenario was characterized by a ground, which had

a concave shape and a significant slope to be considered, many shrubs around the trees and different tree species, which had heterogeneous crown shapes. The ground points could be discarded by using the spectral reflectance since these reflected a lower infrared light than vegetation points. However, the mean reflectance of low vegetation and tree crowns is similar, so trees cannot be clearly identified using only the multispectral features. In this regard, our method was based on the calculation of 3D cutting-planes oriented with the slope of the terrain in order to extract those points, which are in the tree crown. Figure 22 describes the experimental concept for the proposed method in the study area. Firstly, the 3D point with the minimum height (MIN point) was set. Then, a bounding box was calculated on the point cloud in order to determine the boundary ground points (p1, p2, p3 and p4) for each corner. Thus, four slope vectors were calculated by linking the two points with the maximum height (p2 and p4) to the minimum point and to the other boundary points (p1 and p3). As a result, two planes were created by considering the vectors $\vec{c}$ and $\vec{d}$ for the plane P1 as well as the vectors $\vec{a}$ and $\vec{b}$ for the plane P2. In the left image in Figure 22, the Digital Surface Model (DSM) is shown where the MIN point is detected in the green area, which depicts the lower height values. The planes P1 and P2 are also shown, which were determined by the vectors mentioned before. Moreover, in the image on the right, the same concept is described by depicting the cutting-planes on the point cloud from a 3D perspective. By applying this method, all 3D points under the cutting-planes were automatically discarded. Consequently, only the highest 3D points, which usually form the tree crown and the highest branches, were preserved for the identification of every individual tree.

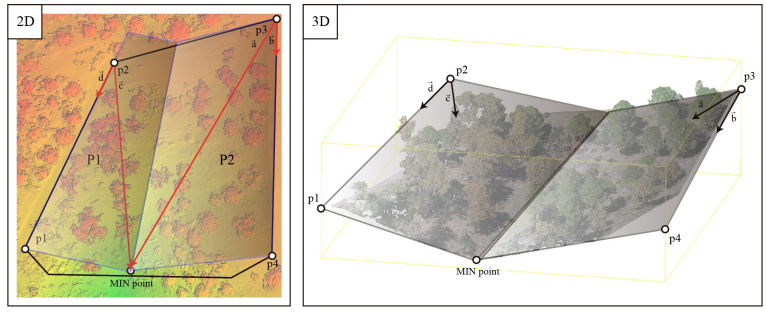

(a) (b)

Figure 22 – The ground removal determined by two cutting-planes (P1 and P2). (**a**) The representation of planes on the elevation map, and (**b**) The position and orientation of planes in 3D.

The segmentation for each tree crown is carried out following an ap-

proach based on spatial clustering. The algorithm proposed by Kanungo et al. [116] is applied in order to extract the tree crowns, which are spatially separated from each other. In the study area, by applying the noise removal on the point cloud, the minimum distance between every tree crown is at least 50 cm. The generation of every cluster is determined as follows: (1) the Euclidean distance between the 3D points must be lower than 50 cm (this value is proportional to the GSD of the dense point cloud) and (2) the angle between normal vectors cannot be wider than 180 The goal of these constraints is to ensure the correct definition of the growing region for each cluster. Thus, the tree crown is segmented by using only the spatial features of the 3D model.

Once the tree crown had been segmented, the final step was the detection of 3D points of the tree trunk in order to acquire a more detailed knowledge of the 3D tree structure. In this regard, the location of the tree crown centre for each tree can determine directly the position of the corresponding trunk for the X and Y axes. For this purpose, instead of calculating the average of coordinates for the points in the tree crown, we propose a novel method based on the creation of 3D alpha-shapes [117]. These geometric structures create a non-convex bounding volume, which envelops a set of 3D points. The vertices of the shape are determined by an alpha radius, which is set as 20 cm in order to produce the tightest fitting alpha shape, which encloses all points of the tree crown. Then, the centroid for each one is calculated and it is used as the seed point in order to search the 3D points points of the tree trunk. To this end, a clustering method was developed in order to detect 3D points, which share the following features: (1) a tolerance of 30 centimetres for the X and Y axes of centroid, (2) the location of points has to be above the 3D cutting planes (P1 and P2) and (3) points have not been considered as part of the tree crown. Figure 23 shows the example of the application of this method on a single tree in the study area. Thus, the trunk and main branches can be correctly identified in the tree.

Finally, an optimization method to improve the results of previous segmentation was developed. The KNN method was applied in order to correct those points which had been labeled wrong class (tree crown or trunk), if most of their neighbours did not share the same class. The search radius was set to 50 cm by considering the GSD of the point cloud and the impact on performance. Hence, the 3D tree structure for each tree could be divided into the trunk and crown.

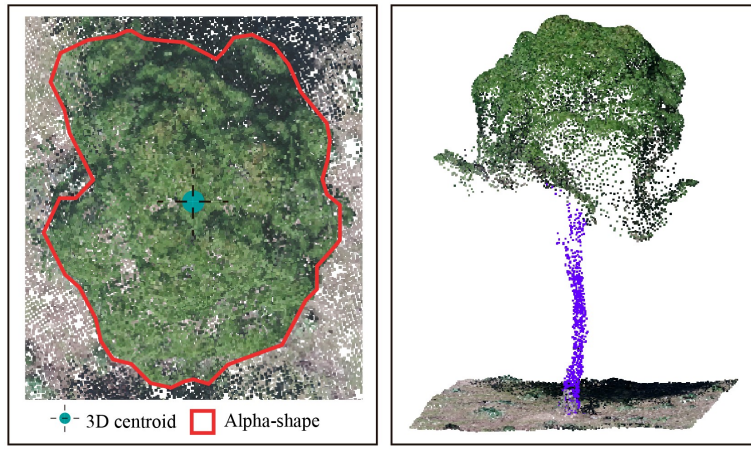

Figure 23 – The segmentation of the tree trunk. (**a**) The top view of the alpha-shape and centroid on the tree crown, and (**b**) The points labeled as the tree trunk.

3.3.6 Structural Feature Extraction

The accurate measurement of canopy architecture and tree crown parameters is critical for the assessment of photosynthesis and the energy transfer. In this study, reflection mapping on the 3D tree structure was used to find out meaningful relationships between the structural features of different tree species and the spectral reflectance, which were observed in the tree canopy.

According to the tree parameters, which were considered in our study, the tree height, the trunk diameter (DBH) and the crown volume were measured for each tree. Firstly, the tree height is a relevant feature which plays a key role in competition for light in the forest canopy. This value was measured by calculating the distance for the Z axis between the lowest point of the trunk and the highest point of the tree crown. Secondly, the trunk diameter was determined by the maximum distance between two points of the trunk at the same height. To this end, a bounding cylinder enveloping the points of the tree trunk, was created and the resulting diameter was considered the trunk diameter. Although the trunk of some trees was partially occluded by the tree crown, the shape of cylinder could be generated by using the visible points, so the lack of tree trunk points could be overcome without a significant negative impact on the calculation of the DBH. Finally, the crown volume is another relevant tree parameter which influences on the light absorption

and tree development. In this study, the space of the tree crown was decomposed by a 3D octree [118] with a spatial resolution of 25 cm. This data structure is based on a tree topology in which every internal node has exactly eight children. Hence, the tree crown was spatially divided by an octree in which a inclusion test was developed in order to check for each leaf node if it contains one 3D point at least. As a result, the crown volume was calculated by the sum of each voxel volume, which was occupied by some parts of the tree crown. These tree parameters were compared with field measurements to verify the accuracy of our methodology.

3.3.7 Reflectance-based Analysis

In this study, a novel methodology has been proposed to analyze the impact of the canopy reflectance on the 3D structure of individual trees. Once the tree parameters were extracted, a statistical analysis was developed to detect key relationships between the mean reflectance and structural parameters of the tree. Our research is focused on the observation of the 3D tree structure and reflected light by the tree canopy of three different tree species (pine, oak and eucalyptus). In the analysis process, the correlation between the studied tree parameters is approached. Regarding the impact of the mean canopy reflectance on the 3D tree structure, it is classified into three categories: (1) high, (2) medium and (3) low. Therefore, the impact of the canopy reflectance by considering tree species is analyzed. Table 7 shows a summary of all studied variables, which were considered for the analysis process.

Feature	Description
Spectra	
Green	The highest plant reflectance of the visible range.
Red	Healthy plants present a high absorption of red light.
NIR	It is the least sensitive band to chlorophyll.
REG	This band is relevant for the assessment of plant stress.
NDVI	It is used for tracking the health of vegetation.
Morphology	
Tree height	Vertical distance from the tree base to the highest point.
DBH	The diameter of the trunk of tree.
Crown volume	The 3D space occupied by the tree crown.

Table 7 – A summary of the studied characteristics for each tree structure.

3.3.8 Validation Process

This section describes the process of determining the geometric quality of the 3D reconstruction. The aim is to validate the 3D model in order to carry out all measurements on the tree structure. On the one hand, a validation of the model scale was carried out using the ground points for georeferencing. On the other hand, field data were acquired in order to measure the quality of the measurements taken on the point cloud like the tree height and tree trunk.

Figure 24 – Field measurements of structural parameters of trees. (**a**) The target tree, (**b**) The manually marking of the lowest point of the tree trunk, (**c**) Leica TCR-805 (TS), and (**d**) The view of the pointing to the pin on each side of the trunk.

3.3.8.1 GNSS Measurements

The use of measurements with the GNSS receiver to give exact coordinates of the points used for the correct geolocation of the images captured with the UAV has already been explained. Furthermore, these points allow us to analyze the geometric quality of the model in terms of preserving scale. The cross validation method was used to evaluate the quality of the scale of the model during the creation of a 3D construction from multispectral images. A set of random points was selected to perform the validation, the rest were used for georeferencing. Then, the quality of the 3D model scale was validated using the root-mean-square error (RMSE), which was calculated for the X and Y axes (Equation 3.5) and the Z axis (Equation 3.6).

$$RMSE_{X,Y} = \sqrt{\frac{1}{n}\Sigma_{i=1}^{n}\Big(X_i - X_{i,GNSS}\Big)^2 + \Big(Y_i - Y_{i,GNSS}\Big)^2} \quad (3.5)$$

$$RMSE_Z = \sqrt{\frac{1}{n}\Sigma_{i=1}^{n}\Big(Z_i - Z_{i,GNSS}\Big)^2} \tag{3.6}$$

where: $X_{i,ref}$, $Y_{i,ref}$ and $Z_{i,ref}$ are the coordinates of the 3D point measured by the GNSS and X_i, Y_i or Z_i are the coordinates of point i of the point cloud.

3.3.8.2 Total Station Measurements

As stated above, the georeferencing of UAV images was carried out from a GNSS receiver in RTK mode. In this work, the tree structure was characterized by field data, which were collected on the tree trunk and the highest branches of the tree crown, to determine the tree height and trunk diameter. These measurements were taken using a TS, Figure 24**c**. According to its manufacturer's manual specifications it has an accuracy of 3 mm ± 2 ppm using a reflectorless for the estimation of the distance and 1.5 mgon for angular measurements. To achieve this accuracy in field data acquisition, some visible marks were fixed on the tree structure in order ensure a high accuracy in the geometric validation. Therefore, some pins with a rounded end (5 mm of diameter) were placed on each side of the tree trunk, Figure 24a and Figure 24d. The lowest point of the tree trunk was measured using a pole, which was set on the base of tree, Figure 24b.

3.4 Results

The forest structure was modeled using multiple UAV-based images, which were captured by a high-resolution camera and a multispectral sensor. In this study, the SfM method was applied to generate a dense point cloud in the study area. For this process, only RGB images were used because these had a greater spatial resolution than multispectral images. Regarding the quality of the 3D reconstruction, the GSD was 1.09 cm, the number of points per cubic meter was 2039.27 and the size of the point cloud was 3.395.368. As a result, the crown, trunk and main branches of the tree structure could be correctly modeled. In addition, the noisy points around the trees were filtered, thereby, 259.194 points of the 3D model were automatically removed.

Once the comprehensive 3D structure of the forest was created and processed, it was enriched by multispectral features. Thus, useful study was carried out to analyze a wide variety of ecosystem functions and the impact of canopy reflectance on structural parameters of trees. In this

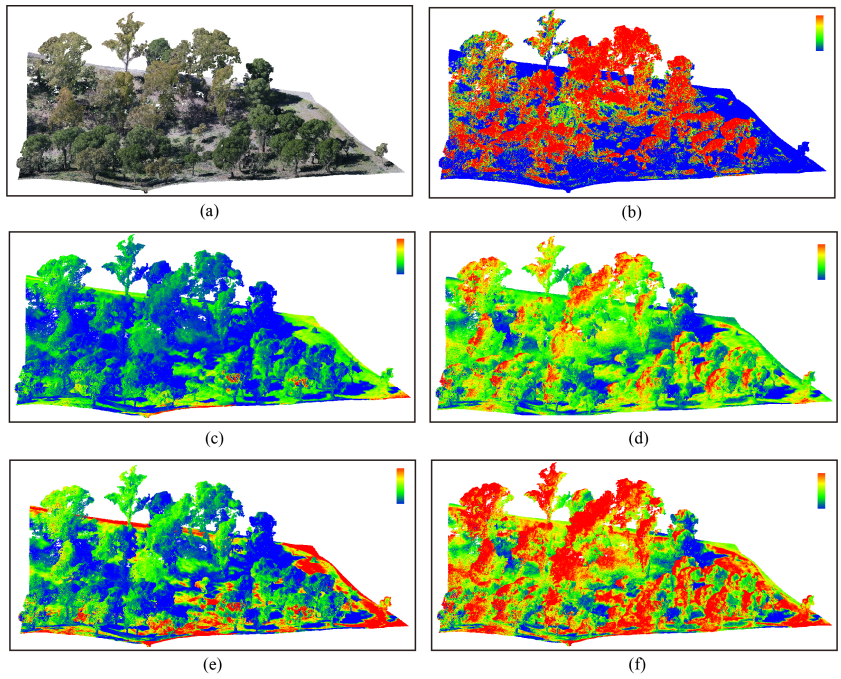

Figure 25 – The 3D forest models. (**a**) The RGB point cloud, (**b**) The point cloud of Green band, (**c**) The point cloud of NIR band, (**d**) The point cloud of Red band, (**e**) The point cloud of REG band, and (**f**) The NDVI point cloud.

work, we focused on the relationship between the tree structure and the spectral response in the tree canopy. Figure 25 shows the results of the point cloud reconstruction as well as the spectral models, which contain the mean reflectance per point in the Red, Green, NIR and REG bands. Moreover, the NDVI point cloud is shown in order to review the overall status of the trees in the study area.

3.4.1 Forest Inventory

To ensure a detailed forest inventory, a spatial clustering was developed in order to detect individual trees in the study area. In addition, the tree structure was segmented by the trunk and crown. The segmented model is shown in Figure 26. As a result, 43 trees were automatically identified in the point cloud. Then, these were manually labeled according to their corresponding tree species. In summary, 10 eucalyptus trees, 7 oak trees and 26 pine trees were identified. Therefore, a detailed analysis of the spectral and structural parameters for each individual tree

was performed and compared with different tree species.

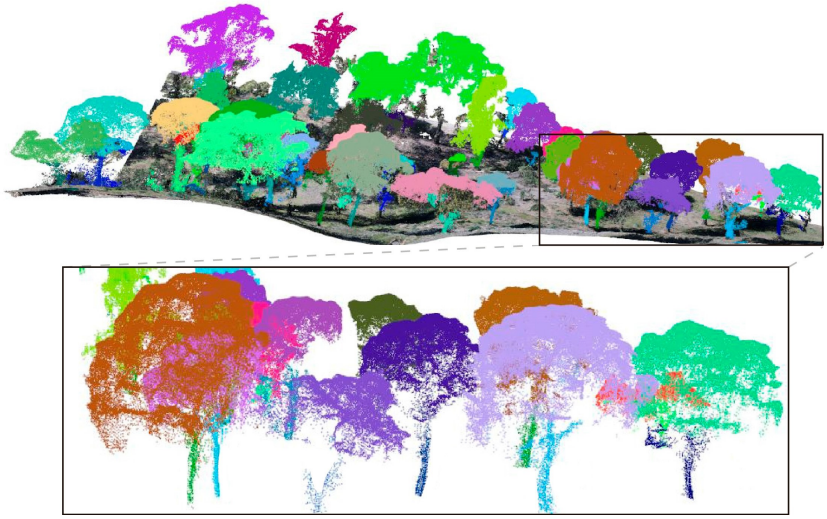

Figure 26 – The segmentation of individual trees and the recognition of the crown and trunk for each tree.

Regarding the performance of methods, which were adopted for processing of data in the study area (0.6 ha), the hardware specifications are: Intel Xeon(R) W-2145 (CPU), 64 GB (RAM) and GeForce RTX 2070 (GPU). The 3D reconstruction was the most computationally expensive process, whose execution time was 3 hours and 20 minutes. The time required to map every multispectral image on 3D model (3.136.174 points) was 0.64 seconds, thus the total time for all images was 14 minutes and 76 seconds. Finally, the processing time for the recognition of individual trees as well as the crown and trunk segmentation for each tree was 5.82 seconds.

3.4.2 Analysis of Tree Parameters

Structural and spectral parameters were automatically measured on the point cloud in order to characterize the 3D shape and the spectral behaviour for single-trees. Regarding the heterogeneity of the forest extension, which was observed in this research, the tree parameters were analyzed by distinguishing the tree species.

Figure 27 shows four boxplots, which depict the variability of studied features for each tree species. According to the structure-based parameters, the eucalyptus tree is characterized by having the highest crown

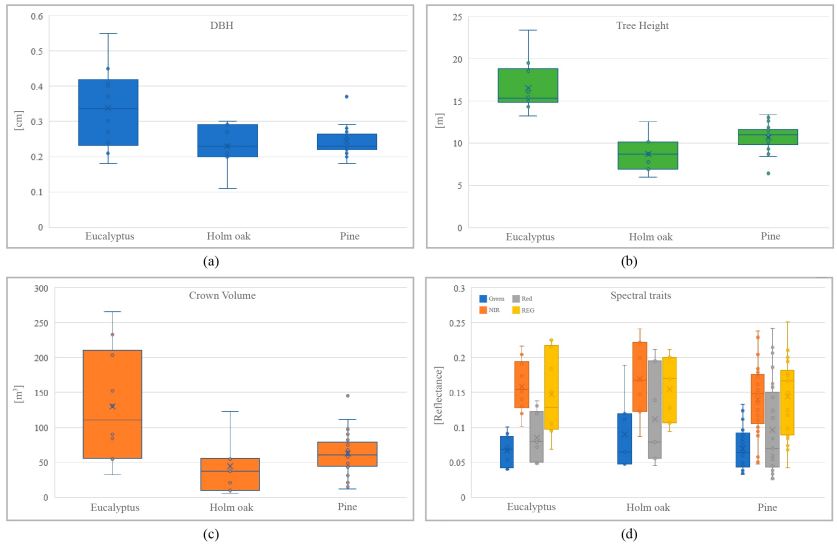

Figure 27 – Tree parameters for each species. (**a**) The diameter breast height, (**b**) The tree height, (**c**) The crown volume, and (**d**) The spectral reflectance.

volume, height and DBH. The mean values are 110.81 m^3, 16.56 m and 0.33 cm respectively. Then, the DBH of pines and oaks is very similar, as close as 0.235 cm. However, pines have higher mean values of tree height and crown volume (10.68 m, 62.57 m^3,) than oaks (8.70 m, 37.12 m^3). According to the mean reflectance, which was measured for each multispectral band, some significant variations can be observed in Figure 27d. Firstly, the eucalyptus reflects the highest quantity of incident sunlight in the REG band and absorbs most of light in the visible range (green and red). Secondly, oaks have the mean highest reflectance in the NIR and REG bands. Moreover, this type of tree is characterized with the highest reflectance in the Red band. Finally, pines have a high absorption in the Green band and the highest reflectance values are observed in the NIR and REG bands. Generally, pines absorb most of green light and heterogeneous reflectance values are detected in the Red band. The cause of these fluctuations are discussed in Section 3.5.

Once the tree parameters were described, the impact of the mean reflectance for each tree species was studied. Regarding Figure 28, a normalization of the studied measurements was carried out, using the Napierian logarithm, in order to study the correlations between them. Regarding the most meaningful relationships between the tree geometry and the canopy reflectance, the crown volume was the structural parameter, which was more closely related to the light reflection or absorption.

Moreover, the height of trees was directly proportional to the canopy reflectance because the highest tree were not under shadows of surrounding trees. Consequently, if the tree height and crown volume increased, the mean reflectance on the tree canopy was higher too. Nevertheless, critical changes were observed on some specific trees, which did not follow this trend. Those were produced by some anomalies in the tree-based functions whose analysis is out of scope of this work. According to the NDVI values, no significant changes were detected between different tree species. They were slightly higher in the canopy of pines (0.64 as average) and they decreased in the canopy of oaks (0.59). By applying the previous analysis, it has been demonstrated that reflectance is directly related to the 3D tree structure. Therefore, our results can be used to assess the biodiversity in a forest as well as detect critical changes of reflectance and structure on single trees.

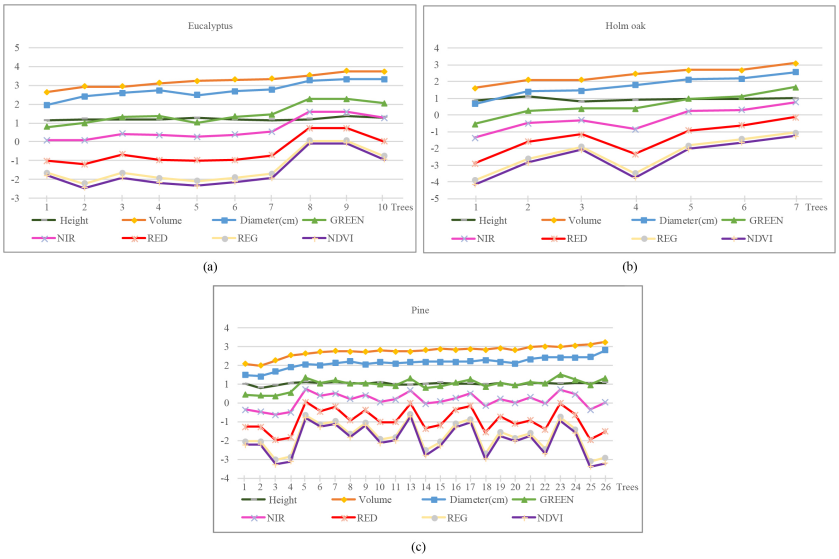

Figure 28 – The distribution of structural and spectral features of trees organized by species. (**a**) Eucalyptus, (**b**) Holm oak, and (**c**) Pine.

3.4.3 Geometry accuracy

The geometric quality of the generated model was analyzed from different points of view. Firstly, the quality of the point cloud was evaluated in terms of preserving the scale, namely, the accuracy of distances measured on the model in any direction. To carry out this analysis, as mentioned in Section 3.3.8, the cross-validation method was applied.

Figure 29 shows a correlation between the geometric quality in the horizontal and vertical direction.

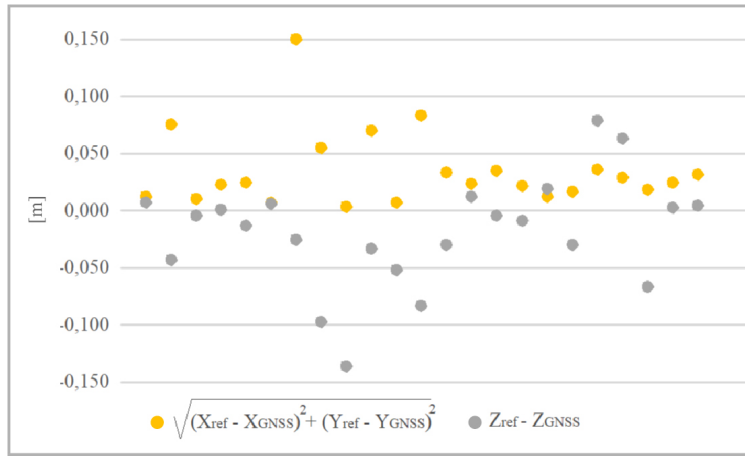

Figure 29 – Differences (m) of GCPs between the coordinates measured with GNSS and those obtained on the point cloud.

In general, the variations between planimetric and altimetric coordinates for each point were very similar. In this regard, the sharpness with which the GCPs were identified in the model was a very important factor. These results demonstrate a high accuracy in the X, Y (RMSE: 0.048 m) and Z (RMSE: 0.050 m) on the point cloud. Consequently, it is feasible to make measurements on the model in both, horizontal and vertical directions, obtaining geometric magnitudes of adequate quality.

Secondly, the assessment of the geometry accuracy was based on the validation of the estimated measurements on the point cloud. For this purpose, the field data acquired by the TS were used to study the mean error for the estimation of the height and DBH. Figure 30 correlates the SfM-derived and field-measured tree heights and trunk diameters for the correctly-detected trees (43 samples). A linear regression is used to fit the lines (marked in blue) and to study the dispersion for each dataset. The tree height measurements on the point cloud (green points) are on the line because the mean error is very low (4 cm) by considering the magnitude of the measure (m). According to the measurements of DBH, a higher accuracy is required because the distances are much lower. Regarding the mean DBH error by the estimation on the point cloud, it was 2.5 cm.

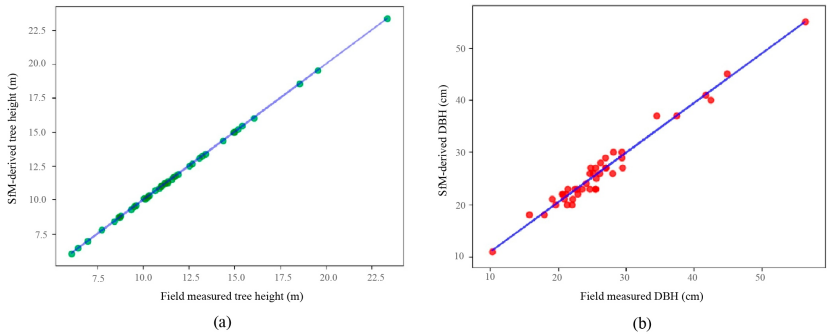

Figure 30 – Field measures with the TS and estimated values on the SfM-based point cloud. (**a**) Tree height, and (**b**) Trunk diameter (DBH).

3.5 Discussion

This paper addressed the methodology of SfM-based remote sensing for individual tree-level forest inventory and the impact-based analysis of canopy reflectance on the 3D tree structure. The study area was researched by using multispectral and high-resolution RGB images. In our previous work, we developed a method for the multispectral image mapping on point clouds [15]. In this research, the proposed methods for the segmentation of trees, the crown and trunk recognition and the characterization of the 3D tree structure went one step further than the existing scheme, by considering different species and more structural parameters of trees.

In order to achieve a comprehensive knowledge of the tree parameters, a novel method was proposed for the detection of individual trees in forest as well as the crown and trunk segmentation on the 3D tree structure. Traditionally, clustering algorithms based on k-means have been used for this purpose. Nevertheless, the pre-defined value of k is one the most important drawbacks because the number of trees in the study area is unknown. To overcome this problem, various CHM-based methods were proposed using LiDAR data or satellite images in order to detect the treetops [119, 120]. In this study, we used the original point cloud rather than rasterized images. It is generally acknowledged that the point-based methods outperform CHM-based approaches [121]. Moreover, we proposed a method for the recognition of the tree on photogrammetric point clouds. Regarding the results, Figure 26 shows that every tree was automatically detected in the point cloud and the tree structure was divided into the crown and trunk. Therefore, tree parameters were extracted such as the tree height, the crown volume and

the trunk diameter (DBH). By considering the tree crown and trunk as single clusters for each tree, we were able to measure the mentioned parameters and characterize the 3D tree structure in large forest stands.

According to the spectral features, the reflected light in the Green and Red bands is often influenced by the leaf chlorophyll content. In fact, the mean reflectance in these bands was lower than in others due to the fact that visible light was highly absorbed by leaves. In the NIR and REG bands, the forest foliage had a higher reflectance owing to the fact that these wavelengths were slightly influenced by chlorophyll pigments. Regarding the spectral response for each tree species, Figure 28 summarizes the variability of the spectral values measured on the tree canopy in every multispectral band. The eucalyptus had the highest absorption in the Red and Green bands (the visible range), so the mean reflectance was close to 15%. The pine had the highest mean reflectance in these bands as well as in the NIR and REG bands. The oak trees presented a higher reflectance in visible bands than the eucalyptus, but a lower reflected light in the NIR and REG bands than the pine. Finally, the highest values of NDVI were detected in the upper canopy of eucalyptus due to the high contrast between the NIR and Red bands.

Regarding the analysis of individual trees, the pine and oak had a high fluctuation in the NDVI, Red and REG bands. On the one hand, one oak was characterized by a more dispersed branching structure so the mean reflectance was significantly low. On the other hand, the variation of reflectance in these bands was determined by the shadow effects, which had an important impact in the Green and Red bands. The results of the analysis by fusing structural and spectral features for each tree of different species showed some meaningful conclusions. The eucalyptus and oak species generally presented higher values of infrared reflectance on trees which had a higher crown volume and height. Specifically, the eucalyptus showed a relevant increase of reflectance when the crown volume was higher than 130 m^3. Regarding the variation of the reflectance of Holm oak, these trees showed a homogeneous increase of the spectral reflectance as the tree size. Nevertheless, only one of them did not follow this trend in the Red and REG bands, as mentioned before. Finally, the spectral responses of the observed pines are the most irregular. The lowest values of reflected light in the infrared bands were not directly related to a lower crown volume or tree height. Multiple pine trees presented a significant decrease of reflected light in the NDVI, Red and REG bands despite their crown volumes were greater than the rest of trees. These critical changes could have been produced by the internal shadow between branches in the tree canopy. A further research will be developed to clarify the main causes of these fluctuations on pines.

Finally, regarding the quality of the geometry of the model, it is important to highlight that the accuracy of the GNSS and TS measurements were higher than the measurements estimated on the point cloud; therefore the procedure applied was feasible to validate the geometric quality of the point cloud. Results showed a high accuracy for the estimation of the tree height and DBH. In summary, the proposed framework can be used for assessing the biodiversity and green capacity of the forest, which is high demanded research in remote sensing.

3.6 Conclusions

This study was focused on mapping and analyzing the spectral reflectance on the 3D structure of individual trees. For the purpose of our research, a Mediterranean forest, where different tree species coexist, was researched using UAV-based sensors (a digital RGB camera and a multispectral sensor). By applying the SfM method, a dense point cloud was generated with a high spatial resolution (GSD: 1.09 cm). Then, the point cloud was characterized by the spectral reflectance from many multispectral observations. One of the main contributions of this work is the semantic segmentation of the point cloud. A spatial clustering was carried out in order to identify every single tree. Then, a fully automatic method was proposed for the recognition of the tree trunk. As a result, 43 trees were correctly identified, and thus the spectral and structural measurements were obtained for each individual tree.

In this research, every single-tree architecture was analyzed by considering the incident sunlight on the tree canopy and its influence on structural parameters such as the tree height, trunk diameter and the crown volume. Regarding the shape and spectral response of each tree, meaningful relationships were determined between the 3D structure and the mean reflectance in the canopy. In general, trees with a higher crown volume and height generally had a higher reflectance in the near infrared range and a strong absorption in the visible range. Nevertheless, some critical changes were observed between the studied tree species. The shadow effect played a key role on the oak trees, which had a lower height. We have concluded that by applying the proposed methodology, researchers can inspect single-trees using the 3D canvas of our tool and observe the spectral reflectance in the tree canopy. The main novelties of this research were the fusion and analysis of spectral and structural features of individual trees as well as the development of methodological advancements of describing competition for light and its impact on the 3D tree structure.

Several open problems can be subject of further research. Regarding

the obtained features about the morphology and spectral response of each tree, we will focus on using neural networks for the recognition of real materials in natural environments. In addition, we would like to accelerate the process for the multispectral image mapping on the point cloud using a GPU-based approach. Finally, the application of this data model for a fully automatic classification of tree species is an interesting topic to approach in the future.

Part III

Semantic segmentation of point clouds

This part is devoted to the segmentation of 3D models. The first chapter presents the proposed method for the recognition of similar materials using a 3D model enriched with multispectral data. The second chapter describes the algorithm for the detection of every grapevine and missing plants in point clouds of vineyards.

4 Semantic Segmentation of Natural Materials on a Point Cloud Using Spatial and Multispectral Features

About this chapter

The work presented in this chapter has been published in the journal *Sensors*. This research is focused on fusing spatial and multispectral characteristics for the unsupervised classification of natural materials in a 3D point cloud. While I led the line of work (under the supervision of Francisco R. Feito and Lidia Ortega), José Luis Cárdenas and Carlos Ogayar participated in the qualitative validation and accuracy assessment of the proposed method.

J.M. Jurado, J.L. Cárdenas, C.J. Ogayar, L. Ortega, and F.R. Feito.
Accurate Plant Modeling based on the Real Light Incidence
Proc. of the International Conference on Computer Graphics Theory and Applications (GRAPP), p. 360, Feb. 2019.

J.M. Jurado, J.L. Cárdenas, C.J. Ogayar, L. Ortega, and F.R. Feito.
Semantic Segmentation of Natural Materials on a Point Cloud Using Spatial and Multispectral Features
Sensors, Vol. 20, no. 8, p. 2244, Apr. 2020.

4.1 Introduction

The precise observation of three-dimensional (3D) natural spaces is a research line in which many recent works have proposed novel solutions with a high impact in the science of materials and remote sensing [122]. The emergence of a wide variety of sensors makes it possible to develop detailed studies about the recognition of meaningful features of every entity in nature. In an ecosystem there are many living organisms and nonliving objects, which are influenced by several environmental effects. The characterization of this scenario by the 3D reconstruction of plants, rocks or trees, as well as the capture of light interactions between them play a key role to gather comprehensive data of the environmental sustainability. However, nature tends to be chaotic and the recognition of all existing entities in a natural space is not a trivial task. These objects usually present a similar appearance in the visible range and can be occluded by some overlapping structures. In this work, we focus on the

extraction and fusion of spectral and spatial properties of a real-life scenario for the semantic segmentation of some natural entities, which are characterized by different materials. Many remote sensing application and monitoring tasks will benefit from having access to the proposed method for the material segmentation in a natural environment. For instance, the creation of a forest inventory, the object recognition to study the ground composition, the survival of a plant species or the impact of environmental pollution may use the proposed material-based segmentation in this research.

The modeling of 3D structures in natural scenarios has been improved through the proposal of recent approaches based on different techniques such as RaDAR [123], Light Detection and Ranging (LiDAR) [124] or structure-from-motion (SfM) [125]. Regarding the improvement of the camera resolution, the use of image-based methods for 3D reconstruction has increased because these are based on a more cost-effective solution than costly LiDAR systems. The potential of close-range photogrammetry (CRP) to produce dense and accurate point clouds has increased in recent years [126, 127]. The resulting 3D models have sufficient geometric details to depict the 3D shape of objects captured. SfM-based [19] methods enable the creation of geometrically precise point cloud datasets based entirely on large sets of overlapping images taken from multiple viewpoints. Recent research has been presented for the 3D reconstruction of urban and natural environments by using conventional cameras [128, 129]. Instead of managing a triangular mesh, which requires an additional computational cost, the point clouds are widely used to provide an accurate representation of existing objects in nature. This geometric characterization is a great opportunity to extract morphological features and to discover the spatial distribution of every entity in this complex scenario. The use of 3D models instead of the image segmentation of materials is one of the contributions of this work. However, the semantic recognition among homogeneous materials in vegetation areas, where many structures also present a similar shape, is challenging. In addition to the use of spatial features and the visual appearance to classify different natural materials, the multispectral sensors provide extra channels to measure the lighting interactions between every entity of the environment.

Multispectral imaging provides meaningful features to differentiate similar materials whose reflectance significantly changes in a specific narrow band [130]. Lighting is one of the most important factors to study the visual appearance of materials. The observation of the object reflectance by multispectral images is a key technique to model the physical process of light interacting with materials [131]. Moreover, the

multispectral images have been used for the shadow removal in urban spaces [132] and image segmentation of materials [133, 134]. In the field of computer vision, some previous works propose different approaches for plant phenotyping considering the spectral response [135], the recognition of different geological formations using a multispectral camera [136] and the detection of urban materials [137, 138]. Other recent approaches have proposed a semantic classification of urban spaces by applying neural networks [139, 140] or using LiDAR data and a clustering approach [141]. Furthermore, the use of deep learning techniques for unsupervised scenarios is a promising research [142, 143]. The automatic recognition of homogeneous materials in a natural space, which contains a high diversity of objects, is one of the fundamental problems of computer vision. This issue is posed in this paper by observing the spectral reflectance on the 3D structure of the studied scenario.

The acquisition of multispectral images is useful to get a comprehensive knowledge of light interactions in natural environments. Recent methods propose solutions using hyperspectral, multispectral and thermal images for the environmental understanding. The merge of geometric properties with other data types like the spectral reflectance reveal some feature patterns, which cannot be easily detected in the visible range. Several studies have proposed different solutions by considering heterogeneous image datasets to extract a comprehensive knowledge of the development of ecosystems. Nevalainen et al. [61] used hyperspectral imaging for an individual tree detection with UAV-based photogrammetric point clouds and Degerickx et al. [3] provided an urban tree health assessment using airborne hyperspectral and LiDAR imagery.

The proposed method aims to extract different types of materials from a 3D model of nature. The study scenario is characterized by the homogeneity of materials, so it is difficult to differentiate them. Our approach is based on the characterization of the 3D model geometry with multispectral data for the semantic segmentation of materials. Therefore, high resolution RGB images and multispectral images have been taken at the same time. Both sensors have been integrated into the same system designed by our team.

This article is structured as follows: Section 4.2 describes the study scenario and the main methods used for data acquisition, fusing and segmentation. In Section 4.4, the results are presented and discussed. Finally, Section 4.6 presents the main conclusions and further research.

4.2 Materials and Methods

The study area characterization, the description of the used sensors and the methods applied to acquire, process, and identify the target materials in the studied natural space are presented in this section. The methodology is based on three main stages: (1) multispectral image mapping on the point cloud, (2) feature extraction and (3) semantic segmentation. Figure 31 presents the main steps of the proposed methodology.

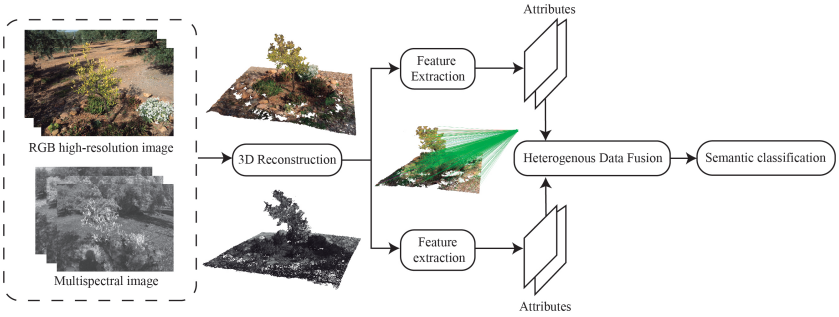

Figure 31 – The flow diagram of the proposed methodology.

4.2.1 The Surveyed Area and Acquisition Process

In this work, we focus on a reduced real-life environment which has been modeled with high detailed geometry. This scenario is characterized by a tree, low vegetation of different species, flowering plants, rocks and rocky ground. Our goal is to identify singular materials in the natural space, which determine a different appearance of the existing entities. Initially, we do not have any previous knowledge about the objects captured in the scene.

According to the acquisition process, a high-resolution RGB camera and a multispectral sensor have been used to capture multiple overlapping images of the studied scenario. Moreover, an Inertial Measurement Unit (IMU) and a Global Positioning System (GPS) is used for georeferencing the RGB images and getting a more accurate 3D reconstruction. Firstly, the full-frame RGB camera (model: Sony Alpha 7 RIII) takes images with 48 megapixels, thereby observing the target scene by a high spatial resolution. These images are georeferenced by using an external IMU/GPS to determine the position and orientation of the camera. Moreover, the external parameters of the camera are set before the acquisition process in order to ensure a correct capture from all viewpoints

(ISO: 100, exposure time: 1/200 and f-number: 8). Secondly, the multispectral sensor (model: Parrot Sequoia) is composed by four lenses in order to capture the reflected radiation on different wavelengths and a sunshine sensor to correct the irradiance incident on the study area. Consequently, for each capture four multispectral images are taken. The observed spectral range is the near-infrared (NIR) from 770 nm to 810 nm, red (640 nm - 680 nm), green (530 nm - 570 nm) and red-edge (REG) from 730nm to 740nm. The multispectral images (1.2 megapixels) present a lower resolution than RGB images and higher geometric distortion due to the wide-angle lenses with a focal length of 4mm. The position and orientation of every image is determined by the GPS and IMU, which take part of the multispectral sensor. Figure 32 shows the observed RGB and multispectral bands in the surveyed scenario.

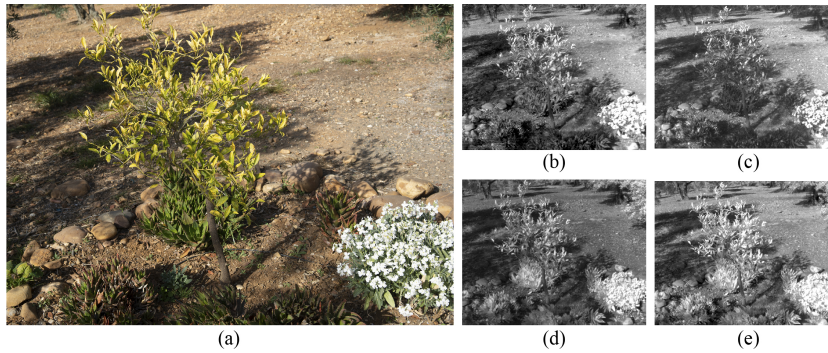

Figure 32 – The captured images: (**a**) RGB image, (**b**) green, (**c**) red, (**d**) NIR, and (**e**) REG.

The integration of sensors, described above, is required for a simultaneous capture of high-resolution RGB and multispectral images. For this purpose, a specific object has been produced by 3D printing in order to create a custom camera rig (Figure 33). As a result, the high-resolution camera and the external GPS/IMU, as well as the multispectral sensor can be used together to model the 3D structure of the target scene and to observe the reflectance response of every object of the scene captured.

According to the proposed acquisition system, multiple overlapping images have been taken by the RGB camera and the multispectral sensor around the study scenario. On the one hand, 82 RGB images are capture by the high-resolution camera. On the other hand, 82 captures are taken by the multispectral sensor and for each one four spectral bands are observed, so 328 multispectral images are acquired. The overlap between all images is 85% in order to get detailed geometry with a high spatial resolution.

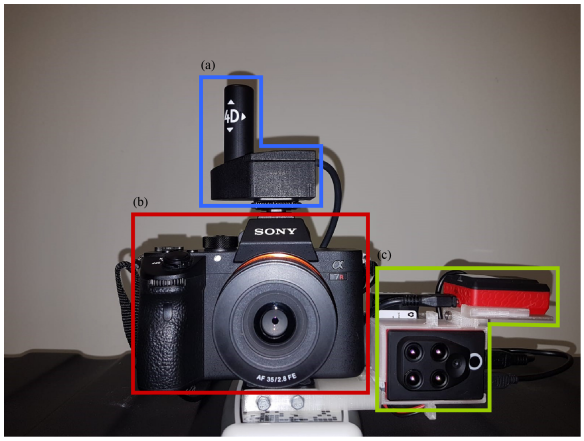

Figure 33 – The acquisition system: (**a**) the IMU and GPS, (**b**) the high-resolution camera, and (**c**) the multispectral sensor.

4.2.2 3D Reconstruction

The 3D modeling of natural environments is not a simple task due to the high complexity of the plant structures and the high occlusion between every object. In nature, many entities are usually overlapped in the same space. Therefore, the correct reconstruction of this type of scenarios requires some considerations. The SfM relies on visual similarities between overlapping images to reconstruct the model. The vegetation has a complex geometry (multiple branches and leaves), which is why it is more difficult to find enough similarities between overlapping images and many images cannot be correctly calibrated. Consequently, it is recommended to set a high overlap between the captured images (upper than 70%) and reduce the image scale on 1/2 for the search of key points in the image.

In this work, the photogrammetric processing is applied through the application of the SfM algorithm [144]. It is an open-source method, which can detect the same regions of overlapping images, determine their geometric relationships and infer the rigid scene structure (point set) with the pose (position and orientation) of all cameras. The resulting 3D structures are modeled as a point cloud instead of a 3D mesh due to the fact that many complex geometric objects cannot be correctly triangulated. Consequently, only the point cloud is the comprehensive 3D model of the study scenario for the extraction of different existing materials. As a result, two point clouds are generated by using RGB and multispectral images. The RGB point cloud has a higher spatial

resolution and the Ground Sampling Distance (GSD) is 0.07 cm. The size of the densified point cloud is 8,394,979. Otherwise, the quality of multispectral images is worse than RGB images due to high geometric distortion and lower image resolution. Consequently, the GSD of the resulting point cloud is 0.97 cm. This temporary point cloud is only used for the data alignment and thus, the initial pose of multispectral cameras is corrected by mapping them on the RGB point cloud. This process is explained in Section 4.2.4.

4.2.3 Multispectral Image Processing

Multispectral imaging provides image information in spectral as well as spatial domains. As mentioned before, various methods have been presented to study the reflectance properties for each natural material by considering different lighting conditions. In natural environments there are similar materials, which characterize different entities. The physiological properties of vegetation play a significant role in the material appearance [145]. The surface bidirectional reflectance distribution function (BRDF) measures the distribution of the reflected light by leaves, which is directly determined by the plant status. Therefore, the mean reflectance of an object is a key feature to find out its corresponding material.

In this work, a multispectral sensor is used to measure the spectral reflectance in a real-life scenario from multiple viewpoints. As mentioned before, this sensor is composed by a camera, which captures the reflected irradiance, and a sunshine sensor, which takes the incident irradiance. The resulting multispectral images provides an accurate measurement of reflectance in some specific narrow-band. Firstly, in the near-infrared (NIR), the vegetation can be easily recognized due to that fact that this band is less sensitive to chlorophyll. Secondly, the green and red bands are very useful to classify similar natural materials according to the light absorption in the visible range. Finally, the REG band captures the reflectance between the red and NIR, so it plays a key role to detect a key contrast from the visible to infrared light.

The capturing spectral reflectance is influenced by several parameters such as changes of ambient light, the shutter speed, etc. Therefore, the multispectral images have to be radiometrically corrected by a calibration target. In our study, the spectral reflectance is calculated by measuring the incoming sunlight irradiance and reflected irradiance by the surface of the object captured. Equation 4.1 is used to estimate the reflectance value of every pixel for each multispectral image.

$$R = K \left(\frac{\Phi_e^r}{\Phi_e^i} \right) \cos(\theta) \tag{4.1}$$

where Φ_e^r is the radiant flux reflected by the object captured, Φ_e^i is the radiant flux incidence by the sun and θ is the angle between the direction vector of sun rays and the direction vector of the sunshine sensor.

The incoming sunlight irradiance (Φ_e^i) is measured by the sunshine sensor, which is mounted on top of the acquisition system. This device is continuously capturing the lighting conditions during acquisition process. Moreover, the angle between the sunshine sensor and the sunlight direction must be considered to compensate the light reflection. A mean value of the incident light is estimated for each multispectral image. The mathematical formulation of this magnitude is defined in Equation 4.2.

$$\Phi_e^i = \frac{\nu}{g\tau} \tag{4.2}$$

where ν is a sensor count value, g is the relative gain factor and τ is the exposure time in seconds.

The next step is to calculate the reflected irradiance (Φ_e^r) by using metadata (Exif) stored in the image. Every pixel $\mathbf{p}$ in the image $\mathbf{I}$ provides a reflected irradiance value, which is calculated by applying the Equation 4.3.

$$\Phi_e^r = f^2 \frac{\rho - B}{A\gamma\varepsilon + C} \tag{4.3}$$

where g is the f-number = 2.2, p is defined by pixel intensity, ε is the exposure time, γ is the ISO parameter = 100 and A, B and C are the calibration coefficients measured per camera in production.

Finally, the plant reflectance has to be radiometrically calibrated. Therefore, a calibration panel is used to calculate the calibration coefficient (K) regarding a known reflectance for every multispectral band. Three images are captured over this panel with different exposure levels. This process is carried out on the beginning and at the end of the acquisition process. Then, the Equation 4.4 is applied to calculate a calibration coefficient K for each observed band.

$$K_i = R_i \left(\frac{\Phi_e^i}{\Phi_e^r} \right) \tag{4.4}$$

where R_i is the known reflectance for each band i, Φ_e^i is the radiant flux incidence from the sunlight and Φ_e^r is the radiant flux reflected by the calibration panel.

Moreover, the reflectance values in the red and NIR bands are combined to estimate the Normalized Difference Vegetation Index (NDVI) [146]. This spectral index is widely used in remote sensing for the assessment of a plant health. Although this study is beyond the scope of this work, the use of NDVI is very interesting to identify the vegetation on the scene and classify different plant classes. As a result, a reflectance and NDVI maps are obtained for each multispectral image and then mapped on the point cloud to characterize it with meaningful spectral traits.

4.2.4 Heterogeneous Data Fusion

In this section, we describe the process to enrich the RGB point cloud using the spectral reflectance in order to get a more detailed knowledge of the behavior of all existing materials. This approach is based on our previous work presented by Jurado et al. [15]. Consequently, the comprehensive 3D model can also contain multispectral features by mapping the reflectance and NDVI maps on the geometry. For this purpose, the proposed method is divided in two processes: (1) the data alignment and (2) the inverse 3D projection.

The alignment of multispectral images and the high-resolution RGB point cloud is carried out by the development of an automatic method to set the same coordinate system for both datasets. To ensure a fully automated multispectral image mapping, we have applied the iterative-closest-point (ICP) algorithm [79] for the geometry-based alignment of multispectral and RGB point clouds. This method assesses the corresponding point pairs based on computing a weighted average from calculation of distance and compatibility of normal vectors. A normal vector defines how a surface responds to lighting. The amount of light reflected by a surface is determined by its normal vector and the direction of incoming light. These normals are directly calculated at the reconstruction step. As a result, a rigid transformation is obtained minimizing the sum of the squared error in Equation 4.5.

$$E(R, \mathbf{t}) = \frac{1}{N_p} \sum_{i=1}^{N_p} ||\mathbf{x_i} - R\mathbf{p_i} - \mathbf{t}||^2 \tag{4.5}$$

where: x_i and p_i are corresponding points, t is the translation vector and R is the rotation matrix.

Then, the inverse projection is developed to determine the matching between the 3D point and its corresponding pixel in the multispectral image. Figure 34 shows the point cloud and main vectors, which are considered for the image mapping. The blue arrow is the direction vector of the camera and the purple arrow is the normal vector of a 3D point. The reflectance values of a multispectral image are weighted during the mapping process by considering the angle between both vectors.

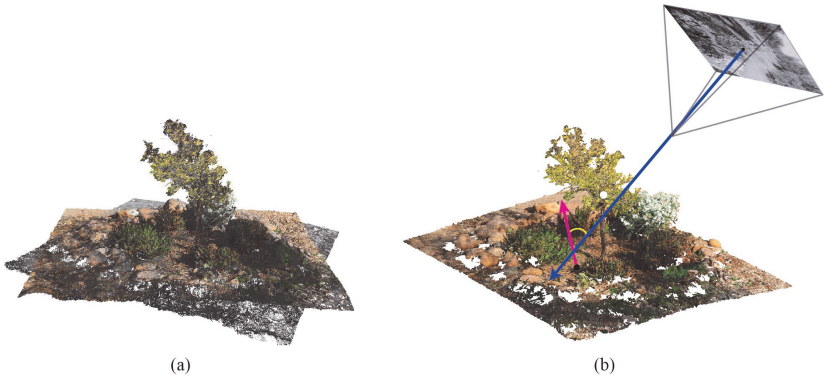

(a) (b)

Figure 34 – Data fusion: (**a**) the point cloud alignment, and (**b**) multispectral image mapping on the point cloud.

By applying our method every 3D point (with coordinates: *X, Y, Z*) is mapped to image coordinates (x_d, y_d) by considering the fisheye model of the multispectral camera. This distortion model is determined by the parameters C, D, E and F, which describe an affine deformation of the circular image in pixel coordinates. The polynomial fisheye, with the coefficients p_2, p_3, p_4, is defined in Equation 4.6.

$$\rho = \theta + p_2\theta^2 + p_3\theta^3 + p_4\theta^4 \tag{4.6}$$

where:

$$\theta = \frac{2}{\pi} \arctan\left(\frac{\sqrt{X^2 + Y^2}}{Z}\right); \theta \epsilon [0, 1]$$

where: X, Y and Z are the coordinates of 3D point.

Thus, the pixel coordinates (x_d, y_d) for the projection of every 3D point can be calculated by the Equation 4.7:

$$\begin{bmatrix} x_d \\ y_d \end{bmatrix} = \begin{bmatrix} C & D \\ E & F \end{bmatrix} \begin{bmatrix} x_{hbt} \\ y_{hbt} \end{bmatrix} + \begin{bmatrix} c_x \\ c_y \end{bmatrix} \tag{4.7}$$

where:

$$\begin{bmatrix} x_{hbt} \\ y_{hbt} \end{bmatrix} = \begin{bmatrix} \frac{\rho X}{\sqrt{X^2+Y^2}} \\ \frac{\rho Y}{\sqrt{X^2+Y^2}} \end{bmatrix}$$

and (c_x, cy) is the principal point in pixel coordinates.

In addition, a visibility test is carried out in order to detect the occlusion of shelf-hidden geometry in the model. In this regard, we propose a novel method to test the visibility of all objects from every camera position (Figure 35). Firstly, 3D points inside the view frustum of each camera are candidates to be projected in the image plane and to estimate their image coordinates (x,y). Secondly, these candidate points are ordered by the Euclidean distance between the camera and the position of viewpoint. Thirdly, from the nearest-to-farthest points, a minimal triangulated surface is formed by considering the target point and their neighbors. The neighbor search is based on the radius distance and the angle among normal vectors. Finally, the resulting surface is used to detect occluded points which are discarded in this capture. This algorithm is iterated until all points are checked.

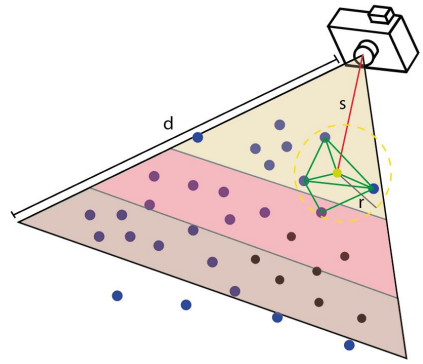

Figure 35 – Occlusion detection on the point cloud. The target point (yellow) and their neighbors create a surface (green) to detect the occluded points (black).

Regarding the efficiency of the proposed method as well as the clustering process, which is described in the following section, the point cloud is spatially indexed using a kd-tree [82] in order to ensure an efficient performance. The value for k in the this spatial-data structure is determined on the three spatial coordinates (X, Y, Z) to reduce the consuming time for the neighbor search in the clustering process.

Finally, a weighting procedure is developed in order to assess the reliability of reflectance from each viewpoint. This algorithm considers the angle between the normal vector of the 3D point and the direction vector of the camera. The multispectral camera captures a more reliable reflectance of an object's surface if its direction vector is similar to the normal vector of such object. If the angle between both vectors is greater, the reflectance detected is more irregular and less reliable. Our method focuses on the comparison between the vector direction of each multispectral view and the normal vector of every 3D point. In this way, reflectance maps are calculated considering three ranges: a perpendicular view (0° to 25°), an oblique view 25° to 60° and an indirect view (greater than 60°).

This phase is very important in order to characterize the geometry with meaningful information about the spectral reflectance of the study area. Thus, the point cloud characterization makes the extraction of the existing materials in the captured scene easier. For each 3D point, we can determine the light which is reflected or absorbed for every observed multispectral band. The reflectance measurements, the RGB color and spatial location are processed like additional attributes.

4.2.5 Semantic Segmentation

In this section, the proposed methodology to identify different natural materials in the target area is described. Our approach is based on spatial and multispectral variables to develop the semantic segmentation of the point cloud. An innovative feature of this work, the point cloud has been enriched by the spectral reflectance observed from several multispectral bands. Therefore, the studied data contain multi-dimensions, which have been considered for the material extraction. Every 3D point is characterized by the spatial position in the scenario (coordinates: X, Y, Z), the reflectance in the green, red, REG and near-infrared bands, the vegetation index (NDVI) and the RGB color. Consequently, this detailed feature vector composed by eleven attributes is used for the semantic segmentation of the point cloud.

According to the above, the key differences between every natural

entity have to be recognized in the target scenario. The relationships between these values and their variability are mainly determined by the properties of the materials. Therefore, the study of reflected light for each object lead to find out the distribution of different materials in the study scenario. In this paper, we propose a method for the semantic segmentation of homogeneous materials by considering the material appearance in the visible and non-visible range of the electromagnetic spectrum. For this purpose, a clustering algorithm is used to recognize every type of material without a labeled dataset. Unlike supervised learning, the clustering techniques are based on unsupervised learning since we do not have ground truth to compare the output of the clustering algorithm to the true labels and evaluate its performance.

In this study, our goal is to identify different types of materials real-life effects such as irregular lighting, hard or soft shadows, indirect illumination between objects, etc. To this end, a hierarchical cluster analysis [147, 148] is developed to find out relatively homogeneous clusters. In contrast to the use of agglomerative clustering, which fails to detect local patterns in the data in local patterns without considering the global distribution of data, divisive clustering is also more accurate in making top-level partitioning decisions. This top-down approach builds the hierarchy on the assumption that all points are included in the same cluster. This cluster is split using a flat clustering algorithm. This procedure is recursively applied until a stopping criterion is introduced or each point is in a singleton cluster.

Our approach is based on the divisive clustering with an unknown number of clusters (k) to be detected in the point cloud. Initially, we do not have a previous knowledge of the classes of objects in the study scenario, therefore, the k value is undetermined. For each iteration of the algorithm, we aim to look for the two clusters which are more heterogeneous from each other. To this end, the most straightforward and generally accepted way to estimate the similarity between every object in a multidimensional space is to calculate Euclidean distances. The mathematical formulation is defined by the Equation 4.8. In this process, the kd-tree is used again to speed up the search for massive points during the step of neighbor search in the point cloud.

$$d(p_i, p_j) = \sqrt{\sum_{k=1}^{n} (x_{ik} - x_{jk})^2} \tag{4.8}$$

where $\mathrm{p}_i = (\mathrm{x}_{i1}, \mathrm{x}_{i2}, ..., \mathrm{x}_{in})$ and $\mathrm{p}_j = (\mathrm{x}_{j1}, \mathrm{x}_{j2}, ..., \mathrm{x}_{jn})$ are two of n

dimension points in point cloud P.

Figure 36 presents a flow diagram of the proposed method. For each iteration, the K-means algorithm [116] is applied to extract the two most heterogeneous clusters. The main objective is to recognize the key feature pairs, which produce a greater heterogeneity of data.

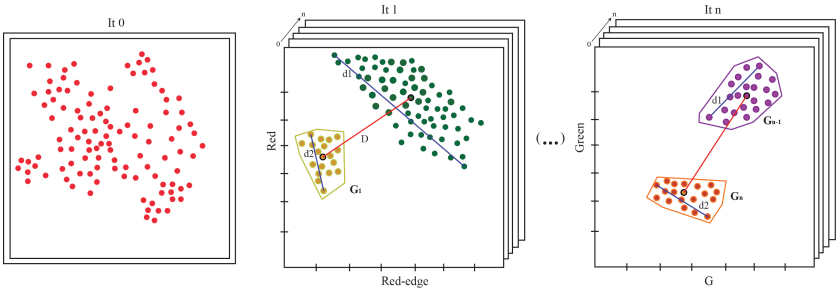

Figure 36 – The main steps of the clustering algorithm.

The splitting criterion is determined by the maximization of the cluster diameter and the distance between the centroid of each cluster (Equation 4.9). Initially, all points are considered into the same cluster. Then, a search of the pair of characteristics is carried out to detect the most significant difference between two groups. This process is recursively iterated until the stopping criterion is met. The condition of the loop end is when the cluster diameter is shorter than the distance between the centroids. For instance, in Figure 36, the diameter (d_2) of cluster G_1 is less than the distance (D) between the centroids, so this group cannot be subdivided again for the next iteration. Therefore, the heterogeneity of every cluster is highly reduced. In the final step, points are segmented into two groups G_n and G_{n-1}, whose diameters are shorter than the distance between their centroids.

$$Max_{x,y\in A}(d(x,y)) \; and \; Max_{x\in A,y\in B}(d(cx,cy)) \tag{4.9}$$

where x and y are points of the same cluster and cx and cy are the centroids of cluster A and B respectively.

4.3 Accuracy Assessment

The proposed method has been evaluated by measuring the accuracy of the process for the multispectral image mapping on the point

cloud. On the one hand, the root-mean-square error (RMSE) is calculated to determine the quality of the alignment method between RGB and multispectral point clouds. The RGB point cloud is considered the reference model because it has a more precise geometry and a higher spatial resolution than the multispectral model. According to the result, the multispectral and RGB point clouds are automatically fixed in the same reference system. The error of this process is measured by applying the Equation 4.10.

$$RMSE = \sqrt{\frac{1}{n}\Sigma_{i=1}^{n}\left(X_{i,P_1} - X_{i,P_2}\right)^2 + \left(Y_{i,P_1} - Y_{i,P_2}\right)^2 + \left(Z_{i,P_1} - Z_{i,P_2}\right)^2} \tag{4.10}$$

where (X, Y and Z) is the coordinates of a 3D point, P_1 is the RGB point cloud, P_2 is the multispectral point cloud and n the size of this last one.

On the other hand, the process of the multispectral image mapping on the RGB point cloud is checked by an image-based test. Figure 37 shows a multispectral image where pixels in the black color mean that these have been projected on the RGB model. The shape of every object captured in the study scene such as the tree, leaves or rocks can be correctly identified in the multispectral image. The background of the image is automatically discarded because it does not take part in the observed scenario.

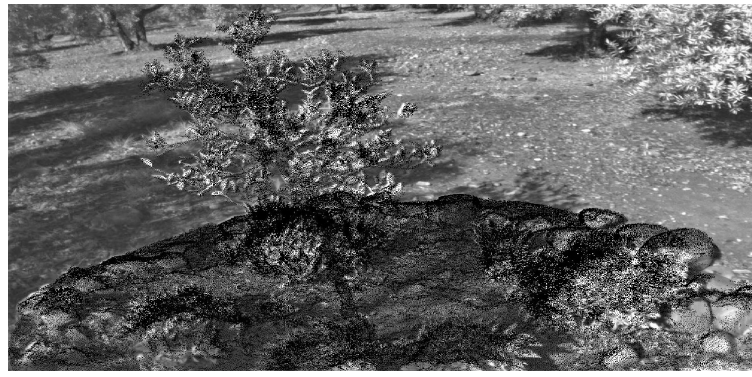

Figure 37 – Qualitative assessment of multispectral image mapping on the point cloud. Black pixels represent those 3D points mapped in the image.

4.4 Results

According to the application of the previous methodology, the observed study scenario can be classified by homogeneous materials with a similar appearance, which belong to different natural objects. The proposed framework demonstrates the contribution of multispectral images to characterize singular materials in nature. These results emphasize the potential of our application to generate a semantic segmentation of the point cloud by fusing spatial and spectral features.

4.4.1 Point Cloud Characterization

In this study, the first step is the geometric reconstruction of the study area. For this purpose, a photogrammetric process is performed by using the RGB images which were taken from multiple viewpoints. This point cloud presents a high spatial resolution (GSD = 0.07 cm). Moreover, multispectral images were captured at the same time in order to measure the spectral reflectance under natural lighting in several narrow bands. In this way, the target scene can be characterized by the spectral response of existing objects.

By applying the proposed method for multispectral image mapping on the point cloud, for each 3D point, we can inspect the spectral response on the 3D model. The error of the point cloud alignment is 0.85 cm, which can be tolerated in our approach because it is lower than the spatial resolution of the multispectral point cloud. Consequently, the point cloud is characterized by 11 attributes (X, Y, Z, R, G, B, red, green, REG, NIR, NDVI), which are used for the process of the point cloud segmentation. Figure 38 presents the enriched model for every information layer, which can be textured on the point cloud. The color scale is defined by the highest values in red color, the medium values in green and the lowest values in the blue color. On the RGB point cloud, blooming plants can be easily recognized but rocks and the tree trunk show a similar appearance as do the leaves and low vegetation. Regarding the highest values in the infrared domain (NIR and REG bands), these are shown by plants, where most of incident light is reflected. In the visible range, the reflectance detected in the vegetation area is lower than the rest due to the effect of chlorophyll pigments. Finally, in the NDVI point cloud vegetation areas can be clearly identified. However, this index is slightly saturated in the ground surface and the tree canopy. For every type of observation on the 3D model, some single entities can be clearly classified but not others. Consequently, the proposed divisible hierarchical clustering is carried out to find out the key feature patterns and extract the homogeneous materials in the study area.

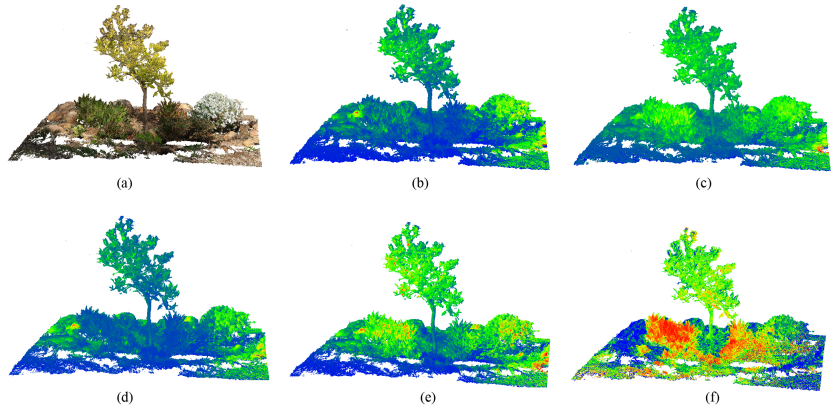

Figure 38 – The studied observations of the point cloud: (**a**) RGB color, and multispectral bands: (**b**) green, (**c**) NIR, (**d**) Red, (**e**) REG, and (**f**) NDVI.

4.4.2 Material Extraction

As a result of the application of the proposed segmentation of the point cloud, meaningful materials have been recognized in the study scenario. In the Figure 39, a detailed image of every identified material is shown. The leaves, the wood of the trunk, blooming plants, rocks, the ground and some shrubs have been detected in the point cloud.

According to the meaningful features used at different levels of the hierarchy, the NDVI and NIR were the first meaningful traits to detect leaves. Secondly, Red, REG and RGB values determined points of the tree trunk. Thirdly, NDVI, REG and Green characterized the shrubs whereas the blooming plants were influenced by NIR and Red bands. Fourthly, rocks were identified by combining the blue visible channel and the Red spectral band. Finally, the ground was recognized by the R and B visible channels and REG. Undoubtedly, all previous characteristics were combined with the spatial location of 3D points, which is considered a key constraint to limit the neighbor search in the point cloud. Figure 40 presents the resulting semantic point cloud, where every cluster is identified like a single color. Moreover, the resulting dataset of the segmented point cloud is available in the supplementary material.

4.5 Discussion

This section presents a discussion regarding the results of the proposed approach. In this study, we propose a novel methodology to ex-

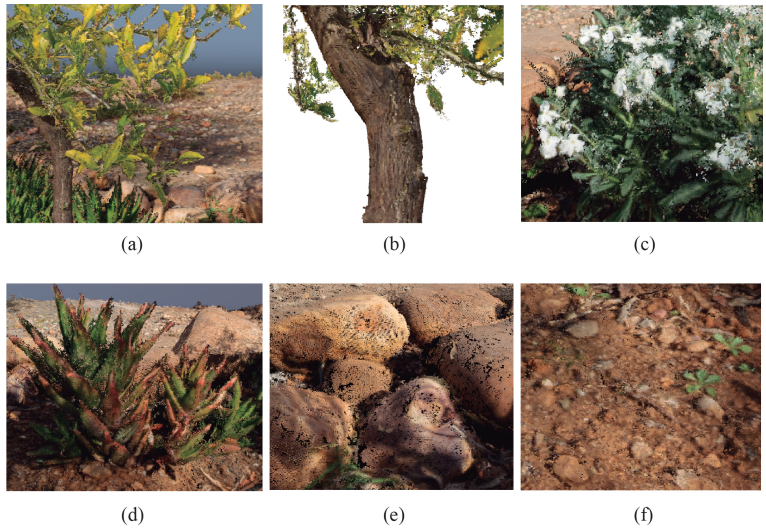

Figure 39 – The identified materials in the scene. (**a**) leaves, (**b**) wood, (**c**) flowers, (**d**) plants, (**e**) rocks, and (**f**) ground.

tract different materials in a natural space. The main goal for this work is to find out key differences between every object captured in the target scenario. Our approach is based on the unsupervised classification, so no previous labeled dataset is not required. Moreover, there is not a fixed number of clusters to be identified because this should change according to the heterogeneity of the study area. By applying our method, an enriched point cloud is generated as the result of the multispectral image mapping. This point cloud is segmented into different type of materials, which can be directly studied to understand the observed environment. Consequently, the results have a high impact and transferability to specific applications of remote sensing.

The material recognition on point clouds without training data is a challenging task. First, we focus on the point cloud reconstruction. The geometry presents a high spatial resolution less than one centimeter, so most object surfaces can be correctly modeled. Recently, the use of image-based approaches for 3D reconstruction has significantly increased because latest cameras are able to capture a high-resolution image and are more cost-effective than LiDAR system. However, the complex geometry as well as the homogeneous appearance of natural in the visible range objects arise some problems the semantic material-based segmentation. To characterize the observed scenario by other meaningful traits, a multispectral sensor was used for capturing four narrow bands. The

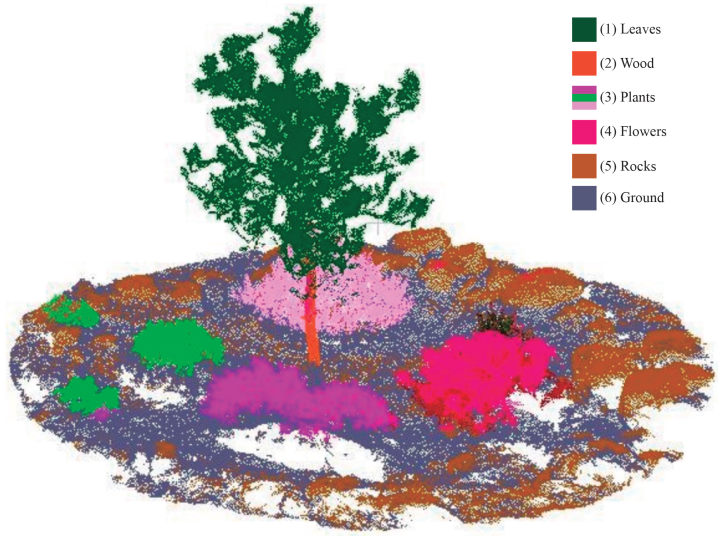

Figure 40 – The semantic segmentation of natural materials in the point cloud.

result of the application of the proposed method for multispectral image mapping on the point cloud enable the fusion of the geometry and the reflected light for each 3D point on specific ranges of the electromagnetic spectrum. The variability of the spectral reflectance between every narrow band has been a key factor to recognize the properties of different natural materials. For instance, the visible light is highly absorbed by healthy vegetation whereas the infrared light is mostly reflected and rocks present a higher contrast in red and REG bands, etc. The NDVI is also considered an important feature because this index works properly for the recognition of vegetation materials. The collection of these heterogeneous attributes provided a comprehensive knowledge of the study scenario. As a result, six materials (leaves, tree trunk, plants, rocks and ground) were identified by applying the process of the semantic segmentation.

In addition, our clustering method has been compared to CANUPO suite [149]. It has been used by applications in geomorphology for the 3D point cloud segmentation of complex natural scenes using a multiscale dimensional criterion. This algorithm uses a training dataset and extracts geometric features to characterize every class. An expert has to label the points on the 3D model, which compose the target material. According to this coarse labeling for every class, CANUPO takes some relevant characteristics to be assigned for this group of points by consid-

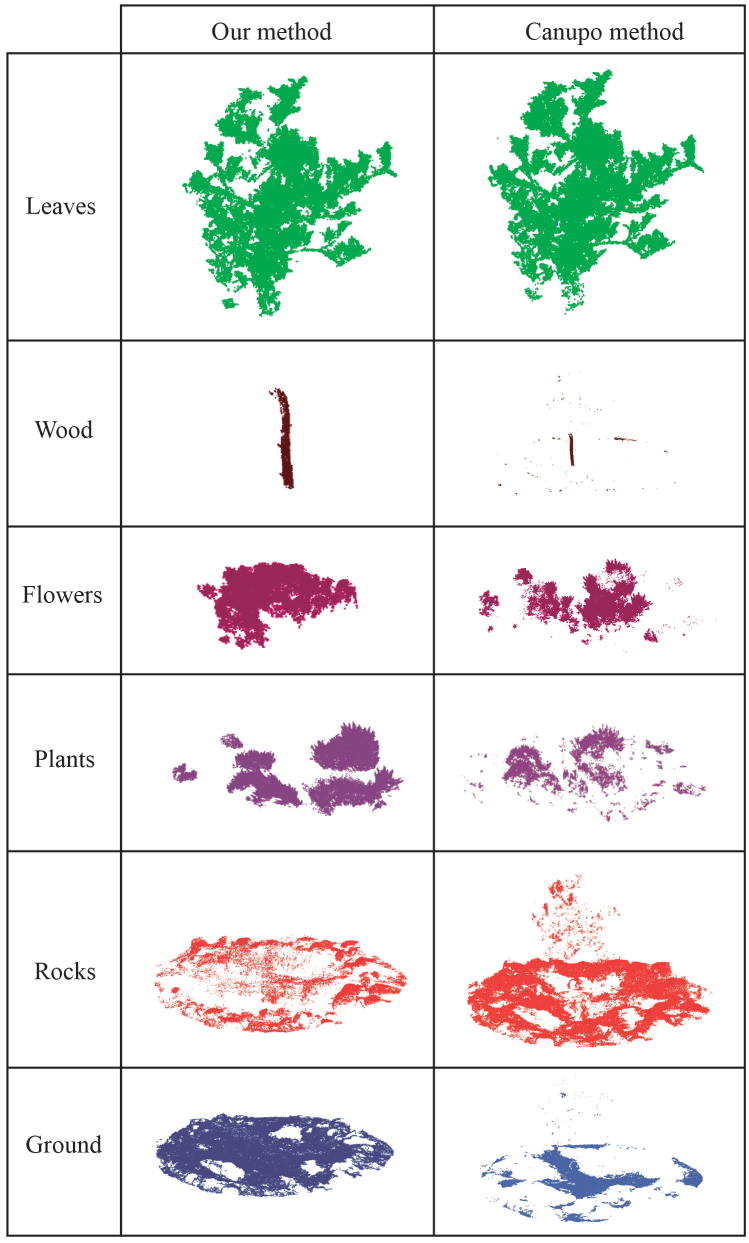

Figure 41 – A visual comparison between results of our method and CANUPO algorithm, considering all materials, which have been automatically recognized in the 3D model.

ering a confidence value. An important drawback of this method is that only binary classification can be performed. Moreover, it requires the human intervention for the point cloud labeling and a training dataset has to be created to enable the classification. A novelty of the proposed method lies in the fact that it does not need (1) a known number of classes to be recognized on the point cloud and (2) training datasets, which have to be tediously created. According to the results, Figure 41 reveals a more accurate recognition of natural material by the proposed method. Relevant differences can be observed for the segmentation of ground, rocks and plants. Flowers are also accurately identified by our method because these points present a higher reflectance in REG and NIR bands. Undoubtedly, the fusion of multispectral and spatial characteristics in the point cloud is essential to detect feature patterns associated to the behavior of every natural material. Our results emphasize the possibility of recognizing different materials in a complex natural space by using 3D model enriched with multispectral images.

4.6 Conclusions

In this study, we have addressed the problem for the semantic segmentation of real-life materials, which present a similar appearance in nature. Scene understanding is a challenging task of the current research in computer vision. The automatic recognition of homogeneous natural materials on a point cloud without a previous labeled dataset is the main contribution of the proposed methodology. Our approach enables the detection of different type of materials by fusing spatial and spectral features of the study scenario. The main novelty is the application of a hierarchical divisive clustering by using an enriched photogrammetric 3D model, which has been characterized by the spectral reflectance observed from many multispectral images.

A custom rig camera was produced in order to integrate a high-resolution camera and a multispectral sensor, thus enabling the capture of multiple images by both devices from different viewpoints around the target scene. The study area was a controlled environment whose geometry was not too complex and contained some natural materials. Therefore, the proposed method could be validated and then, it could be applied for larger scenarios. Initially, the RGB images were used in the photogrammetric process to generate the point cloud. The resulting geometry had a high spatial resolution, 0.07 cm. Then, the multispectral sensor was used to measure the spectral reflectance in four narrow bands (Green, Red, NIR, REG). Moreover, NIR and Red bands were used together for the calculation of the NDVI. In this way, the material properties could be studied by observing the reflectance from every wave-

length. By applying the proposed method, multispectral images can be correctly mapped on the point cloud, thus the 3D point is associated by a feature vector, which describes a more detailed behaviour of all objects captured. Our approach is based on heterogeneous data fusion on a 3D space. Consequently, we obtain a meaningful set of characteristics for the unsupervised classification of the point cloud.

According to this enriched point cloud, a hierarchical divisible clustering was proposed for the material recognition. In this study, we did not have any previous information about a fixed number of clusters in the dataset. Therefore, the clustering process did not require a previously labeled dataset as well as a known number of clusters to be classified. Moreover, the performance in clustering method was enhanced by the spatial indexing of a kd-tree structure. The results demonstrated the potential of our method to detect similar entities like rocks, the trunk, and ground as well as different type of vegetation materials (see the supplementary material). Furthermore, our material-based segmentation was compared to the CANUPO algorithm based on a supervised classification. In spite of the fact that this method needs a manual labelling of target materials on the point cloud, our approach is able to get a more accurate identification of every material. Specifically, 3D points of rocks, the ground, the tree trunk can be correctly identified, whereas comparable methods can only detect the leaves and some parts of low vegetation.

In the future, our aim is the use of the proposed method to create an accurate ground-truth for using autoencoders and training 3D neural networks. We hope to extend our data structure to propose a more realistic physically-based rendering of natural environments using the Graphics Processing Unit (GPU). In addition, we would like to test our method for the recognition of urban materials.

5 Automatic Grapevine Trunk Detection on UAV-Based Point Cloud

About this chapter

The work presented in this chapter has been published in the journal *Remote Sensing*. This research is focused on the recognition of key geometrical parameters to ensure the existence of every grapevine in the 3D model of a vineyard. While I led the line of work (under the supervision of Francisco R. Feito), this work was conducted in collaboration with Uni-versidade de Trás-os-Montes e Alto Douro. In particular, Luís Pádua collaborated with data acquisition and validation and Joaquim J. Sousa supervised every phases of this research.

J.M. Jurado, L. Pádua, F.R. Feito and J.J. Sousa.
Automatic Grapevine Trunk Detection on UAV-Based Point Cloud
Remote Sensing, Vol. 12, no. 18, p. 3043, Sep. 2020.

5.1 Introduction

The monitoring and management of agricultural crops, particularly with regard to nutrient level, water stress, diseases and pests, and phenological status, are vital for successful agricultural operations [150]. Traditionally, these activities are carried out through visual examinations of the crops, or by analyzing plants and soil, which are time-consuming and invasive approaches [151]. Considering the fact that it is necessary to maximize yield and resources, while reducing environmental impacts, mainly by optimizing the use of water and significantly reducing fertilizers and pesticides [152]. This can only be achieved by obtaining data that allow the intelligent and sustainable management of agricultural parcels [153]. It will then be possible, in a rational and economical way, to resort differentiated and localized actions with regard to the use of water and nutrients, and to control the soil and vegetation cover, as well as the plant's phytosanitary status.

The technological advances in recent years, have enabled the miniaturization of electronic components and a significantly reduction in prices, taking Precision Agriculture (PA) to another level. For example, the advent of Unmanned Aerial Vehicles (UAVs) capable of capturing aerial high resolution data using different kind of sensors (RGB, multi and hyperspectral, thermal and LiDAR), together with new photogrammetric

processing methods, allow the computation of diverse outcomes such as orthophoto mosaics, vegetation indices and 3D point clouds [57]. UAVs are a popular tool in PA and the obtained aerial imagery is turned into information which can be used to optimize crop inputs through variable rate applications [154, 155, 156].

In a short period of time PA approaches and practices have become very popular and were introduced in all agricultural sectors [157]. The vine and wine sector is among those that have most benefited of precision farming techniques, applied to optimize vineyard performance [158]. Thus, the Precision Viticulture (PV) concept was introduced and can be defined as a particular field of PA, whose purpose is maximizing grape yield and quality while minimizing environmental impacts and risks [159]. Therefore, it is possible to avoid unnecessary treatments, which can be harmful and polluting, and reduce costs [160]. The ability of UAVs to obtain high spatiotemporal resolution and geocoded images from different sensors, make them a powerful tool for a better understanding of the spatial and multi-temporal heterogeneity of vineyard plots, allowing the estimation of parameters that directly affect its state. Thus, individual grapevine identification and location is of great importance to precisely assess the vineyard status estimating different parameters per individual plant [1]. However, there are many features in vineyards that make these scenarios very complex to develop automatic methods for trunk individual detection and location [14]. Therefore, segmentation methods that consist of processes of dividing input data into several disjoint areas that maintain the unique and homogeneous features from surrounding have to be employed.

Regarding vineyard vegetation detection, several methods were already proposed based on different approaches using the photogrammetric outcomes from UAV-based imagery by applying image processing techniques, machine learning methods and by filtering dense 3D point clouds and Digital Elevation Models (DEMs) [14, 161, 162, 163, 164]. Those methods are capable of distinguishing grapevine from non-grapevine vegetation and to extract different vineyard macro properties such as the number of vine rows, row spacing, width and height, potential missing plants and vineyard vigor maps.

The outcomes resulting from photogrammetric processing applied to UAV-based imagery can be used to estimate individual geometrical and biophysical grapevine parameters, providing a plant-specific application for PV [165]. In this scope some studies can be found in the literature. De Castro et al. [166] developed an Object-Based Image Analysis (OBIA) method applied to high-resolution vineyard Digital Surface

Models (DSMs) to estimate grapevine vegetation. Then, the individual position of grapevines were marked, assuming a constant space between plants. This way, missing plants were also estimated and some geometrical parameters were estimated. In a different study, proposed by Matese and Di Genaro [167], missing plants detection was assessed in a semi-automatic procedure by filtering the DSM and by manually placing small polygons, representing individual plants and, then, analyzing the number of pixels intercepted by each polygon by using a five-classes approach based on quantiles to verify the probability of a missing plant presence. A binary multivariate-logistic regression model was used by Primicerio et al. [168] for the individual detection of grapevines, including missing grapevines, in orthophoto mosaics. In the referred studies it is highlighted that the integration of other sensors data could allow the extraction of single plant vigor, health and water status. In this regard, Pádua et al. [1] performed an individual grapevine estimation for site-specific management in a multi-temporal context, helping winegrowers to fully explore the potential of the high-resolution data provided by UAVs and to combine data resultant from the different imagery sensors for a more precise decision support and a quick vineyard inspection.

More recently, several studies have explored 3D point clouds resulting from UAV-based imagery photogrammetry processing to identify vineyards. Point cloud models consist of large datasets of points representing the surface of visible objects and can be derived from UAV-based imagery by photogrammetry and computer vision algorithms such as, for example, Structure from Motion (SfM). Alternatively, 3D point clouds can be directly provided by Light Detection and Ranging Systems (LiDAR). Comba et al. [169] proposed an unsupervised algorithm for vineyard detection and vine-rows features evaluation, based on 3D point-cloud maps processing. However, as final result, only the vineyards and local evaluation of vine rows orientation were retrieved. Comba et al. [170] applied a multivariate linear regression model to crop canopy descriptors derived from the 3D point cloud, to estimate vineyard's Leaf Area Index (LAI). Marie Weiss and Frédéric Baret [163], applied a SfM algorithm to extract 3D dense point cloud over the vineyard and used the terrain altitude, extracted from the dense point cloud, to get the 2D distribution of height of the vineyard. Then, a threshold on the height was applied to separate the rows. Mesas-Carrascosa et al. [171] used 3D point clouds generated using photogrammetric techniques to RGB images acquired by UAV to derive vineyard canopy information. Additionally, to the geometry, each 3D point also stored the color which was used to discriminate between vegetation and bare soil. Aboutalebi et al. [172] used UAV-based 3D information to monitor and assess vineyard plant's condition. Different aspects of 3D point cloud were used to estimate height, volume, surface area, and projected surface area of plant's canopy. Then biomass

information was used to assess its relationship with in situ LAI. Other studies, such as that by Moreno et al. [124], used terrestrial LiDAR sensors to reconstructed vineyard crops. Although accurate, these methods are time-consuming and very expensive.

As it can be concluded, through the studies previously presented, there are many groups of researchers who are dedicated to the development of methods to extract useful information from vineyards. Although it is considered by everyone of fundamental importance the detection and location of individual plants, there are no methods capable of making it fully automatic. Indeed, the various methods found in the literature, are able to estimate the position of trunks, but using prior knowledge related to the number of plants per row and the distance between plants. Therefore, a fully automatic method able to detect and locate grapevine trunks is desirable and would have the potential to create base maps for most PV studies.

In this article, we present an innovative and fully automatic method able to detect and locate individual grapevine trunks, by exploring 3D point clouds derived from photogrammetric processing of UAV-based RGB imagery. The proposed method proved to be effective even when applied to complex vineyards plots. It is able to distinguish posts from trunks and to mark missing plants.

5.2 Materials and Methods

5.2.1 Study Area

To develop the method proposed in this manuscript, several commercial vineyards (Figure 42a), in the northern region of Portugal, were selected to its application.

Commercial vineyards usually present the great advantage of a proper management, where the best practices are applied to improve yield and quality. Therefore, these vineyards present well treated rows with a regular vegetative wall, facilitating the individual grapevine detection. Then, in the scope of this study, a complex and challenging vineyard plot was analyzed (Figure 42b, $41^{\prime}08.1^{\prime\prime}$ N, $74^{\prime}09.9^{\prime\prime}$ W, 472 m altitude). The main purpose of using this vineyard, located in the campus of the University of Trás-os-Montes e Alto Douro (UTAD), Vila Real, Portugal, in the Douro demarcated region, was to push the method's application to its limit. The plot has an area of 3200 m^2 and is composed of 55 rows, and a double guyot trained system is used. The selection of this

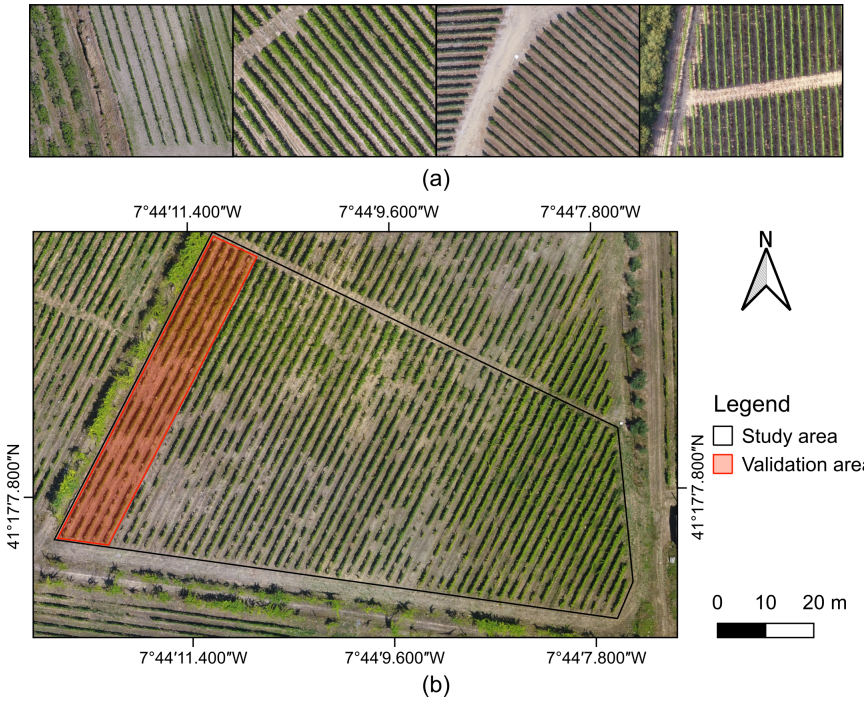

Figure 42 – General overview of the study areas: (**a**) some examples of commercial vineyards, and (**b**) vineyard plot used for validation and to assess the limits of the proposed methodology. Coordinates in WGS84 (EPSG:4326).

vineyard is based on the different levels of vigor and missing plants along the vine rows, providing a diverse variety of cases that are hard to be found in commercial vineyards.

5.2.2 UAV-Based Data Acquisition

Aerial RGB imagery acquisition was performed using the multi-rotor UAV DJI Phantom 4 (DJI, Shenzhen, China). Its native camera was used for RGB imagery acquisition, FCC 3 model, a CMOS sensor with 12.4 MP resolution mounted in a 3-axis electronic gimbal.

Different flights were conducted over distinct areas using a single-grid configuration and a flight height varying between 30 m (June and July flight campaigns) and 50 m (flights from January to May), from the UAV take-off position and with an imagery frontal overlap of 90% and 80% side overlap. The missions were planned and executed using DroneDeploy

Figure 43 – The three moments of the vegetative cycle that influence camera parameterization and flight height. Phase 1 (beginning of the wine campaign), where the influence of leaves is negligible— camera can be used facing down and the flight altitude can be higher; Phase 2 (critical phase of phenological development); and Phase 3 (preparation of the vintage and estimating production)— In these phases the camera should be used with an angle and the flight height must be low (20–30 m).

(California, CA, USA) in an Android smartphone. Regarding the most complex test site (Figure 42b), the flight was performed on 30 July 2019 and a total of 228 images were acquired. The whole flight campaign was carried in 13 min, five minutes for UAV assembly/disassembly operations and mission uploading, while the duration of the flight was eight minutes. The camera can be facing down, i.e., in the nadir direction, in all the flights conducted during the season preparation period. In the remaining flights, conducted in the growing and/or harvesting preparation period, the camera was used with an inclination angle of 65 relative to the nadir direction. This choice was done due to the absence or presence of leaves, capable of obstructing trunk detection (respectively, Phase 1 and Phases 2 and 3, of Figure 43).

5.2.3 Proposed Method

The main steps of the automatic grapevine trunk detection method based on a geometric segmentation on point cloud data are presented in Figure 44.

Firstly, the RGB aerial imagery are used to generate a 3D dense point cloud which was geometrically corrected using ground control points (GCPs). Then, a noise reduction is applied to remove many points which usually are close to the plant body. This step is important to achieve a more accurate trunk detection on areas with dense vegetation. Secondly, the location of vine rows is obtained in the form of lines using

the method proposed in Pádua et al. [14]. In this way, the search area is confined to the vine rows only, optimizing the whole process. Consequently, 3D points close to these lines were selected from the rest of the point cloud. Thirdly, a geometric segmentation is carried out in order to remove 3D points representing the ground and leaves. Thus, points belonging to trunks are isolated and spatial clustering can be performed. Finally, the 3D position for each grapevine is determined and, therefore, the number of existing and missing plants is calculated. The method was developed and implemented in C++ using the Point Cloud Library (PCL) [111].

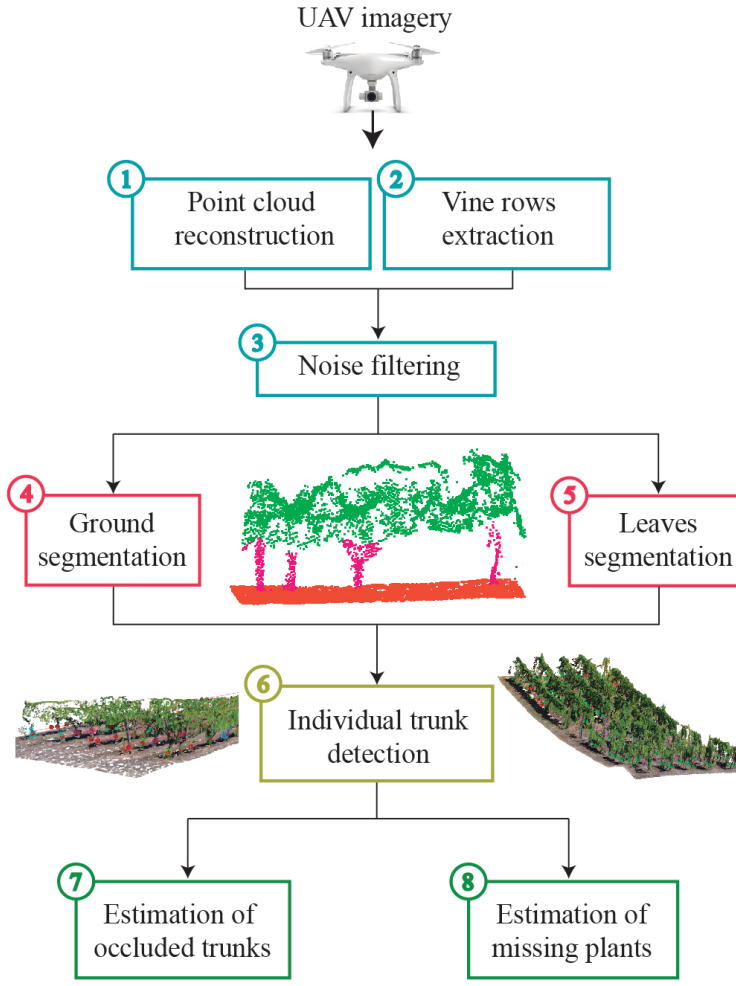

Figure 44 – The flowchart diagram of the proposed methodology.

5.2.3.1 SFM and Noise Removal

SfM techniques [8] are widely used for 3D reconstruction of multiple scenarios of the real-world [173]. These image-based methods are able to identify and match key points between overlapping images. In contrast to LiDAR-based solutions [124], the application of SfM enables collecting the fit-for-purpose data to model the geometry from some viewpoints. In general, plant modeling poses some challenges due to irregular surfaces, occlusion and varying illumination. In this regard, some considerations should be taken into account to process data correctly. For this study, 3D dense point clouds were generated over vineyard plots, by considering the following processing options: (1) a high overlapping rate ($\geq$80%), (2) a valid key point must be visible in at least three images and (3) the image scale is set to 1/2 in order to increase recognizable key points per image. The photogrammetric processing of the acquired RGB imagery was performed using Pix4Dmapper Pro (Pix4D SA, Lausanne, Switzerland). A 3D dense point cloud was generated using the multi-scale half-image size, a high point density and a minimum of three matches per image. It was exported in polygon file format (PLY). Moreover, raster products were also computed after 3D point cloud interpolation using Inverse Distance Weighting (IDW).

Noisy points that inevitably surround the vegetation areas have to be removed in order to make an accurate geometric segmentation on the 3D model. The point cloud is filtered applying a noise filter which is provided by PCL, this method is based on the computation of distance between neighbors [174]. For each 3D point, the mean distance from it to all its neighbors is computed. Thus, all points whose mean distances are outside an interval defined by the global distances mean and standard deviation are considered to be outliers. The neighbor search was developed by considering a specific radius which is related to the point cloud density. The several tests performed allowed to conclude that 0.05 m should be used to increase method's and results' quality. By applying this noise filter to the 3D point cloud, most of erroneous 3D points in the lower parts of the grapevines were removed, allowing a better recognition of the trunks.

5.2.3.2 Vine Rows Extraction

In order to reduce the research area, the method proposed by Pádua et al. [14] is first applied. In this way, the vector lines representing individual axis of vine rows are identified. In short , the identification of the lines is based on the use of a crop surface model—computed from the subtraction of the Digital Elevation Model (DEM) to the Digital Surface

Model (DSM)—in combination with the green percentage index (G%) [175], computed using the red, green and blue bands of the orthophoto mosaic. Then, grapevine vegetation is estimated from the threshold and concatenation of both raster products— the Canopy Surface Model (CSM), according to a height range and the G%, by using the Otsu's method [176]. After this procedure, a binary image is generated with a set of clusters of pixels mostly representing the grapevine vegetation. In this way, the vine rows and its central lines are estimated, considering the orientation of the most representative clusters.

Thus, the estimated vine rows axis (central lines) are used as a virtual guide to create a buffer allowing identifying points which compose the plant geometry and the surrounding soil (see Figure 45a). Since the vegetative wall width of grapevine plants usually varies between 30 and 50 cm, it was decided to create a 60 cm buffer to selected 3D points to be analyzed. As it is shown in Figure 45b, the green points represent the selected points considering 30 cm width to each side the vine row.

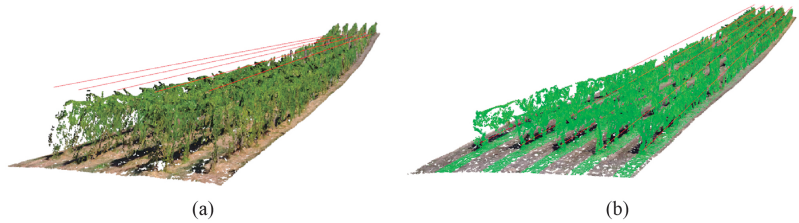

(a) (b)

Figure 45 – Example of a segmentation of vine rows: (**a**) visualization of the 3D vine rows generated as presented in Pádua et al. [14], and (**b**) 3D points selection in the point cloud, using a 60 cm buffer.

5.2.3.3 Ground and Leaves Segmentation

The vine rows extraction method enables removing 3D points, which were outside of 3D buffers. However, in addition to points, which potentially may define the trunk's geometry, there are other 3D points in the vine row space to be discarded. In order to isolate trunk points, it is necessary to remove those 3D points representing leaves, which usually appear in the upper section of the point cloud and ground points, which are located in the lower part of the 3D model. For this purpose, only geometric and spatial features as well as the point color were considered, and the following three steps strategy was applied: (1) spatial subdivision of the vine row buffers, based on height thresholds, (2) ground removal (3) leaves removal. This process is fully automatic and no human intervention is required. In effect, the method has the ability to be

applied even in vineyard plots with irregular slope, distinct density of plant foliage and voids (missing plants) along the vine row.

However, and before the application of the this procedure, 3D buffers need to be divided in different segments (Figure 46). This subdivision is determined based on the buffer's length and the terrain's slope. In this task, it is crucial to apply height thresholds, mainly important if the terrain slope varies. In flat terrains this step could be avoided, still to keep the method as general as possible, it was decided to include this step. If the terrain's slope is irregular, a higher number of segments will be required to allow a better fit. By default, the segment length is set to 1 m since it proved to fit most scenarios.

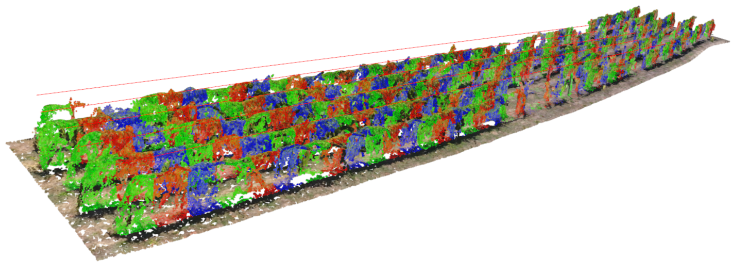

Figure 46 – Subdivision of the vine row into n segments.

The leaves and ground removal operation is carried out by considering the vine row buffers segmentation. In fact, the following geometric operations were developed for each segment. Firstly, 3D points with the highest and lowest heights are detected. Then, the terrain's slope is fitted by changing the orientation of a cutting plane for n iterations. Thus, ground points which are under this plane were automatically discarded. Figure 47 shows the main iterations of this step.

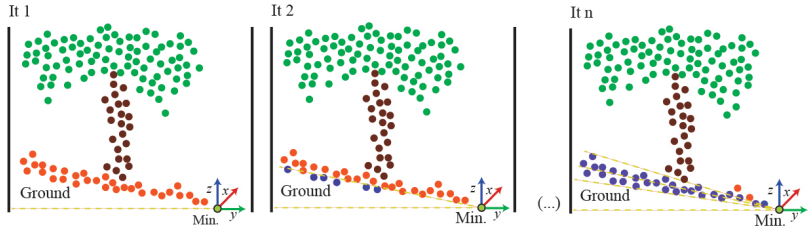

Figure 47 – Cutting plane adjustment for the ground removal in the first segment of the vine row.

Initially, this 3D plane is fixed by the point with the minimum height and the up vector ($\mathbf{v}$ = 0,0,1), whose direction is perpendicular to the horizontal plane. Then, for each iteration, the plane is rotated 5round the x-axis. This geometric transformation was performed by applying the rotation matrix showed in Equation (5.1). The stopping criterion was determined by several 3D points, selected in each iteration, i.e., those which were under the cutting plane influence. The plan inclination angle is set to the value allowing a proper fit of 3D plane to the terrain slope. Finally, to determine the location of points relative to the cutting plane, the point-normal equation for the cutting plane was applied. If the result is lower than zero, the point is under the plane (Equation 5.2), so it is classified as ground and automatically removed in the point cloud.

$$R_x = \begin{pmatrix} 1 & 0 & 0 \\ 0 & \cos(\alpha) & -\sin(\alpha) \\ 0 & \sin(\alpha) & \cos(\alpha) \end{pmatrix} \tag{5.1}$$

$$A(x - x1) + B(y - y_1) + C(z - z_1) < 0 \tag{5.2}$$

where A, B and C represent the coefficients of the normal vector, (x, y, z) represent the coordinates of the point on the plane and (x_1, y_1, z_1) represent the coordinates of 3D points.

Regarding the leaves removal, the same inclination angle used for the ground cutting plane was applied. To fix the position of this upper plane, an offset value was calculated considering points with the maximum and minimum height for each segment. This procedure is illustrated in Figure 48.

After ground and leaves points removal, the next step consists in the identification of individual trunks. This is done based on the application of a spatial segmentation especially developed for that purpose. In this regard, the trunk is considered to be a 3D geometric shape, and a clustering method sharing the following features was developed: (1) the Euclidean distance between the 3D points must be lower than 50 cm (this value is estimated considering the typical distance between grapevines, which is never of this order); and (2) the minimum number of points for clustering is set to five. According to these constraints, a correct limitation of the growing region was determined for each cluster. Therefore, n groups of points were segmented for each vine row.

The value h represents the vertical height of plants in the segment, while the value f represents the offset obtained by applying Equation (5.3).

$$f = |Z_{Max} - Z_{Min}|\dot{0}.6 \tag{5.3}$$

According to this setting, the top plane was adapted by the geometric features for each segment. After several tests, the 60% of the maximum height is the most adequate value to determine the position of the cutting plane. In this case, upper points to the cutting planes, which were considered vegetation, were removed in the point cloud. However, some outlying points could not be correctly filtered by the cutting plane. For this reason, another filter was applied based on the point color. A threshold for the green channel was fixed in order to remove vegetation points characterized by the green channel higher than 120 as well as red and blue channel lower than 80. This combination was considered adequate and derived from the many tests performed. Lower values would cause the removal of points belonging to the trunks.

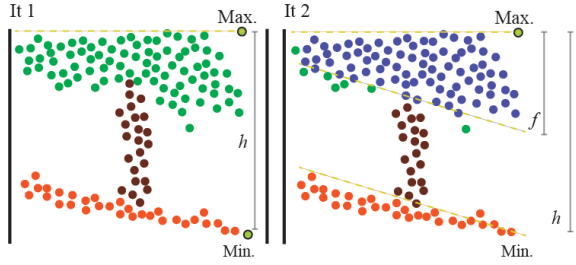

Figure 48 – Cutting plane adjustment for the leaves removal.

5.2.3.4 Trunk Detection

After ground and leaves points removal, the next step consists in the identification of individual trunks. This is done based on the application of a spatial segmentation developed for that purpose. In this regard, the trunk is considered to be a 3D geometric shape, and a clustering method sharing the following features was developed: (1) the Euclidean distance between the 3D points must be lower than 50 cm (this value is estimated considering the typical distance between grapevines, which is never of this order); and (2) the minimum number of points for clustering is set to five. According to these constraints, a correct limitation of the growing region was determined for each cluster. Therefore, k groups of points were segmented for each vine row.

Regarding the results of spatial clustering, two optimizations are considered to improve the final results. The first optimization focuses on

solving errors related to the spatial segmentation. In areas characterized by dense vegetation, where the trunk was partially occluded by leaves, the trunk's 3D reconstruction is, in general, generated with a lower detail. In these cases, the trunk is potentially composed by a few real points and many noisy points. Consequently, an inaccurate segmentation is achieved, which causes false positives in those regions. This issue is overtaken by testing the angle (α) between two vectors: (1) the direction vector of the vine row axis; (2) the direction formed by two consecutive centroids of clusters. A maximum deviation of 20s allowed. This value proved to be adequate to remove clusters which are not correctly segmented. As illustrated in Figure 49, green points are valid centroids and red points are those centroids which are discarded. The blue arrows depict the correct patch formed by all plants of the row. This test is performed along the vine row in the same direction on the x-axis.

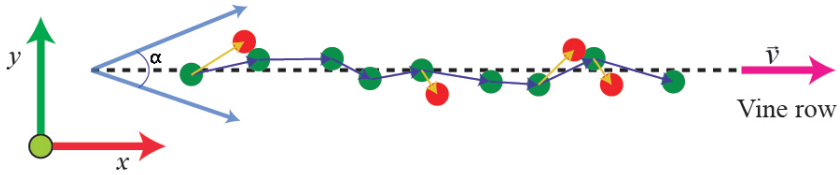

Figure 49 – Optimization of the clustering segmentation procedure.

The second optimization consists on the automatic recognition of posts, which are considered to be trunks, since geometrically both are very similar. For this purpose, key geometric features were considered to detect posts for each vine row. In Figure 50a, trunks and posts are marked by a green and yellow rectangle, respectively. The main difference is the number of vegetation points around them. As shown in Figure 50b, a neighbor search is developed for each centroid, limited by a radius ($r = 80$ cm). This value is the most adequate considering the mean size of grapevines in the dataset. To check points which were into this spherical-searching region, Equation (5.4) is applied. Then, the point color is also considered in order to detect vegetation points. Vegetation points are characterized by a threshold for the R, G and B channels so, if some of them are located inside the search area, the cluster is considered to be trunk. Likewise, if no vegetation points are found, the cluster is classified as a post.

$$x^2 + y^2 + z^2 - r^2 < 0 \tag{5.4}$$

where for each cluster, x, y and z represent the coordinates of a 3D point and r the radius of the search region.

Figure 50 – Recognition of posts: (**a**) post location in the point cloud, and (**b**) the search of vegetation points around the trunk.

5.2.3.5 Estimation of Missing Plants

Depending on the epoch of the year in which data are acquired, vegetation may occlude trunks (Figure 43). The proposed method is also prepared to deal with such scenarios, being able to estimate the position of no visible trunks and missing plants. In general, and mostly in recent commercial vineyards, each vine row is formed by plants which are equidistant from each other. However, the presented method estimates the space between plants automatically, which makes its use universal and fully automatic. For testing this feature, the method was applied on a complex vineyard plot presented in Figure 42. Therefore, the method can be used in any vineyard even in those which present challenging features such as the irregular distance between plants, replanted grapevines with different trunk diameter and some plants not visible from aerial images due to a dense foliage (Figure 51).

Figure 51 – Cases where the trunks are occluded or cannot properly modeled.

The estimation of missing plants and occluded trunks is useful in order to optimize the results of plant recognition as well as to know the number of voids along the vine rows, which could be occupied by new plants. For this purpose, the resulting data from the individual grapevine

detection were used in order to identify areas where no plants were found. Firstly, the distances between consecutive grapevines are calculated and sorted from the lowest to the highest, considering all plants detected in a given vine row.

Then, all distances less than 50 cm are discarded and the top 10% values of the sorted list are used to calculate the average distance (d). This value was calculated for each vine row and is also used to highlight areas that can potentially contain missing plants or occluded grapevines. If the distance between two consecutive plants (D) is higher than d, and the rate d/D is higher than one, the integer part of the quotient represents the number of plants that should be detected in the area. Then, missing plants and/or occluded trunks are marked using the average distance (d) as reference. Figure 52 illustrates the representation of two detected grapevines and the area between them where there are missing plants and occluded trunks. The last step consists in determining if the marked point represents a missing plant or an occluded trunk. To this end, a point inclusion test in a three-dimensional cylinder (height of 1 m and a radius of 20 cm) is implemented, considering the same constrains which were used for the trunk detection.

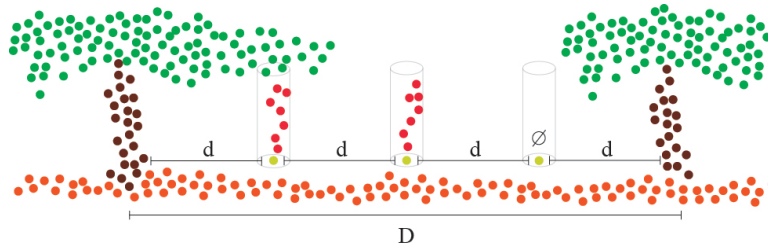

Figure 52 – Recognition of missing or occluded plants.

5.2.4 Validation Process

To analyse the robustness and effectiveness of the proposed method in all its features, five vine rows of the complex study area (polygon highlighted in Figure 42) were used. A field campaign was performed in order to map the real state of vine rows and to determine the location of missing plants. This way, for each vine row, the results provided by the application of the proposed method were compared with ground-truth data allowing computing the overall accuracy of the whole validation area and of each estimation.

Grapevine estimation evaluation was conducted based on the number of correct (true positive—TP) and incorrect (false positive—FP)

grapevine estimations and also considering the correct/incorrect estimation of missing plants along the vine rows as, respectively, true negatives (TN) and false negatives (FN). From theses data precision, recall, F1score and the overall accuracy were computed for each vine row and for the whole validation area.

5.3 Results

5.3.1 Point Cloud Reconstruction and Processing

The proposed method works perfectly when it is applied to well-maintained commercial vineyards plots, using aerial data acquired as described in Section 5.2.2. In those cases, the method is able to detect all existing trunks. However, the method was pushed to its limit, being applied to a complex area, arising from the existence of distinct vegetation density/vigor areas, several voids caused by missing plants, and new plants that were replaced defective or dead plants.

As results, a 3D point cloud formed by 26.656.371 points was generated and the time for point cloud densification was 01 h:29 m:23 s. Figure 53 shows the generated point cloud and the virtual lines that represent the vine rows axis. Most of plants could be fully modeled, but there are some grapevines whose trunks were partially occluded by leaves. Moreover, noisy points were produced around the trunks, between the leaves of plants and the ground. These 3D points negatively affect the recognition of trunk's shape. To address this problem, a noise filter was applied and most of noising points could be removed. This process was applied using a kernel size of 0.05 m. In summary, 10.448.046 points were discarded in the generated dense point cloud.

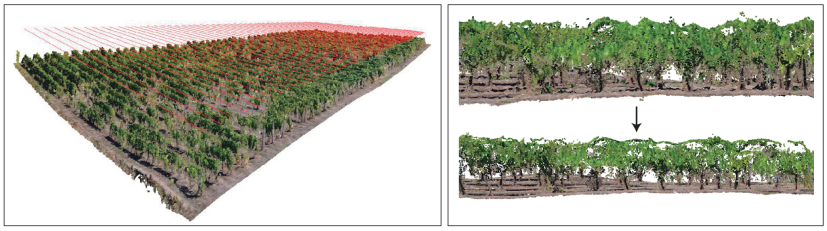

Figure 53 – 3D model generated of the complex vineyard plot: (**a**) the reconstruction of study area using all the 3D points, and (**b**) final model, after application of noise filter.

5.3.2 Individual Grapevine Detection

Once the point cloud is generated and the noisy points filtered out, the 3D model is segmented in order to discard ground and leaves points. Figure 54 shows the results of this step, when the method is applied to the vine rows of the validation area. Consequently, red points (classified as ground and leaves, Figure 54b) are discarded and just trunk points, which will be used as input data for the spatial clustering, remain.

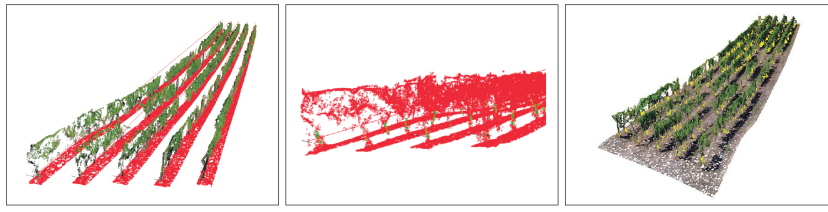

Figure 54 – Main steps for individual trunk detection: (**a**) ground points identification and removal, (**b**) vegetation/leaf points identification and removal, and (**c**) trunk detection.

The method was applied to the whole plot and the location of detected and missing plants was analyzed in the QGIS software. This output is presented in Figure 55, with the orthophoto mosaic in the background. A total of 1916 grapevines were estimated and 402 plants were classified as being missing.

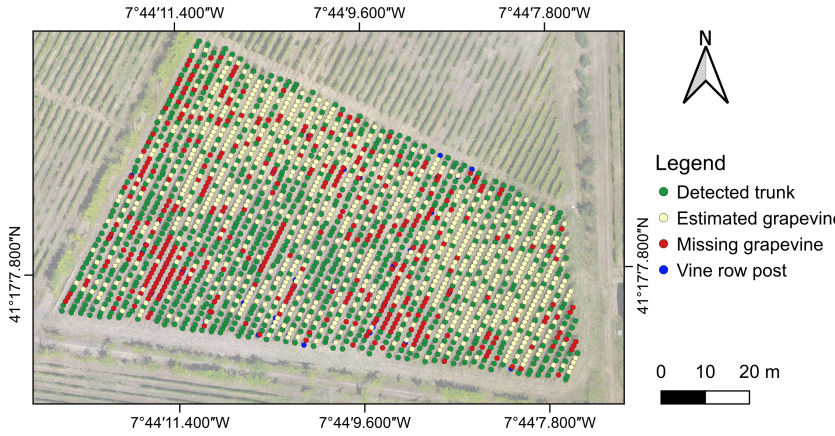

Figure 55 – Overview of the results obtained applying the proposed method to the whole complex plot. Coordinates in WGS84 (EPSG:4326).

Regarding the efficiency of this method, the time required for the automatic recognition of each individual grapevine in the whole plantation was 38 s using a PC with CPU (Intel Xeon(R) W-2145) and RAM (64 GB). The low time required for computing the methods makes possible the use of portable devices for on-site processing.

5.3.3 Grapevine Estimation Accuracy

The results of the grapevine estimation from the application of the proposed method to the five validation vine rows are presented in Table 8.

Vine row	N.º of grapevines			Missing grapevines			Row Total		
	Obs.	Est.	OA	Obs.	Est.	OA	Obs.	Est.	OA
1	46	43	93.5	12	15	75.0	58	58	100.0
2	39	37	94.9	18	21	83.3	57	58	98.2
3	42	45	92.9	15	12	80.0	57	57	100.0
4	40	46	85.0	17	9	52.9	57	55	96.5
5	49	50	98.0	7	7	100.0	56	57	98.2
Total	216	221	97.7	69	64	92.8	285	285	100.0

Table 8 – Number of plants and overall accuracy (OA, %) of the proposed method compared to the ground-truth data of five vine rows. Row total values are also provided.

Regarding the total number of grapevines presented in the evaluated vine rows (ranging between 39 to 46), an overestimation of five plants is observed. Under detection of grapevines is verified in two rows, differing in three and two grapevines, respectively. The opposite is observed in the other three vine rows, with ten plants being overestimated (respectively, three, six and one). According to the number of missing grapevines (69, in total, ranging between 7 to 18 per row, average of 14 missing plants) the results obtained by the method show an overestimation of six missing grapevines in two vine rows (three in each) and one vine row is in agreement with the ground-truth data. As for the other vine rows the under estimation of missing plants diverges from three to eight plants (64 missing plants in total, with an average of 13 missing plants per row, 93% overall accuracy). As for the total number of possible grapevines in a given vine row (sum of the grapevines and missing grapevines), a mean of 57 plants were estimated, the same number when observing the ground-truth data, being the total also 285 plants, obtaining three rows with the same number of plants, two rows with one plant less, and one row with two plants more. For this specific parameter, the overall

accuracy ranges between 97% (underestimation) and 100% considering all vine rows. According to the capability of the proposed method in the automatic detection of grapevines, 157 grapevines (71%) were directly detected from the grapevine trunk, and by the analysis of the point cloud density 64 grapevines were estimated. Moreover, several posts were also detected along the vine rows and therefore, were automatically discarded.

To further validate the spatial accuracy of the methods outputs, each detection was analyzed to assess if the estimations were correctly located. By using the ground-truth data, false negatives and false positives results—grapevines classified as being missing and the inverse, missing plants classified as being grapevines—are evaluated. Table 9 presents these results. In total, from the 221 estimated plants 197 plants were correctly detected and classified (89%), as for missing plants, 41 (64%) were correctly classified, the overall accuracy considering all data is approximately 84%.

Figure 56 shows the 3D location of each plant on the test area. Green points represent the centroids of plants that are directly detected in the 3D model. The centroids' position were then checked against its corresponding vine row in order to identify centroids wrongly classified as trunk (red points). These wrong classifications are caused due to points of vegetation, which are around the trunk and could not be totally removed by the noise filter. Then, posts were distinguished from the grapevine trunks (blue points). Finally, missing plants (pink points) and occluded trunks (yellow points) were estimated. In terms of quantitative data, in the validation area, the proposed method was able to detect 221 plants and 64 missing plants.

Vine Row	**TP**	**FP**	**TN**	**FN**	**Precision**	**Recall**	**F_1**	**OA**
1	39	4	8	7	0.91	0.85	0.88	81.0
2	32	5	16	5	0.86	0.86	0.86	82.8
3	40	5	7	5	0.89	0.89	0.89	82.5
4	42	4	6	3	0.91	0.93	0.92	87.3
5	45	5	4	3	0.90	0.94	0.92	86.0
Total	198	23	41	23	0.90	0.90	0.90	83.9

Table 9 – Evaluation of the classification grapevines and missing grapevines for the following parameters: precision, recall, F_1 (F1-score), and overall accuracy (OA, %). The ground-truth of five vine rows was used. TP: true positive; FP: false positive; TN: true negative; FN: false negative.

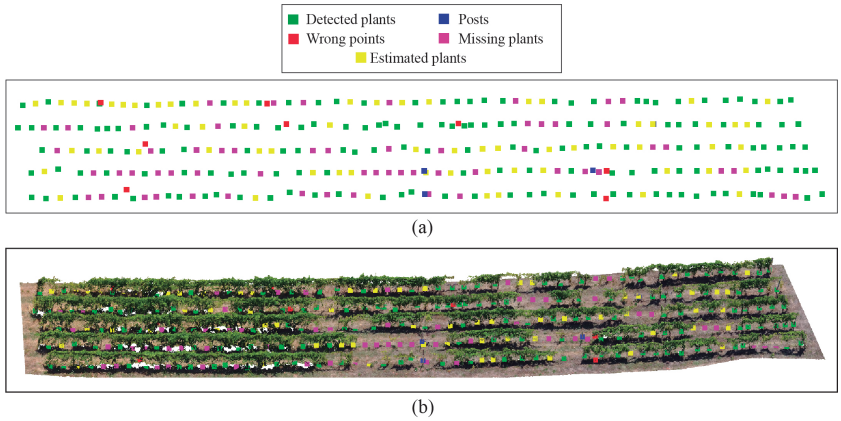

Figure 56 – Individual grapevine delineation applying the proposed method in the validation area: (**a**) points to represent detected plants (visible and occluded trunks), missing plants, wrong clusters and posts, and (**b**) 3D point cloud and points computed for the plant location.

5.4 Discussion

5.4.1 Point Cloud Reconstruction and Processing

The generation of point clouds for remote sensing applications was enhanced by the proliferation of innovative UAV-based technologies such as high-resolution cameras and LiDAR systems. By applying photogrammetric techniques, point clouds can be obtained using multiple overlapping images. Other option is the use of LiDAR scanners which provide dense point clouds of natural environments but these are more expensive than digital cameras [177]. LiDAR data discriminate better plant's canopy since it penetrates vegetation [178, 95, 179], and, therefore, potentially making the identification of the grapevine trunks easier. Moreover, photogrammetric techniques tend to estimate erroneous points in the cases where some points from the ground are estimated along a post. One of the advantages of the proposed method is that it remains operational even when using point cloud data from other type of sensors, reinforcing that when LiDAR sensors for UAVs become more affordable the method can still be employed. The proposed method is not dependent on any technology, although to get proper results is required enough geometric quality of the 3D model to ensure a partial reconstruction of the trunks at least. In this sense, to avoid noisy points around the trunk and vegetation, the presented solution integrates a noise filter. Hence, the proposed method can be applied using any point cloud data with

accurate results.

5.4.2 Individual Grapevine Detection

There are several methods for the automatic detection and parameters extraction on 3D models using crop height models [180], combining terrestrial laser scanner and UAV photogrammetric point clouds [97], fusing RGB and multispectral point clouds to extract individual tree parameters [17], computing 3D vegetation indices in olive groves [15], and obtaining forest structural attributes [181]. However, given the complexity and the unique characteristics of vineyard plots, such methods are not suitable to be applied. Studies focusing on the use of photogrammetric point clouds, generated from UAV-based imagery, were dealing with vineyard detection [169] or detect and describe some of its general properties [163, 171, 182]. Studies for individual grapevine detection using UAV-based raster outcomes often rely on the coarse position of each vine assuming a mean distance of separation between grapevines along the vine row [1, 166, 167]. The proposed method addresses all these limitations, using point cloud data and geometrical characteristics, to automatically identify points belonging to grapevine's trunk. Hence, individual plants can be detected and missing plants estimated.

The complex vineyard plot analyzed in this study had been used in another study [1] with data acquired in 2018. The whole plot contained 2266 plants and was evaluated by the method with an accuracy of 98%. However, the aerial imagery was acquired in an early phase of the vegetative state [183] with a lower vegetation density, which can help in the detection of missing plants. Furthermore, a constant distance between individual plant was also used. The results presented in Section 5.2.4 present an overestimation of 2% (Table 8) according to the number of grapevines and an under-estimation of 8% considering the number of missing plants. This fact is related to the presence of vegetation from adjacent grapevines in areas with missing plants that could cover the void. The results are improved by selecting an early period (preferably belonging to phase 2—Figure 43) to conduct grapevine detection, with grapevines with a lower leaf cover, preventing the existence of vegetation in areas with no plants [167]. In Di Gennaro and Matese [184], 3D and 2.5D methods were compared for vineyard biomass and plant detection, but individual grapevine detection was not performed. In that study, as for missing plants, an overestimation was observed in the 3D-based method, false negatives were related to the existence of new plants while some false positives were due to different grapevine canopy thickness. Similar findings were detected in the miss-classifications observed in this study (Table 9). Moreover, proximal sensing approaches

for grapevine trunk detection using ground vehicles were also tested by research groups, either using LiDAR [185, 186] or depth cameras [187]. However, in contrast to UAVs, such approaches are more expensive—due to the equipment used—and time-consuming, since the vehicles need to go through all vine rows, where some obstacles can also be present in their way.

5.5 Conclusions

The innovative method presented in this study is proved to be effective for a rapid access of the vineyard status using UAV-based 3D point clouds, with automation levels that allow its applicability in different vineyards, not relying on predefined parameters as the distance among plants. The proposed method is able to detect occluded trunks with reliable accuracy rates and missing plants, where in the vineyard context represents the occurrence of voids along the vine rows. The major contribution of this work is that the approach is fully automatic, not requiring any a prior knowledge of the distance between plants or number of plants per row, as in existing approaches. Moreover, the computational complexity of the proposed technique does not require high-performance computing and is appropriate for use on mobile in-field computing devices.

The applicability of the proposed method can be extended to other types of purposes related to the estimation of biophysical parameters of grapevines, providing a more efficient understanding of data for vineyard management and the validation of the use of UAV-based point clouds. Indeed, its impact is increased in a multi-temporal context. In this way, the estimated canopy of each detected grapevine can be studied to measure its volume which can help in the decision-making process for canopy management operations and, consequently, yield optimization. To improve data quality and to extend the method capabilities, an in-depth investigation of the flight parameters optimization (flight height, imagery overlap, camera angle) is required, which can also make possible an automatic detection grape bunches. The results of this study might influence on further research related to individual monitoring of every grapevine, multi-temporal studies and making accurate support decision systems for an optimal vineyard management.

Part IV

Concluding Remarks

6 Conclusions

In this thesis, a series of contributions have been presented in the fields of Remote Sensing and Computer Vision: (1) the multispectral characterization of 3D models and (2) the semantic segmentation and recognition of geometric shapes in point clouds. The multidisciplinary nature of this research highlights the author's motivation to propose advances in different areas that undoubtedly converge in fields of application where the innovation requires a transverse perspective. The first part of this thesis focuses on the characterization of 3D models from multispectral images. The second part aims to develop methods for the semantic segmentation of materials in a 3D natural scenario and the recognition of the 3D geometric shape of grapevines trunks for the automatic location of plants in a vineyard. As a result of this research, the GEU software (Geospatial and Environmental tools of University of Jaén) has been developed, which integrates the set of methods implemented. In this way, it is intended to bring our solution closer to the industrial sector and to promote the transfer of the results derived from this research.

6.1 Main Contributions and Future Work

Multispectral characterization of 3D models. In this first part, two lines of work have been presented. Firstly, in Chapter 2 the method for mapping multispectral images on point clouds relating to an olive plantation has been described. The development of this method has enabled the study of both morphological and spectral variables of individual plants, which have been automatically identified in the point cloud considering several key spectral traits. Moreover, the proposed method enables testing the occlusion in the 3D scenario in order to avoid mapping occluded points, which are not directly visible in the image. The resulting point cloud is enriched with multispectral data, so that each 3D point is characterized by a series of reflectance values observed at different wavelengths. In addition to the development of the method, we have created the user interface and 3D canvas of GEU to achieve an optimal visualization of results. Thus, an interactive visual inspection of the 3D model is provided, thus enabling a more accurate analysis and evaluation of the health status of surveyed crops. Finally, in this work a multi-temporal study has been developed by monitoring morphological and spectral features of olive trees over the period of two years. We have developed our research using the olive grove as the study object, thus resulting advances directly have a positive impact on the olive sector,

which plays a key role in Jaén, and has a significant presence on the international scene. As future work several applications are planned related to the detection of diseases and early prediction of harvest using all attributes collected for each olive tree. The work carried out in this thesis provides a key information for harvest prediction, such as the volume, height and multispectral features for each individual olive tree.

Secondly, in Chapter 3 we have worked on the multispectral characterization of different tree species (pine, oak and eucalyptus) and on the analysis of their 3D structures. Next, the correlation between morphological and spectral parameters of each species has been studied from the individual detection of each modeled tree. The aim is to analyze the impact of the reflectance observed in the treetops on the three-dimensional structure of the plant. This study demonstrates the usefulness of the method proposed in the previous work to carry out a detailed characterization of a natural scenario, in which high and low vegetation coexist. Likewise, this development enables possible a detailed monitoring of every tree, whose structure and health status is influenced by natural effects and conditions of the environment. Undoubtedly, this tool of GEU is useful for the forest inventory and tree specie classification, achieving a detailed view of forest areas even with difficult access. Future research will be centered on the study of biodiversity and the realistic simulation of the plant growth, considering the competition for natural resources.

Semantic segmentation of point clouds. In this second part of this thesis, several advances have been proposed for the recognition of materials in a 3D real-word environment and the individual location of plants in vineyards based on the trunk recognition. Firstly, in Chapter 4, the problem of segmentation of materials with a similar appearance in the visible spectrum has been addressed. The proposed method is based on hierarchical clustering and multispectral characterization of the 3D scene to recognize each material. Spatial and multispectral variables are used together in order to identify each level the subset of points, which presents a greater difference with respect to the others. In this way, it is possible to detect the rocks, the terrain, the trunk, the leaves and low vegetation in the surveyed scenario. The result is a point cloud labeled with those materials which have been identified. This set of data may be used by many applications of computer vision for object tracking and deep-learning methods. These fields will be explored as further research.

Secondly, Chapter 5 presents a fully automatic segmentation of vines using only point-cloud data, which have been acquired from UAV-based images. The proposed method integrates a series of geometric algorithms for the recognition of each trunk by first removing noisy points. Initially,

the soil and leaves are discarded to isolate points of the trunk. Then, a spatial clustering is applied in order to segment the point cloud and recognize every trunks of modeled grapevines. As a result, the method enables determining the location of each plant along the vine row, as well as those gaps which can be filled by new plants. Thus, this method aims to solve current limitations for the individual plant detection in vineyards by making use of the knowledge extracted from 3D models. This advance involves many opportunities for interesting future work such as the monitoring of individual grapevines and the development of more accurate decision-making support systems, thus increasing the final production in vineyards and other plantations as intensive olive groves.

This thesis has presented significant contributions to promising research, in which there are still open problems. As future work, our aim is to increase the functionalities of the GEU software by providing solutions related to (1) integration of thermal data for crop analysis, (2) processing of hyperspectral images, (3) generation of hyperspectral point clouds, (4) segmentation of real-world materials from hyperspectral images and (5) GPU acceleration of the method for mapping images on large point clouds. Currently, part of this future work is already well advanced and is pending to be published in several research journals with a high scientific impact. There is no doubt that the advances resulting from this doctoral thesis open up new fields for research, innovation and development, with the contribution of knowledge obtained from 3D models of real-world scenarios and which have been also enriched from multi-source remote sensing data.

6.2 Personal reflection

In my own personal view, this thesis has allowed me to gain matureness as a researcher and as a person in general to overcome challenging situations and adapt to different working environments. During this time, I have improved my technical skills but more important, I have been successful in working in collaborative environments. I have also learned how to reach compromise, taking into account different points of view. Moreover, I have had the chance to work with many researchers and several competitive teams have built with expertise in several fields, which has enriched and greatly benefited this research. In addition, supervising students has been another opportunity to learn the way to motivate them and to propose the most adequate path considering their objectives. Also, having the chance to participate in research projects imposed on me a great challenge but it was paired up with a high satisfaction. Undoubtedly, these years have been an invaluable and greatly enriching experience.

Part V

Appendices

A

GEU Documentation

This appendix describes main functionalities and applications of GEU (v 1.0). The development of each GEU module involves significant advances in different research fields related to Remote Sensing and Computer Vision. GEU integrates a set of methods focused on multispectral image processing, the generation of 3D models enriched with multispectral data, the segmentation of natural materials and the analysis and visualization of point clouds in a 3D interactive environment. The following sections present: (1) a brief summary of GEU, (2) the user interface, (3) the data model, and (4) the acceleration of 3D mapping algorithms using GPU (graphics processing unit).

A.1 Introduction to geu

GEU is a research-orientated tool written in portable C++ 17. It consists of a small set of libraries and its own methods which implement several functionalities ranging from image processing and 3D mapping to analysis of enriched point clouds which represent real-world scenarios. GEU can help researchers to process multi-temporal remote sensing data automatically, to map multi spectral data on huge 3D point clouds and to recognize some specific feature patterns of natural entities. The resulting 3D models may be efficiently visualized in a 3D interactive scenario in order to accurately inspect the surveyed area.

According to libraries used in GEU, the Point Cloud Library (PCL) [138] is used to manage and visualize 3D point clouds, OpenCV [12] to process and extract key features of multispectral images and Exif library to read image metadata. In addition, Mlpack library has been recently included to apply some machine learning methods [112]. Finally, to enable the use of GPU, the CUDA 11.0 (Compute Unified Device Architecture) platform is also supported in GEU. With the integration of these libraries into the framework of GEU, we have developed several methods in order to propose significant advances, which have been presented in this doctoral dissertation. One of the main characteristics of GEU is that all methods are fully automatic and no human intervention is required to obtain the results. During the research period for this thesis, a high number of experiments and multiple acquisitions of remote sensing data have been developed in order to provide all utilities of GEU. A big picture of GEU software is presented in Figure 57.

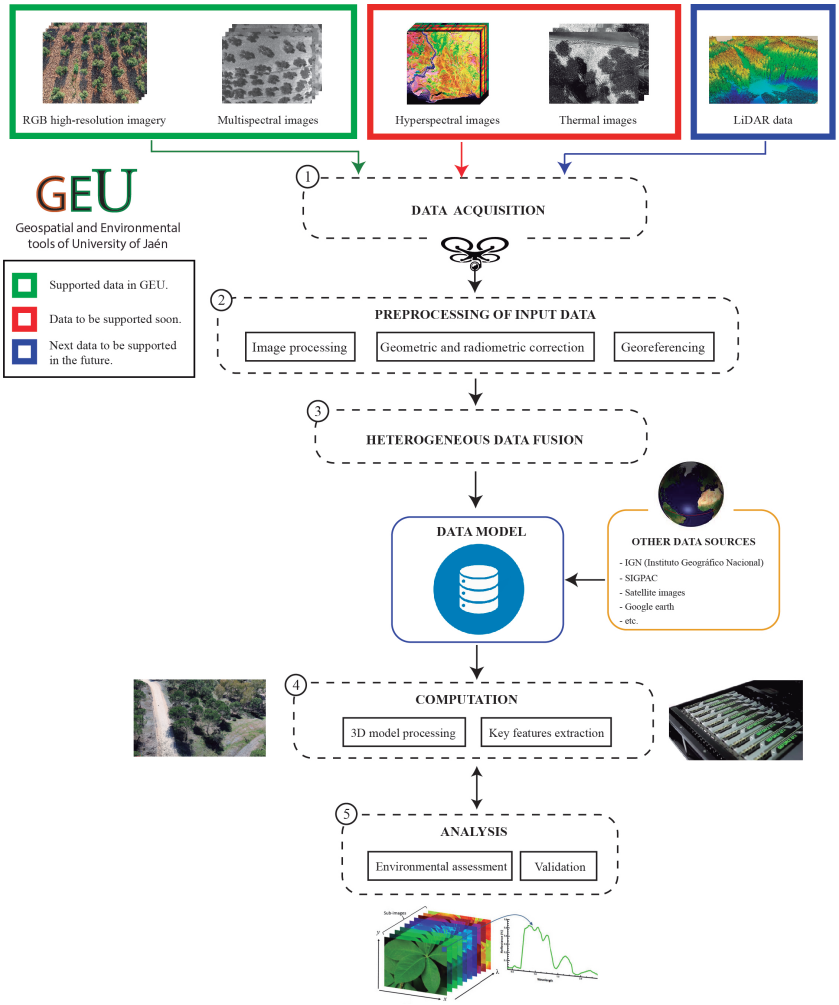

Figure 57 – An overview of GEU framework.

The current version of GEU, v 1.0, enables processing and mapping multispectral images on 3D models. Multispectral data may be used to analyze multiple features of surveyed scenarios, as vegetation reflectance is a meaningful indicator to study the health or stress status of vegetation, the appearance of materials, the branching structure of trees and many physical effects in a natural ecosystem. Regarding input multispectral images, GEU enables the radiometric calibration to generate accurate reflectance maps for each image. This process takes part to the stage of preprocessing data, see the second phase in Figure 57. Then, a data model is designed to manage the results from fusing multispectral

data and 3D point clouds. It is used to store geometric and spectral data related to the surveyed 3D model. Finally, several operations may be performed for the computation and analysis of enriched 3D point cloud with multispectral data, see the fourth and fifth stage in Figure 57.

The main goal of GEU is to enhance the research of a wide variety of fields related to the monitoring and analysis of environmental scenarios from fusing 3D models and multiple multispectral variables, which describe the spectral behavior of natural entities. According to main functionalities of GEU, these are listed below:

- Generation of reflectance maps from each multispectral capture.
- Multispectral image mapping on 3D point clouds.
- Generation of multi-temporal models.
- Interactive visualization of enriched point clouds with several information layers.
- Detection of individual trees/crops in natural scenarios.
- Estimation of volume and height of trees.
- Morphological and spectral characterization of tree species.
- Recognition of natural materials in a 3D environment.
- Some specific operations to manage 3D models of vineyards and olive plantations.

Regarding main application fields, which directly benefit from using GEU, we highlight the farming sector, in which the management of plantations can be improved and a higher harvest production can be achieved. In fact, GEU has been tested using olive groves and several vineyards as surveyed areas to test the proposed methods. In addition, the study of biodiversity in forest may be enhanced by using GEU, thus achieving an accurate characterization of observed entities in a 3D environment. In this regard, the semantic segmentation is a meaningful tool to recognize some target materials or even to identify some outliers and patterns, which could be interesting to be analyzed from real-world scenarios.

A.2 User interface

An important requirement of GEU is to be easy-to-use software. To this end, we have developed both a user interface to manage all available

methods and a 3D canvas to visualize the results. An all-new cross-platform user interface is provided for running GEU on any platform.

Figure 58 shows the user interface which contains several tool bars in the panel designed for launching all functionalities of the GEU tools. To provide an interactive visualization of results, a 3D canvas is developed, as seen in Figure 59. On the one hand, users can upload input images and check the camera position and orientation for each image. On the other hand, the 3D point cloud can be visualized from multiple views using friendly actions to navigate around the virtual scenario. Moreover, a detailed inspection can be carried out observing different information layers of the 3D model. An example of the application to study the health status of olive trees, applying the proposed method for mapping multispectral images on the 3D model, is shown in Figure 60.

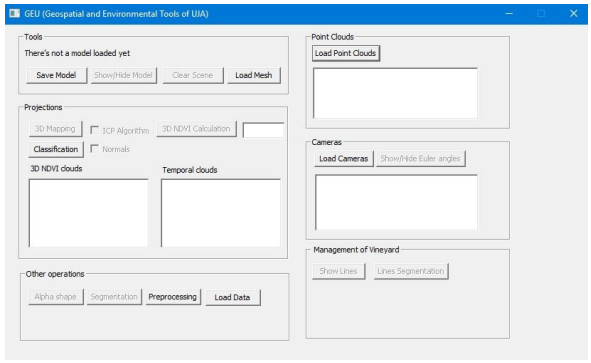

Figure 58 – A snapshot of the user interface of GEU characterized by several tool bars for uploading data, point cloud processing and 3D mapping.

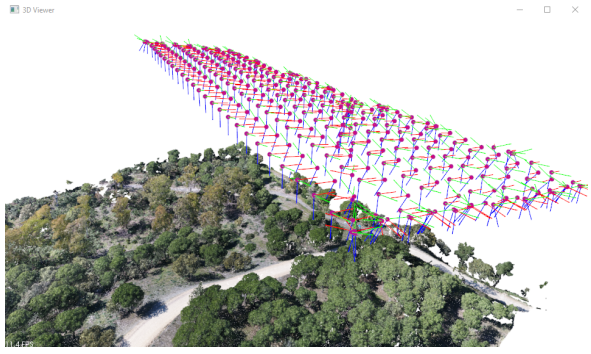

Figure 59 – The visualization of a 3D point cloud and multispectral cameras (position and orientation) using the 3D canvas of GEU.

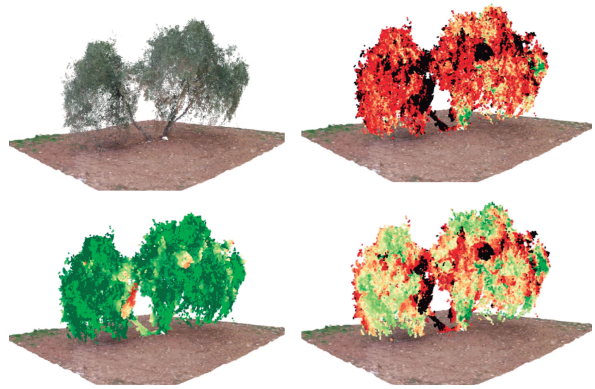

Figure 60 – A 3D visualization of an olive tree model which has been characterized by several traits and vegetation indices.

A.3 Data model

According to the data model, several data structures have been used to manage multispectral data linked to the 3D model. A 3D point of the model is considered as the minimal study object in such a way that for each one several attributes (listed below) are associated:

- 3D position (X, Y, Z).
- Red-green-blue channels.
- Array of reflectance values in the near infrared.
- Array of reflectance values in the red-edge band.
- Array of reflectance values in the red band.
- Array of reflectance values in the green band.
- Array of vegetation indices.

These attributes provide a detailed knowledge for each 3D point, which takes part of any surface of modeled objects. Consequently, since one object is formed by many hundreds of 3D points, we can also learn about the spectral behavior of every observed entity along their surface. To manage the point cloud indexing as an efficient way, a spatial data structure, an octree, is used to accelerate the selection of those points which are visible from each multispectral image. As a result of this operation, the second data structure is generated. This is determined by a 3D matrix which stores the identifiers of visible points in each

multispectral image, as well as the distance from the camera position to the point location. This data structure is used to develop the test occlusion in the 3D scenario.

In this research, experimental results are obtained using binary files to store temporal data corresponding to different flight campaigns. Although it may be an adequate solution for testing the proposed methods, a large scale study of multiple crop plantations and huge forest regions requires the development of a multidimensional and multitemporal database. In fact, the design of this database is just carried out, as shown in Figure 61.

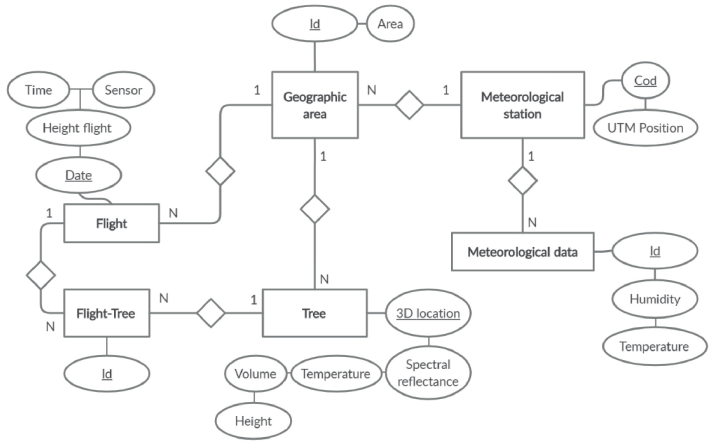

Figure 61 – The entity relationship data model of GEU.

This database stores remote sensing data acquired by different UAV-based sensors. It is available in the current version of GEU and will be used to develop future applications based on machine learning. The deployment of this database enables several spatial and topological operations with massive data and new functionalities towards visual analytics in order to address new promising applications.

A.4 GPU Acceleration

GPU programming is particularly suitable to accelerate time-consuming problems which can be addressed as parallel calculations of datasets (data parallelism). The main goal is the simultaneous use of multiple re-sources to perform concurrent operations. Our parallelization approach is based on CUDA (Compute Unified Device Architecture). The CUDA programming model is a heterogeneous model in which both the CPU

and GPU can be used simultaneously. In CUDA, the host refers to the CPU and its memory, while the device refers to the GPU and its memory. A code run on the host can manage memory on both the host and the device, and it also launches kernels which are functions executed on the device. These kernels are executed by many GPU threads in parallel.

Initially, the development of the method for multispectral image mapping on point clouds is based on CPU, but recently we have developed a preliminary solution, which uses the GPU to accelerate the performance using huge 3D point clouds. This option has been already included in the current version of GEU, as a preview module (note that this is not yet complete). Our solution is focused on minimizing the number of transfers between CPU and GPU, in order to have a coalesced memory access, combining multiple memory accesses into a single transaction, and on maximizing the use of shared memory in the GPU. There are some kinds of memory on a CUDA device, each with a different scope, lifetime, and caching behavior. In particular, we focus on efficient global memory access. This memory is the main memory used for data transfers between the host and the device, as well as for data input to and output from kernels. However, the global memory presents the lowest access and a high latency. This has a negative impact on the performance, so these should be reduced, for instance by applying an asynchronous-based approach for launching every process on the GPU. Data stored in the global memory are visible by any thread block [1] which is running on the GPU.

An out-of-core solution is proposed,as the memory capacity of GPU is not a constraint and does not limit a maximum size of the point clouds to be processed in GEU. To this end, the available global memory is divided into two logical parts: the lock memory and the dynamic memory. The lock memory is occupied by data which are always required during the mapping process such as metadata of images, a 3D matrix for testing the occlusion in the scene, etc. The dynamic memory is occupied by a part of the 3D model to be processed. The point cloud has to be split into multiple sets of points, whose size depends on the available capacity of the dynamic memory. The data computation is based on an asynchronous concurrence of both, the memory transfer tasks and the execution of kernels in the GPU. Figure 62 depicts a scheme of our solution based on launching two kernels in parallel. All memory transfers between CPU and GPU are asynchronous and thus the time required for data transfers and GPU computation is overlapped. Therefore, the dynamic memory is divided into two memory blocks with the same size,

[1] Thread block: it is a programming abstraction that represents a set of threads that can be executed in parallel.

which is used as reference to split the 3D model. The input and output data are stored in these two blocks, by the execution of the first kernel corresponding to the first stream [2] and the second kernel to the second stream

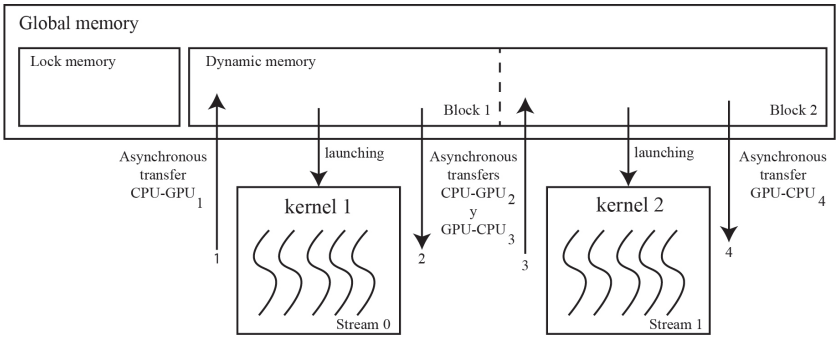

Figure 62 – GPU-based method for multispectral image mapping on point clouds.

In the below pseudocode, Algorithm 2, main steps of the proposed method are shown. For each iteration, a pair of blocks is processed, launching memory transfers and kernel executions in parallel on the GPU. A great advantage of this approach is the significant reduction of time required by memory transfers in such a way that while one block is being computed, data on the other block are being transferred from CPU to GPU.

A.4 Performance Analysis

In this section, a summary of tests to assess the performance of multispectral image mapping method is presented. To develop the performance analysis, a workstation has been used with the following hardware specifications: x86-64 architecture, a Intel processor with 4 cores (cores) i7-4790, 24 GB of memory (RAM) and a NVIDIA GPU (TITAN V) with 5120 cores and 12 GB (VRAM). The training dataset is characterized by a point cloud formed by 66.374.475 3D points and 12 multispectral images. Then, a second dataset is considered using the same point cloud but increasing the number of multispectral images to 180.

The performance evaluation of the sequential method has been carried out using the Intel C Compiler (icc^{TM}), v 10.2. This enables the code compilation applying several levels of optimization. Table 10 shows the overall time and time required for mapping and occlusion test.

[2]Stream: a sequence of operations that execute in issue-order on the GPU.

Algorithm 2: Multispectral image mapping on GPU.

```
Input: block 1, block 2 and some constant variables;
Result: 3D point cloud enriched with multispectral data;
for each iteration do
    Inicialization of block1;
    Inicialization of block2;
    cudaMemcpyAsync(cb1,block1, numBytes,cudaMemcpyHostToDevice,
      StreamA);
    kernel1«<...,StreamA»>();
    cudaMemcpyAsync(cb2,block2, numBytes,cudaMemcpyHostToDevice,
      StreamB);
    cudaMemcpyAsync(cb2,block2, numBytes,cudaMemcpyDeviceToHost,
      StreamA);
    kernel1«<...,StreamB»>();
    cudaMemcpyAsync(cb2,block2, numBytes,cudaMemcpyDeviceToHost,
      StreamB);
end
```

Optimization level	3D mapping	Occlusion	Total
No opt. (-O0)	4338.51	1548.48	5887.01
Opt level 1 (-O1)	2398.85	565.347	2964.22
Opt level 2 (-O2)	903.77	567.345	1471.14
Opt level 3 (-O3)	920.96	575.93	1496.92
Opt level fast (-Ofast)	873.87	566.84	1440.75

Table 10 – The execution time (ms) of the sequential method for multispectral image mapping on point clouds using the compiler icc^{TM}.

After testing the sequential method, the results obtained from the parallel method are presented. Table 11 shows the overall time for mapping 12 and 180 multispectral images on a point cloud of 66 millions 3D points. In this performance evaluation, three executions have been launched, changing the block size to 32, 64 and 128 threads.

Nº of Threads	Overall time (12 images)
32 threads	1243.62
64 threads	902.717
128 threads	893.94

Table 11 – Overall time for mapping 12 multispectral images using the GPU.

In this regard using a block size of 128 threads, an acceleration of 38 % is achieved. Finally, regarding the second training dataset formed by 180

multispectral images, there is a significant increase of the performance in GPU, achieving an acceleration of 91% (Figure 63). While in CPU the executing time is around 24 seconds, the GPU is able to complete the mapping process in two seconds. Undoubtedly, as the dimensionality of data is higher, the performance of the CUDA-developed method achieves a higher acceleration.

Figure 63 – Performance comparison between the sequential and parallel method: (**a**) mapping 12 multispectral images on 3D model, and (**b**) mapping 180 multispectral images on the 3D model.

B

Documentación en Castellano

La actual normativa de la Universidad de Jaén para la defensa de tesis doctorales, adaptada a las directrices del R.D. 99/2011, y aprobada en Consejo de Gobierno el 6 de febrero de 2012 establece que todas las tesis doctorales escritas en un idioma distinto al castellano deberán incluir los siguientes apartados en dicho idioma: título, índice, introducción, resumen y conclusiones. En base a esta normativa se ha incluido el siguiente anexo.

Caracterización espectral y segmentación semántica de modelos 3D complejos en entornos naturales

Juan Manuel Jurado Rodríguez

Directores:
Francisco Ramón Feito Higueruela
Lidia Ortega Alvarado
Juan José Cubillas Mercado

Universidad de Jaén

Departamento de Informática
Escuela Politécnica Superior de Jaén
Universidad de Jaén

Noviembre 2020

Contenidos

Introducción

El uso de modelos tridimensionales para obtener características espaciales y geométricas de escenarios del mundo real se ha hecho cada vez más frecuente gracias al desarrollo de nuevas técnicas dirigidas a su adquisición, procesamiento, visualización o análisis desde distintos campos de investigación como la visión por ordenador, la informática gráfica y la teledetección. Durante los últimos años, la proliferación de una amplia variedad de sensores y cámaras de alta resolución ha dado lugar a la generación de enormes conjuntos de datos de entornos urbanos y naturales para múltiples propósitos. Esta tesis doctoral pone el foco sobre nuevos avances relacionados con la fusión de datos heterogéneos (para integrar datos procedentes de distintos sensores), la visión por ordenador (para obtener información clave de las imágenes y modelos 3D) y el mapeo 3D (para generar modelos 3D enriquecidos a partir de imágenes multiespectrales). Como resultado de esta investigación, se ha desarrollado el software GEU (Geospatial and Environmental tools of University of Jaén) dirigido a la creación, procesamiento y visualización interactiva de escenarios 3D enriquecidos con distintas capas de información temporal.

Esta tesis presenta contribuciones en dos áreas diferentes dentro del campo de la teledetección y la visión por computador: (1) la caracterización multiespectral de modelos 3D (Parte II) y (2) la segmentación semántica de nubes de puntos (Parte III). En el presente capítulo se ofrece una breve introducción a estos ámbitos de estudio, destacando los principales hitos alcanzados en cada uno de ellos.

Caracterización multiespectral de modelos 3D

La primera parte de esta tesis doctoral se centra en la caracterización multiespectral de modelos tridimensionales, con el objetivo de proveer de una herramienta para la monitorización y análisis de entornos reales que han sido modelados en 3D y enriquecidos con rastos espectrales. En la actualidad, el uso de sensores a bordo de Vehículos Aéreos no Tripulados (UAVs, por sus siglas en inglés) hace posible una adquisición eficiente y de alta resolución, tanto espacial como espectral, de escenarios de nuestro entorno. En consecuencia, cada vez son más los estudios que utilizan sensores sobre drones para la captación de distintas variables medioam-

bientales [1, 2]. Los resultados obtenidos en estas aportaciones científicas ponen de manifiesto la calidad de los datos obtenidos con este tipo de sensores logrando una observación más detallada en comparación con otros sistemas de adquisición basados en el uso de satélites o avionetas. No cabe duda que el volumen de datos sobre el territorio está creciendo exponencialmente lo que suscita el desarrollo de nuevas metodologías y técnicas para su óptima explotación y análisis. En esta línea de trabajo, es cada vez más frecuente la utilización conjunta de distintos tipos de sensores con el fin de capturar un mayor número de características del entorno. Sin embargo, la integración de datos para llevar a cabo el proceso de análisis requiere metodologías para la fusión de información heterogénea. En relación, a los avances propuestos en esta tesis doctoral se presenta un método para la fusión de nubes de puntos 3D y datos multiespectrales con el fin de analizar una serie de características que no pueden ser directamente reconocidas en imágenes. Nuestro enfoque se fundamenta en la generación de un modelo 3D, que representa la geometría del área de estudio, y sobre el que se conoce su signatura espectral, que ha sido medida a partir de imágenes multiespectrales tomadas desde múltiples puntos de vista con un sensor espectral a bordo de un dron. Para ello, en primer lugar, se modela el escenario mediante fotogrametría y a continuación, se desarrolla un método capaz de mapear las imágenes multiespectrales sobre el modelo 3D y estudiar la oclusión en la escena. En la Figura 64 se muestran los sensores y tipos de imágenes utilizados para la generación del conjunto de datos de estudio en esta investigación. El software GEU integra este método lo que posibilita un avance significativo en el estado de arte para, de forma totalmente automática, generar, procesar y visualizar eficientemente modelos 3D enriquecidos con rasgos espectrales de carácter multitemporal.

La reconstrucción tridimensional de escenarios naturales supone una tarea compleja, ya que la estructura de la vegetación es irregular, coexisten un gran número de entidades superpuestas y la apariencia cambiante de los materiales dificulta la modelización de ciertas partes del entorno. Sin embargo, el uso sensores abordo de drones hace posible la adquisición de imágenes oblicuas y de alta resolución desde un gran numero de perspectivas con el fin de capturar el entorno con la mayor completitud posible. En cuanto a las principales técnicas utilizadas para la generación de nubes de puntos 3D de escenarios del mundo real se destacan las siguientes: (1) reconstrucción de modelos a partir de sistemas LiDAR

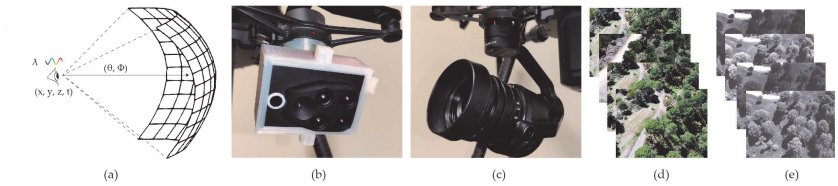

Figura 64 – Materiales y datos utilizados en esta investigación: (**a**) parámetros de captura de una imagen: posición de la cámara (x,y,z), orientación (θ, Φ), ancho de banda (λ) y momento de captura (t), (**b**) sensor multiespectral, (**c**) cámara digital de alta resolución, (**d**) imágenes aéreas RGB y (**e**) imágenes multiespectrales.

(*Light Detection and Ranging*) [3, 4], (2) modelado de entornos a partir de cámaras de profundidad (RGB-D) [5] (3) uso de tecnología SAR (*Synthetic Aperture Radar*), [6] y (4) fotogrametría [7, 8]. En cuanto al uso de las cámaras RGB-D, estos sistemas presentan limitaciones para el modelado de vegetación puesto que la resolución de imagen no es suficiente p ara g enerar l a g eometría c ompleja i nherente a l a m ayoría de estructuras arbóreas o vegetales. Las nubes de puntos SAR se utilizan comúnmente para generar mapas de deformación de la superficie a gran escala o modelos digitales de elevación, así como para proporcionar información 4D. En lo que respecta a la tecnología LiDAR, ésta puede utilizarse para obtener modelos 3D de alta calidad, pero dicha solución es bastante costosa y en muchas ocasiones implica tediosas tareas de adquisición. En lo que respecta a los métodos basados en imágenes, estos están siendo cada vez más utilizados para la modelización de escenarios del mundo real alcanzando resultados de alta calidad geométrica. El conocido algoritmo *structure from motion* (SfM) se integra como parte de la metodología de modelado para generar nubes de puntos en 3D a partir de imágenes tomadas con un alto grado de superposición. El aumento en la resolución de la imagen, así como la captura de múltiples tomas desde distintos puntos de vista hace posible la reconstrucción con un alto detalle geométrico de modelos tridimensionales que representan formas complejas en entornos reales. En este sentido, la nube de puntos es el tipo de datos más utilizado para la representación en 3D de escenarios representativos de nuestro entorno. A pesar de que la generación de modelos volumétricos es posible mediante la aplicación de métodos de triangulación o modelado inverso [9], en esta investigación se toma la nube de puntos como objeto de estudio sobre el que se van a aplicar el conjunto de algoritmos desarrollados.

La observación de fenómenos físicos más allá del espectro visible es en muchos casos la técnica de monitorización más utilizada para la detección de características significativas en entornos naturales. Esto se debe al impacto que tiene la respuesta espectral de las entidades naturales sobre su apariencia, estado fisiológico y morfológico. La reflectancia espectral es una característica clave que ha sido estudiada para conocer las propiedades de los materiales, estado de salubridad de las plantas e impacto de distintos efectos medioambientales en entornos naturales. La medición de la reflectancia puede llevarse a cabo utilizando sensores multiespectrales o hiperespectrales [10]. Estos son capaces de obtener la cantidad de luz reflejada que posteriormente es calibrada considerando la luz incidente para generar los mapas de reflectancia. Tradicionalmente, los datos multiespectrales se han estudiado a partir de la generación de mapas bidimensionales lo que supone una importante pérdida de información acerca de las partes laterales e internas de estructuras vegetales. Para superar esta limitación, el método que se propone, para la generación de modelos 3D enriquecidos con datos multiespectrales, posibilita una nueva metodología de estudio y evaluación del desarrollo de escenarios naturales, atendiendo a la relación de sus estructuras tridimensionales y su comportamiento espectral. Además, estos escenarios naturales, que habitualmente son bastante extensos, pueden ser inspeccionados en un entorno 3D sobre el que se puede interaccionar y gestionar la visibilidad de varias capas de información que representan diferentes características del modelo o distintas series temporales. Esto significa un importante avance para el procesamiento de los datos multiespectrales en un entorno tridimensional y así, alcanzar un análisis más preciso sobre entornos naturales caracterizados por su carácter cambiante y por su complejidad desde el punto de vista geométrico.

En particular, esta tesis aporta las siguientes contribuciones: (i) fusión de información capturada con distintos sensores, (ii) mapeo de imágenes multiespectral sobre nubes de puntos 3D, (iii) test de oclusión desde múltiples puntos de vista en un escenario 3D, (iv) monitorización multitemporal en plantaciones de olivar y (v) caracterización espectral y morfológica de especies arbóreas en zonas forestales.

Segmentación semántica de nubes de puntos

El reconocimiento de escenarios del mundo real se ha hecho cada vez más frecuente debido al desarrollo de métodos orientados a la segmentación semántica en el campo de la visión por ordenador. En los últimos años, se ha propuesto una amplia variedad de estudios basados en aprendizaje profundo (*Deep Learning*) para reconocer automáticamente distintos tipos de objetos en imágenes espectrales o RGB [11, 12]. Más recientemente, la rápida adquisición de datos 3D, mediante el uso de sensores que aportan información de profundidad de la escena capturada, requiere el desarrollo de nuevos enfoques dirigidos a trabajar sobre escenarios tridimensionales de los que se conoce su geometría e información adicional como la reflectancia espectral [13]. En esta investigación, la fusión de datos procedentes de distintos sensores y el desarrollo de métodos basados en el procesamiento de modelos 3D es la base de la innovación hacia nuevos avances relacionados con la segmentación semántica de materiales en entornos naturales y el reconocimiento de patrones geométricos en nubes de puntos 3D.

La caracterización de entornos naturales a partir de la observación precisa sobre el comportamiento espectral que presentan los materiales existentes es de gran interés en el ámbito de la teledetección y la visión por computador. Con la llegada de nuevos sensores capaces de adquirir eficientemente variables de nuestro entorno se genera un conocimiento detallado sobre el conjunto de entidades naturales que coexisten en el ecosistema. A pesar de que se logra la modelización de entornos naturales cada vez a mayor resolución espacial, el reconocimiento y clasificación semántica del conjunto de elementos que lo componen no es una tarea trivial. La segmentación automática de materiales del mundo real es una tarea compleja puesto que se tratan escenas geométricamente complejas y que presentan una apariencia cambiante debido a una iluminación muy irregular. Nuestra investigación en esta área, pretende aportar soluciones para (i) la segmentación de materiales naturales que pueden presentar una apariencia similar en el espectro visible y (ii) el reconocimiento automático de la posición de cada vid a lo largo del viñedo para poder así, llevar a cabo una monitorización individual de cada cultivo.

En primer lugar, se ha desarrollado un método que se sirve de los modelos 3D enriquecidos con información multiespectral para detectar

distintos tipos de materiales en una nube de puntos donde coexisten varios tipos de entidades naturales. La adquisición de los datos se ha llevado a cabo utilizando un sistema que integra una cámara de alta resolución y un sensor multiespectral de tal forma que se puede capturar simultáneamente tanto imágenes RGB como imágenes multiespectral sobre el área de estudio. Inicialmente, las imágenes RGB de entrada se procesan para generar una nube de puntos aplicando el algoritmo *structure from motion* (SfM). A continuación, las imágenes multiespectrales son mapeadas sobre la nube de puntos con el fin de enriquecer la geometría del modelo con valores reflectancia medidos en distintos longitudes de onda (verde, rojo, bordes rojos e infrarrojo cercano). Así, cada punto 3D del modelo queda caracterizado por la reflectancia, su color visible y su posición en la escena. Todas estas características son utilizadas para reconocer aquellos puntos 3D que presentan un patrón similar atendiendo a sus rasgos espectrales y a la proximidad entre ellos. Para ello, se aplica un método basado en agrupamiento jerárquico con el fin de generar varios subconjuntos en la nube de puntos que compartan características similares. Como resultado, el tronco del árbol, las hojas, la hierba, el suelo y las rocas pueden ser reconocidas en el área de estudio. Estos resultados demuestran la viabilidad de nuestro método para reconocer materiales naturales en escenarios 3D, incluso aquellos que presentan una apariencia similar en el espectro visible pero diferencias claves en algunas longitudes de onda estudiadas. Del mismo modo, esta aplicación pone en valor el uso de modelos 3D enriquecidos con información espectral para la segmentación semántica de materiales en entornos naturales.

En segundo lugar, hemos presentado un método que supone un avance significativo en la monitorización sobre viñedos. En concreto, se ha desarrollado un algoritmo para el reconocimiento de troncos de vides utilizando características geométricas extraídas de una nube de puntos que representa un viñedo. En este sentido, para alcanzar una gestión eficiente de los viñedos se requiere de herramientas capaces de identificar plantas individuales de forma automática. En los últimos años, el uso de drones se ha convertido en una de las principales fuentes de información para la monitorización en aplicaciones relacionadas con la viticultura de precisión. De hecho, gracias a estos sistemas de adquisición se pueden capturar imágenes con las generar modelos 3D de gran densidad de puntos de tal forma que se pueda modelar la estructura y forma tridimensional de las vides. Esto hace posible el reconocimiento de

importantes características geométricas de cara a identificar cada planta aislando el resto de geometría del entorno. A pesar de la proliferación de tecnologías innovadoras en la viticultura, la identificación de las vides individuales se sirven en técnicas de segmentación basadas en imágenes, considerando generalmente una distancia fija de separación entre ellas. Nuestro método se centra en el reconocimiento de parámetros geométricos clave para asegurar la existencia de cada planta en el modelo 3D. Esta solución representa un avance importante para posibilitar un seguimiento exhaustivo de cada vid existente en la plantación a partir de su ubicación que se obtiene aplicando el método propuesto.

En resumen, las principales contribuciones en este campo son: (i) la segmentación automática de materiales naturales basada en clasificación no supervisada, (ii) una metodología eficiente para generar modelos 3D etiquetados, (iii) el reconocimiento automático de vides individuales a partir de parámetros geométricos, sin requerir ningún conocimiento previo sobre la plantación y (iv) la estimación de las plantas que faltan y que deben ser replantadas en los viñedos para optimizar la producción de la cosecha.

Objetivos

El objetivo general de esta tesis es proponer varios avances para la caracterización espectral de entornos naturales y la segmentación semántica de escenarios 3D. El núcleo principal de esta investigación es la generación de nubes de puntos enriquecidas a partir de imágenes multiespectrales. Los modelos resultantes son de gran ayuda a fin de potenciar la investigación en el campo de la teledetección y visión por computador. En esta investigación se han desarrollado varias casos prácticos que ponen en valor el uso de modelos 3D enriquecidos con información espectral tales como la monitorización multitemporal sobre una plantación de olivar y el estudio del impacto de la reflectancia sobre la estructura 3D de distintas especies arbóreas. Los hitos conseguidos en esta primera parte nos han conducido al desarrollo de nuevos métodos orientados a la segmentación semántica de escenarios naturales. En este sentido se ha trabajado en el reconocimiento automático de materiales analizando tanto características espaciales y multiespectrales de cada uno de los objetos reconstruidos. Por último, se propone un método innovador en el sector de la viticultura para el reconocimiento de la posición de cada vid, así

como la detección de huecos sin plantas a lo largo del viñedo.

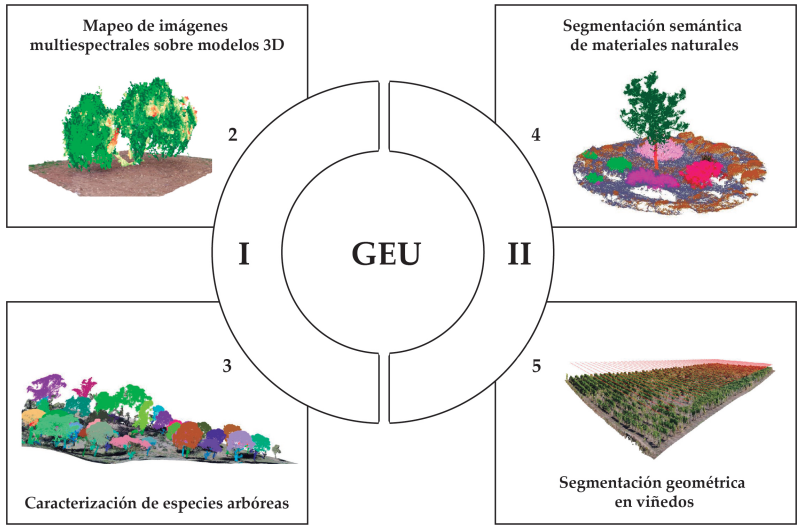

Figura 65 – Objetivos principales abordados en esta tesis doctoral.

En la Figura 65 se presenta una visión general de los resultados obtenidos en cada una de las partes que componen esta investigación. Esta tesis doctoral se caracteriza por su carácter multidisciplinar, puesto que los avances y metodologías propuestas aportan soluciones en distintos campos de estudio relacionados con el procesamiento de imágenes multiespectrales, la fusión de datos heterogéneos, el inventario forestal, la monitorización multitemporal en cultivos de olivar y viñedos y la segmentación semántica de materiales en escenarios 3D. Como resultado de esta investigación se ha desarrollado la herramienta GEU, que integra el conjunto de métodos propuestos. Actualmente, se está trabajando sobre nuevas funcionalidades de GEU para abordar varios problemas, que son presentados como trabajo futuro en el Capítulo 6.

A continuación, se enumeran los objetivos específicos abordados en cada trabajo:

- El desarrollo de un nuevo método de mapeo de imágenes multiespectrales sobre nubes de puntos que representan escenarios del mundo real. Este método debería ser capaz de procesar imágenes multiespectrales para (1) obtener los mapas de reflectancia para cada captura, (2) cálculo de la oclusión en el entorno 3D, (3) mapear

cada punto 3D sobre aquellos píxeles desde los que es visible en la imagen y (4) posibilitar la integración de datos multitemporales en el modelo 3D. Los resultados deben ser modelos 3D enriquecidos con varias capas de información, que pueden ser inspeccionados mediante una visualización eficiente e interactiva en un entorno 3D.

- El desarrollo de una aplicación, que se sirva del método anterior, para caracterizar varias especies de árboles sobre una nube de puntos representativa del bosque Mediterráneo y así, estudiar la relación entre los rasgos morfológicos y multiespectrales de cada una de ellas. Para ello, se requiere la detección de árboles individuales en la nube de puntos, obtener características relativas a la estructura 3D y analizar el impacto que tiene sobre esta la reflectancia espectral.

- La segmentación semántica de nube puntos para el reconocimiento de materiales del mundo real aplicando técnicas de clasificación no supervisada. El algoritmo propuesto utiliza variables espaciales extraídas de una nube de puntos y rasgos multiespectrales para identificar materiales naturales similares. Como resultado se genera un modelo etiquetado en el que para cada punto 3D se conoce su material. La técnica presentada es de gran utilidad para la generación automática de modelos 3D etiquetados, ampliamente utilizados en trabajos relacionados con el aprendizaje profundo.

- El desarrollo de un método para la detección del tronco de la vid, utilizando características espaciales y geométricas de la nube de puntos. Este avance se centra en el reconocimiento de parámetros geométricos clave para asegurar la existencia de cada planta en el modelo 3D. El método propuesto es capaz de identificar los troncos individuales, los postes y aquellos huecos sin plantas permitiendo así, una localización tridimensional exacta de cada planta y la posibilidad de desarrollar estudios multitemporales.

Estructura de la tesis

La presente tesis doctoral queda dividida en cuatro partes organizadas en un conjunto de capítulos:

- PARTE I: se incluye el presente capítulo para presentar un panorama general del tema de investigación y las principales contribuciones y objetivos de esta tesis doctoral. Además, se mencionan los resultados y contribuciones logradas hasta la fecha.

- PARTE II: se presenta el núcleo principal de la herramienta GEU que tiene como principal objetivo la caracterización multiespectral de modelos 3D. En el Capítulo 2 se aborda el problema de la fusión de datos heterogéneos, imágenes multiespectrales y nubes de puntos. Se describen las principales etapas del método para asociar cada punto 3D con sus correspondientes píxeles en la imagen multiespectral. Además, en este proceso, se estudia la oclusión en la escena con el fin de evitar mapear puntos que son ocluidos. Así, se genera una nube de puntos enriquecida de tal manera que cada punto 3D almacena varios valores de reflectancia espectral correspondientes a diferentes longitudes de onda. Actualmente, este método se está optimizando utilizando la unidad de procesamiento gráfico (GPU) para acelerar el rendimiento y, por lo tanto, permitir el uso de modelos 3D de mayor tamaño y densidad. Este último trabajo se presenta como una investigación futura, ya que esta implementación está aún en desarrollo. En el Capítulo 3 abordamos un novedoso estudio centrado en la caracterización de rasgos morfológicos y espectrales de diferentes especies de árboles en una zona forestal. Este avance posibilita la documentación detallada del comportamiento espectral que presentan arboles de igual o distinta especie y el estudio de la biodiversidad, teniendo información detallada acerca de la geometría de la planta y la reflectancia espectral a lo largo de su estructura tridimensional.

- PARTE III: se proponen una serie de avances entorno a un problema de gran interés por la comunidad científica relacionado con la segmentación semántica de modelos 3D, que han sido reconstruidos del mundo real. El Capítulo 4 se centra en la segmentación de materiales naturales utilizando tanto características espaciales como espectrales del modelo 3D. Como resultado, se obtiene una nube de puntos etiquetada que resulta de gran interés para su aplicación en campos relacionados con el aprendizaje profundo. En el Capítulo 5 se describe el desarrollo de un método para la detección individual de plantas en viñedos mediante la detección de troncos, aplicando algoritmos geométricos sobre la nube de puntos. Ade-

más, el método propuesto es capaz de distinguir postes, así como los huecos sin plantas que hay a lo largo de cada hilera del viñedo. Los resultados de este estudio posibilitan el seguimiento individual de cada vid, estudios multitemporales y la elaboración de sistemas de decisión de apoyo más precisos para una gestión óptima de los viñedos.

- Parte IV: se concluye destacando las principales contribuciones de la tesis doctoral y se mencionan una serie de desafíos sobre varios problemas abiertos que pueden abordarse como investigación futura.

Esta investigación y sus contribuciones no habrían sido posibles sólo por mí mismo. De hecho, muchos de los trabajos presentados en esta tesis doctoral han sido realizados en colaboración con otros investigadores. Para favorecer la legibilidad, al principio de cada capítulo se describe y contextualiza el trabajo presentado.

Conclusiones

En esta tesis se han presentado una serie de contribuciones en áreas relacionadas con la teledetección y la visión por computador: (1) la caracterización multiespectral de modelos 3D y (2) la segmentación semántica y reconocimiento de formas geométricas en nubes de puntos. El carácter multidisciplinar de esta investigación pone de manifiesto la motivación del autor por el avance del conocimiento en distintas áreas que sin duda convergen en campos de aplicación cuya innovación requiere de una perspectiva transversal. La primera parte de esta investigación se centra en la caracterización de modelos 3D a partir de imágenes multiespectrales. La segunda parte tiene como objetivo el desarrollo de métodos para la segmentación semántica de materiales en un escenario natural 3D y el reconocimiento de patrones geométricos como el tronco de una vid para su localización automática en una plantación. Como resultado de la investigación llevada a cabo en esta tesis, se ha desarrollado el software GEU (Geospatial and Environmental tools of University of Jaén) que integra el conjunto de métodos implementados. De esta forma, se pretende acercar nuestra solución al sector industrial y promover la transferencia de los resultados derivados de esta investigación.

Principales contribuciones y trabajo futuro

Caracterización multiespectral de modelos 3D. En esta prime-ra parte de la tesis se han descrito dos líneas de trabajo. En primer lugar, en el Capítulo 2 se ha presentado el método para el mapeo de imágenes multiespectrales sobre nubes de puntos relativas a una plantación de oli-var. El desarrollo de este método ha posibilitado el estudio conjunto de variables morfológicas y espectrales de plantas individuales que han sido automáticamente identificadas en la nube de puntos atendiendo a su sig-natura espectral. El método propuesto integra el cálculo de la oclusión para evitar el mapeo de puntos ocluidos sobre píxeles desde donde no son visibles en la imagen. Como resultado, se obtiene una nube de puntos en-riquecida con información espectral de tal modo que para cada punto 3D se tienen una serie de valores de reflectancia en cada una de las longitudes de onda observadas. Junto al desarrollo del método, se ha trabajado en la visualización de los resultados con el fin de mejorar la inspección vi-sual del modelo 3D y poder así realizar un análisis y evaluación más precisos sobre el estado de salubridad de los cultivos.

En este trabajo se ha desarrollado un estudio multitemporal comparando la evolución, entre dos campañas, de las variables morfológicas y espec-trales monitorizadas para cada planta. Nuestra investigación toma como objeto de estudio el olivo, de tal forma que los avances alcanzados tienen un impacto directo sobre la gestión eficiente de plantaciones de olivar, un sector que desempeña un papel fundamental en Jaén y en el panorama internacional, y que requiere de nuevas soluciones para la maximización de la rentabilidad en cada etapa del ciclo productivo. Como trabajos futuros se prevén varias aplicaciones basadas en el desarrollo de modelos predictivos para el estudio de enfermedades y la predicción temprana de cosecha utilizando todos los atributos que nuestro método asocia a cada olivo. El trabajo realizado en esta tesis proporciona una información clave para continuar en la propuesta de nuevos métodos en el marco del software GEU y otras investigaciones transversales que tengan como objetivo potenciar el sector del olivar.

En segundo lugar, en el Capítulo 3 se ha trabajado en la caracterización multiespectral de distintas especies arbóreas (pino, encina y eucalipto) y el estudio de sus estructuras en 3D. Seguidamente, se ha estudiado la correlación entre parámetros morfológicos y espectrales de cada especie a partir del estudio individualizado de cada árbol. Se pretende así, analizar el impacto de la reflectancia observada en la copa de los árboles sobre la estructura tridimensional de la planta. En este otro campo de aplicación se demuestra la utilidad del método propuesto, en el trabajo anterior, para llevar a cabo una caracterización detallada de un escenario en el que coexiste vegetación alta y baja, así como distintos tipos de árboles cuyo crecimiento está influenciado por variables de su entorno. En esta línea surgen trabajos futuros de gran interés centrados en el estudio de la biodiversidad, creación de un inventario forestal y estudio sobre el desarrollo de la vegetación en relación a la competencia de recursos naturales y el impacto que esta tiene sobre su crecimiento. Esta utilidad provista en GEU supone un gran avance tanto para investigaciones en curso sobre la conservación y monitorización de zonas boscosas, así como para trabajos futuros hacia una gestión integral para conocer el estado y evolución de extensas áreas de bosque.

Segmentación semántica de nubes de puntos. En esta segunda parte de la tesis se han propuesto una serie avances para el reconocimiento de materiales en un entorno natural reconstruido en 3D

y para la localización individual de plantas en viñedos a partir del reconocimiento del tronco. En primer lugar, en el Capítulo 4 se ha abordado el problema de la segmentación de materiales que presentan una apariencia similar en el espectro visible. El método propuesto se basa en el agrupamiento jerárquico y la caracterización multiespectral de la escena 3D para reconocer cada material. Se utilizan variables espaciales y multiespectrales para identificar para cada nivel aquel subconjunto de puntos que presentan una mayor diferencia con respecto a los demás. Se consigue así, diferenciar las rocas, el terreno, el tronco, las hojas y vegetación baja en el entorno muestreado. Como resultado se obtiene una nube de puntos etiquetada por cada uno de los materiales identificados. La generación de estos conjuntos de datos, ya clasificados, son de gran interés para aplicaciones relacionadas con la visión por computador y metodologías basadas en Deep Learning, campos de exploración que se pretende abordar a futuro.

En segundo lugar, en el Capítulo 5 se presenta el trabajo llevado a cabo para la segmentación de vides utilizando únicamente la nube de puntos que ha sido reconstruida a partir de imágenes aéreas tomadas con un dron. El método desarrollado integra una serie de algoritmos geométricos para el reconocimiento de cada tronco eliminando primeramente el terreno y las hojas. Posteriormente, se aplica un agrupamiento espacial para segmentar el modelo y reconocer los troncos de las vides modeladas. Como resultado del método se obtiene la localización de cada vid y se identifican aquellos huecos que no contienen plantas a lo largo de cada línea del viñedo. Así, este método pretende resolver las limitaciones existentes para la detección individual de plantas en viñedos haciendo uso del conocimiento extraído del modelo 3D. Este avance da paso a trabajos futuros relacionados con la monitorización individual de cada vid y el desarrollo de nuevos sistemas de apoyo a la toma de decisión más precisos para aumentar la producción en viñedos.

El conjunto de trabajos presentados en esta tesis asienta la base de una línea de investigación sobre la que se continúa trabajando con relevantes aportaciones científicas en marcha que pretende incrementar las funcionalidades del sistema GEU aportando soluciones relacionadas con: (1) la integración de datos térmicos para análisis en cultivos, (2) procesamiento de imágenes hiperespectrales, (3) generación de nubes de puntos hiperespectrales, (4) segmentación de materiales del mundo real a

partir de imágenes hiperespectrales y (5) aceleración en GPU del método para el mapeo de imágenes sobre nubes de puntos de gran tamaño. Algunos de estos trabajos ya están muy avanzados pendientes aún de su publicación en revistas de investigación de alto impacto científico. No cabe duda que los avances resultantes de esta tesis doctoral abren nuevos campos para la investigación, innovación y desarrollo teniendo por bandera el aporte del conocimiento obtenido a partir de modelos 3D que representan escenarios del mundo real y que, además, son enriquecidos por información procedente de distintos sensores.

Reflexión personal

El trabajo realizado en esta tesis me ha permitido adquirir madurez tanto en lo profesional como en lo personal resolviendo problemas complejos y trabajando en equipo para la resolución de los mismos. Durante estos años he mejorado mis conocimientos en áreas de trabajo marcadas por su carácter multidisciplinar y he desarrollado nuevas habilidades de cara a trabajar de forma cooperativa entre investigadores de distintas áreas que aportan visiones diferentes para abordar los retos estudiados. No cabe duda que gracias a la composición de estos equipos de trabajo, esta investigación se ha visto enormemente potenciada hacia campos de aplicación diferentes entre sí. Por otro lado, la oportunidad de supervisar a los estudiantes ha sido una labor gratificante con la que he aprendido a motivarlos y aconsejarlos por el camino más adecuado teniendo en cuenta sus objetivos. Asimismo, tener la oportunidad de participar en proyectos de investigación supuso un gran desafío, pero al mismo tiempo una gran satisfacción. Sin duda, estos años han sido una experiencia muy enriquecedora.

Bibliography

[1] L. Pádua, T. Adão, A. Sousa, E. Peres, and J. J. Sousa, "Individual grapevine analysis in a multi-temporal context using uav-based multi-sensor imagery," *Remote Sensing*, vol. 12, no. 1, p. 139, 2020.

[2] L. Comba, A. Biglia, D. R. Aimonino, P. Barge, C. Tortia, and P. Gay, "2d and 3d data fusion for crop monitoring in precision agriculture," in *2019 IEEE International Workshop on Metrology for Agriculture and Forestry (MetroAgriFor)*, pp. 62–67, IEEE, 2019.

[3] J. Degerickx, D. Roberts, J. McFadden, M. Hermy, and B. Somers, "Urban tree health assessment using airborne hyperspectral and lidar imagery," *International Journal of Applied Earth Observation and Geoinformation*, vol. 73, pp. 26 – 38, 2018.

[4] S. Hu, Z. Li, Z. Zhang, D. He, and M. Wimmer, "Efficient tree modeling from airborne lidar point clouds," *Computers and Graphics*, vol. 67, pp. 1 – 13, 2017.

[5] M. Zollhöfer, P. Stotko, A. Görlitz, C. Theobalt, M. Nießner, R. Klein, and A. Kolb, "State of the art on 3d reconstruction with rgb-d cameras," *Computer Graphics Forum*, vol. 37, no. 2, pp. 625–652, 2018.

[6] M. Heublein, F. Alshawaf, B. Erdnüß, X. X. Zhu, and S. Hinz, "Compressive sensing reconstruction of 3d wet refractivity based on gnss and insar observations," *Journal of Geodesy*, vol. 93, no. 2, pp. 197–217, 2019.

[7] J. Iglhaut, C. Cabo, S. Puliti, L. Piermattei, J. O'Connor, and J. Rosette, "Structure from motion photogrammetry in forestry: A review," *Current Forestry Reports*, vol. 5, no. 3, pp. 155–168, 2019.

[8] J. L. Schönberger and J. Frahm, "Structure-from-motion revisited," in *2016 IEEE Conference on Computer Vision and Pattern Recognition (CVPR)*, pp. 4104–4113, 2016.

[9] O. Stava, S. Pirk, J. Kratt, B. Chen, R. Mundefinedch, O. Deussen, and B. Benes, "Inverse procedural modelling of trees," *Comput. Graph. Forum*, vol. 33, p. 118–131, Sept. 2014.

[10] T. Adão, J. Hruška, L. Pádua, J. Bessa, E. Peres, R. Morais, and J. J. Sousa, "Hyperspectral imaging: A review on uav-based sensors, data processing and applications for agriculture and forestry," *Remote Sensing*, vol. 9, no. 11, p. 1110, 2017.

[11] M. Siam, M. Gamal, M. Abdel-Razek, S. Yogamani, and M. Jagersand, "Rtseg: Real-time semantic segmentation comparative study," in *2018 25th IEEE International Conference on Image Processing (ICIP)*, pp. 1603–1607, IEEE, 2018.

[12] L. Jiang, H. Zhao, S. Liu, X. Shen, C.-W. Fu, and J. Jia, "Hierarchical point-edge interaction network for point cloud semantic segmentation," in *Proceedings of the IEEE International Conference on Computer Vision*, pp. 10433–10441, 2019.

[13] Y. Xie, J. TIAN, and X. Zhu, "Linking points with labels in 3d: A review of point cloud semantic segmentation," *IEEE Geoscience and Remote Sensing Magazine*, p. 0–0, 2020.

[14] L. Pádua, P. Marques, J. Hruška, T. Adão, J. Bessa, A. Sousa, E. Peres, R. Morais, and J. J. Sousa, "Vineyard properties extraction combining uas-based rgb imagery with elevation data," *International Journal of Remote Sensing*, vol. 39, no. 15-16, pp. 5377–5401, 2018.

[15] J. M. Jurado, L. Ortega, J. J. Cubillas, and F. R. Feito, "Multispectral mapping on 3d models and multi-temporal monitoring for individual characterization of olive trees," *Remote Sensing*, vol. 12, p. 1106, Mar 2020.

[16] J. Jurado, L. Ortega, and F. Feito, "3D Mapping Approach to Analyze the Evolution of Vegetation Using Multispectral Imagery," in *Spanish Computer Graphics Conference (CEIG)* (I. García-Fernández and C. Ureña, eds.), The Eurographics Association, 2018.

[17] J. M. Jurado, M. Ramos, C. Enríquez, and F. Feito, "The impact of canopy reflectance on the 3d structure of individual trees in a mediterranean forest," *Remote Sensing*, vol. 12, p. 1430, May 2020.

[18] J. M. Jurado, J. L. Cárdenas, C. J. Ogayar, L. Ortega, and F. R. Feito, "Semantic segmentation of natural materials on a point cloud using spatial and multispectral features," *Sensors*, vol. 20, p. 2244, Apr 2020.

[19] J. M. Jurado., J. L. Cárdenas., C. J. Ogayar., L. Ortega., and F. R. Feito., "Accurate plant modeling based on the real light incidence,"

in *Proceedings of the 14th International Joint Conference on Computer Vision, Imaging and Computer Graphics Theory and Applications - Volume 1: GRAPP,*, pp. 360–366, INSTICC, SciTePress, February 2019.

[20] J. M. Jurado, L. Pádua, F. R. Feito, and J. J. Sousa, "Automatic grapevine trunk detection on uav-based point cloud," *Remote Sensing*, vol. 12, p. 3043, Sep 2020.

[21] L. M. Ortega, J. M. Jurado, J. L. L. Ruiz, and F. R. Feito, "Topological data models for virtual management of hidden facilities through digital reality," *IEEE Access*, vol. 8, pp. 62584–62600, 2020.

[22] C. Enríquez, J. M. Jurado, A. Bailey, D. Callén, M. J. Collado, G. Espina, P. Marroquín, E. Oliva, E. Osla, M. I. Ramos, and et al., "The uas-based 3d image characterization of mozarabic church ruins in bobastro (malaga), spain," *Remote Sensing*, vol. 12, p. 2377, Jul 2020.

[23] M. I. Ramos, J. J. Cubillas, J. M. Jurado, W. Lopez, F. R. Feito, M. Quero, and J. M. Gonzalez, "Prediction of the increase in health services demand based on the analysis of reasons of calls received by a customer relationship management," *The International Journal of Health Planning and Management*, vol. 34, no. 2, pp. e1215–e1222, 2019.

[24] M. I. Ramos, J. M. Jurado, J. L. Cárdenas, C. Enríquez, L. Ortega, M. L. Martínez, F. R. Feito, and J. J. Cubillas, "High precision geomatic tools for improving harvest of olive grove in advance," in *International Congress on Engineering and Sustainability in the XXI Century*, pp. 691–700, Springer, 2019.

[25] J.-L. Cárdenas, J.-M. Jurado, L. Ortega, M.-I. Ramos, C. Enríquez, and F. Feito, "3d farm management information system for precision agriculture," in *International Congress on Engineering and Sustainability in the XXI Century*, pp. 778–785, Springer, 2019.

[26] D. J. Rodríguez, J. M. J. Rodríguez, L. O. Alvarado, and F. R. F. Higueruela, "3D Environment Understanding in Real-time Using Input CAD Models for AR Applications," in *Spanish Computer Graphics Conference (CEIG)* (D. Casas and A. Jarabo, eds.), The Eurographics Association, 2019.

[27] A. L. Ruiz, J. M. J. Rodríguez, C. J. O. Anguita, and F. R. F. Higueruela, "Multispectral Registration, Undistortion and Tree

Detection for Precision Agriculture," in *Spanish Computer Graphics Conference (CEIG)* (D. Casas and A. Jarabo, eds.), The Eurographics Association, 2019.

[28] J. M. Jurado, A. Graciano, L. Ortega, and F. R. Feito, "Web-based gis application for real-time interaction of underground infrastructure through virtual reality," in *Proceedings of the 25th ACM SIGSPATIAL International Conference on Advances in Geographic Information Systems*, SIGSPATIAL '17, (New York, NY, USA), Association for Computing Machinery, 2017.

[29] J. Carlos Rodriguez-Cohard and M. Parras, "The olive growing agri-industrial district of jaén and the international olive oils cluster," *The Open Geography Journal*, vol. 4, no. 1, 2011.

[30] D. J. Mulla, "Twenty five years of remote sensing in precision agriculture: Key advances and remaining knowledge gaps," *Biosystems engineering*, vol. 114, no. 4, pp. 358–371, 2013.

[31] K. Karantzalos and D. Argialas, "Towards automatic olive tree extraction from satellite imagery," in *Geo-Imagery Bridging Continents. XXth ISPRS Congress*, pp. 12–23, Citeseer, 2004.

[32] M. Ramos, A. Gil, F. Feito, and A. García-Ferrer, "Using gps and gis tools to monitor olive tree movements," *Computers and electronics in agriculture*, vol. 57, no. 2, pp. 135–148, 2007.

[33] I. N. Daliakopoulos, E. G. Grillakis, A. G. Koutroulis, and I. K. Tsanis, "Tree crown detection on multispectral vhr satellite imagery," *Photogrammetric Engineering & Remote Sensing*, vol. 75, no. 10, pp. 1201–1211, 2009.

[34] G. Sepulcre-Cantó, P. J. Zarco-Tejada, J. Jiménez-Muñoz, J. Sobrino, E. De Miguel, and F. J. Villalobos, "Detection of water stress in an olive orchard with thermal remote sensing imagery," *Agricultural and Forest Meteorology*, vol. 136, no. 1-2, pp. 31–44, 2006.

[35] R. Calderón, J. Navas-Cortés, and P. Zarco-Tejada, "Early detection and quantification of verticillium wilt in olive using hyperspectral and thermal imagery over large areas," *Remote Sensing*, vol. 7, no. 5, pp. 5584–5610, 2015.

[36] P. Zarco-Tejada, C. Camino, P. Beck, R. Calderon, A. Hornero, R. Hernández-Clemente, T. Kattenborn, M. Montes-Borrego, L. Susca, M. Morelli, *et al.*, "Previsual symptoms of xylella fastidiosa infection revealed in spectral plant-trait alterations," *Nature plants*, vol. 4, no. 7, p. 432, 2018.

[37] J. Gago, C. Douthe, R. Coopman, P. Gallego, M. Ribas-Carbo, J. Flexas, J. Escalona, and H. Medrano, "Uavs challenge to assess water stress for sustainable agriculture," *Agricultural Water Management*, vol. 153, pp. 9 – 19, 2015.

[38] F. López-Escudero, C. Del Río, J. Caballero, and M. Blanco-López, "Evaluation of olive cultivars for resistance to verticillium dahliae," *European Journal of Plant Pathology*, vol. 110, no. 1, pp. 79–85, 2004.

[39] G. Grenzdörffer, A. Engel, and B. Teichert, "The photogrammetric potential of low-cost uavs in forestry and agriculture," *The International Archives of the Photogrammetry, Remote Sensing and Spatial Information Sciences*, vol. 31, no. B3, pp. 1207–1214, 2008.

[40] S. Manfreda, M. F. McCabe, P. E. Miller, R. Lucas, V. Pajuelo Madrigal, G. Mallinis, E. Ben Dor, D. Helman, L. Estes, G. Ciraolo, J. Müllerová, F. Tauro, M. I. De Lima, J. L. M. P. De Lima, A. Maltese, F. Frances, K. Caylor, M. Kohv, M. Perks, G. Ruiz-Pérez, Z. Su, G. Vico, and B. Toth, "On the use of unmanned aerial systems for environmental monitoring," *Remote Sensing*, vol. 10, no. 4, 2018.

[41] G. Tmušić, S. Manfreda, H. Aasen, M. R. James, G. Gonçalves, E. Ben-Dor, A. Brook, M. Polinova, J. J. Arranz, J. Mészáros, R. Zhuang, K. Johansen, Y. Malbeteau, I. P. de Lima, C. Davids, S. Herban, and M. F. McCabe, "Current practices in uas-based environmental monitoring," *Remote Sensing*, vol. 12, no. 6, 2020.

[42] P. K. Freeman and R. S. Freeland, "Agricultural uavs in the us: potential, policy, and hype," *Remote Sensing Applications: Society and Environment*, vol. 2, pp. 35–43, 2015.

[43] F. Vanegas, D. Bratanov, K. Powell, J. Weiss, and F. Gonzalez, "A novel methodology for improving plant pest surveillance in vineyards and crops using uav-based hyperspectral and spatial data," *Sensors*, vol. 18, no. 1, p. 260, 2018.

[44] J. Maschler, C. Atzberger, and M. Immitzer, "Individual tree crown segmentation and classification of 13 tree species using airborne hyperspectral data," *Remote Sensing*, vol. 10, no. 8, p. 1218, 2018.

[45] J. A. J. Berni, P. J. Zarco-Tejada, L. Suarez, and E. Fereres, "Thermal and narrowband multispectral remote sensing for vegetation monitoring from an unmanned aerial vehicle," *IEEE Transactions on Geoscience and Remote Sensing*, vol. 47, pp. 722–738, March 2009.

[46] L. Santesteban, S. Di Gennaro, A. Herrero-Langreo, C. Miranda, J. Royo, and A. Matese, "High-resolution uav-based thermal imaging to estimate the instantaneous and seasonal variability of plant water status within a vineyard," *Agricultural Water Management*, vol. 183, pp. 49–59, 2017.

[47] J. Torres-Sánchez, F. López-Granados, and J. Peña, "Mapping olive-tree geometric features from 3d models generated with an unmanned aerial vehicle," in *Precision agriculture'15*, pp. 89–99, Wageningen Academic Publishers, 2015.

[48] A. I. De Castro, P. Rallo, M. Suárez, J. Torres Sánchez, L. Casanova, F. M. Jiménez-Brenes, A. Morales-Sillero, R. Jiménez, and F. López-Granados, "High-throughput system for the early quantification of major architectural traits in olive breeding trials using uav images and obia techniques," *Frontiers in Plant Science*, vol. 10, p. 1472, 2019.

[49] X. Dong, Z. Zhang, R. Yu, Q. Tian, and X. Zhu, "Extraction of information about individual trees from high-spatial-resolution uav-acquired images of an orchard," *Remote Sensing*, vol. 12, no. 1, p. 133, 2020.

[50] J. Torres-Sánchez, F. López-Granados, N. Serrano, O. Arquero, and J. M. Peña, "High-throughput 3-d monitoring of agricultural-tree plantations with unmanned aerial vehicle (uav) technology," *PloS one*, vol. 10, no. 6, p. e0130479, 2015.

[51] R. Díaz-Varela, R. de la Rosa, L. León, and P. Zarco-Tejada, "High-resolution airborne uav imagery to assess olive tree crown parameters using 3d photo reconstruction: application in breeding trials," *Remote Sensing*, vol. 7, no. 4, pp. 4213–4232, 2015.

[52] P. Zarco-Tejada, R. Diaz-Varela, V. Angileri, and P. Loudjani, "Tree height quantification using very high resolution imagery acquired from an unmanned aerial vehicle (uav) and automatic 3d photo-reconstruction methods," *European Journal of Agronomy*, vol. 55, pp. 89 – 99, 2014.

[53] M. Moran, Y. Inoue, and E. Barnes, "Opportunities and limitations for image-based remote sensing in precision crop management," *Remote Sensing of Environment*, vol. 61, no. 3, pp. 319 – 346, 1997.

[54] S. Candiago, F. Remondino, M. De Giglio, M. Dubbini, and M. Gattelli, "Evaluating multispectral images and vegetation indices for precision farming applications from uav images," *Remote Sensing*, vol. 7, no. 4, pp. 4026–4047, 2015.

[55] J. Peñuelas and I. Filella, "Visible and near-infrared reflectance techniques for diagnosing plant physiological status," *Trends in plant science*, vol. 3, no. 4, pp. 151–156, 1998.

[56] E. Neuwirthová, Z. Lhotáková, and J. Albrechtová, "The effect of leaf stacking on leaf reflectance and vegetation indices measured by contact probe during the season," *Sensors*, vol. 17, no. 6, p. 1202, 2017.

[57] L. Pádua, J. Vanko, J. Hruška, T. Adão, J. J. Sousa, E. Peres, and R. Morais, "Uas, sensors, and data processing in agroforestry: A review towards practical applications," *International journal of remote sensing*, vol. 38, no. 8-10, pp. 2349–2391, 2017.

[58] S. Thomas, M. T. Kuska, D. Bohnenkamp, A. Brugger, E. Alisaac, M. Wahabzada, J. Behmann, and A.-K. Mahlein, "Benefits of hyperspectral imaging for plant disease detection and plant protection: a technical perspective," *Journal of Plant Diseases and Protection*, vol. 125, pp. 5–20, Feb 2018.

[59] H. K. Suh, J. W. Hofstee, and E. J. van Henten, "Improved vegetation segmentation with ground shadow removal using an hdr camera," *Precision Agriculture*, vol. 19, no. 2, pp. 218–237, 2018.

[60] C. Hakkenberg, R. Peet, D. Urban, and C. Song, "Modeling plant composition as community continua in a forest landscape with lidar and hyperspectral remote sensing," *Ecological Applications*, vol. 28, no. 1, pp. 177–190, 2018.

[61] O. Nevalainen, E. Honkavaara, S. Tuominen, N. Viljanen, T. Hakala, X. Yu, J. Hyyppä, H. Saari, I. Pölönen, N. Imai, *et al.*, "Individual tree detection and classification with uav-based photogrammetric point clouds and hyperspectral imaging," *Remote Sensing*, vol. 9, no. 3, p. 185, 2017.

[62] C. Tarantino, F. Casella, M. Adamo, R. Lucas, C. Beierkuhnlein, and P. Blonda, "Ailanthus altissima mapping from multitemporal very high resolution satellite images," *ISPRS Journal of Photogrammetry and Remote Sensing*, vol. 147, pp. 90 – 103, 2019.

[63] L. Malambo, S. Popescu, D. Horne, N. Pugh, and W. Rooney, "Automated detection and measurement of individual sorghum panicles using density-based clustering of terrestrial lidar data," *ISPRS Journal of Photogrammetry and Remote Sensing*, vol. 149, pp. 1 – 13, 2019.

[64] Y. Tan, S. Wang, B. Xu, and J. Zhang, "An improved progressive morphological filter for uav-based photogrammetric point clouds in river bank monitoring," *ISPRS Journal of Photogrammetry and Remote Sensing*, vol. 146, pp. 421 – 429, 2018.

[65] J. P. Dash, M. S. Watt, G. D. Pearse, M. Heaphy, and H. S. Dungey, "Assessing very high resolution uav imagery for monitoring forest health during a simulated disease outbreak," *ISPRS Journal of Photogrammetry and Remote Sensing*, vol. 131, pp. 1 – 14, 2017.

[66] M. Mohan, C. Silva, C. Klauberg, P. Jat, G. Catts, A. Cardil, A. Hudak, and M. Dia, "Individual tree detection from unmanned aerial vehicle (uav) derived canopy height model in an open canopy mixed conifer forest," *Forests*, vol. 8, no. 9, p. 340, 2017.

[67] E. Lindberg and J. Holmgren, "Individual tree crown methods for 3d data from remote sensing," *Current Forestry Reports*, vol. 3, pp. 19–31, Mar 2017.

[68] L. Wallace, A. Lucieer, and C. S. Watson, "Evaluating tree detection and segmentation routines on very high resolution uav lidar data," *IEEE Transactions on Geoscience and Remote Sensing*, vol. 52, pp. 7619–7628, Dec 2014.

[69] P. Marques, L. Pádua, T. Adão, J. Hruška, E. Peres, A. Sousa, and J. J. Sousa, "Uav-based automatic detection and monitoring of chestnut trees," *Remote Sensing*, vol. 11, no. 7, p. 855, 2019.

[70] A. K. Jain, "Data clustering: 50 years beyond k-means," *Pattern recognition letters*, vol. 31, no. 8, pp. 651–666, 2010.

[71] S. Ullman, "The interpretation of structure from motion," *Proceedings of the Royal Society of London. Series B. Biological Sciences*, vol. 203, no. 1153, pp. 405–426, 1979.

[72] L. Pádua, P. Marques, J. Hruška, T. Adão, E. Peres, R. Morais, and J. Sousa, "Multi-temporal vineyard monitoring through uav-based rgb imagery," *Remote Sensing*, vol. 10, no. 12, p. 1907, 2018.

[73] J. Xue and B. Su, "Significant remote sensing vegetation indices: A review of developments and applications," *Journal of Sensors*, vol. 2017, 2017.

[74] P. J. Zarco-Tejada, J. R. Miller, A. Morales, A. Berjón, and J. Agüera, "Hyperspectral indices and model simulation for chlorophyll estimation in open-canopy tree crops," *Remote sensing of environment*, vol. 90, no. 4, pp. 463–476, 2004.

[75] A. Gertsis, D. Fountas, I. Arpasanu, and M. Michaloudis, "Precision agriculture applications in a high density olive grove adapted for mechanical harvesting in greece," *Procedia Technology*, vol. 8, pp. 152–156, 2013.

[76] R. D. Jackson and A. R. Huete, "Interpreting vegetation indices," *Preventive veterinary medicine*, vol. 11, no. 3-4, pp. 185–200, 1991.

[77] J. Jorge, M. Vallbé, and J. A. Soler, "Detection of irrigation inhomogeneities in an olive grove using the ndre vegetation index obtained from uav images," *European Journal of Remote Sensing*, vol. 52, no. 1, pp. 169–177, 2019.

[78] J. F. Shroder, *Biological and environmental hazards, risks, and disasters*. Elsevier, 2015.

[79] P. J. Besl and N. D. McKay, "A method for registration of 3-d shapes," *IEEE Transactions on Pattern Analysis and Machine Intelligence*, vol. 14, no. 2, pp. 239–256, 1992.

[80] E. Salamí, A. Gallardo, G. Skorobogatov, and C. Barrado, "On-the-fly olive tree counting using a uas and cloud services," *Remote Sensing*, vol. 11, no. 3, p. 316, 2019.

[81] J. M. Keller, M. R. Gray, and J. A. Givens, "A fuzzy k-nearest neighbor algorithm," *IEEE Transactions on Systems, Man, and Cybernetics*, vol. SMC-15, no. 4, pp. 580–585, 1985.

[82] K. Zhou, Q. Hou, R. Wang, and B. Guo, "Real-time kd-tree construction on graphics hardware," *ACM Transactions on Graphics (TOG)*, vol. 27, no. 5, pp. 1–11, 2008.

[83] M. Lu and Y. He, "Organization and indexing method for 3d points cloud data," *Geo-Information Science*, vol. 2, 2008.

[84] A. Miranda-Fuentes, J. Llorens, J. L. Gamarra-Diezma, J. A. Gil-Ribes, and E. Gil, "Towards an optimized method of olive tree crown volume measurement," *Sensors*, vol. 15, no. 2, pp. 3671–3687, 2015.

[85] Z. Yan, R. Liu, L. Cheng, X. Zhou, X. Ruan, and Y. Xiao, "A concave hull methodology for calculating the crown volume of individual trees based on vehicle-borne lidar data," *Remote Sensing*, vol. 11, no. 6, p. 623, 2019.

[86] M. Wang and Y.-H. Tseng, "Lidar data segmentation and classification based on octree structure," *parameters*, vol. 1, p. 5, 2004.

[87] G. Yang, H. Shen, L. Zhang, Z. He, and X. Li, "A moving weighted harmonic analysis method for reconstructing high-quality spot vegetation ndvi time-series data," *IEEE Transactions on Geoscience and Remote Sensing*, vol. 53, pp. 6008–6021, Nov 2015.

[88] J. Trochta, M. Krůček, T. Vrška, and K. Král, "3d forest: An application for descriptions of three-dimensional forest structures using terrestrial lidar," *PLOS ONE*, vol. 12, pp. 1–17, 05 2017.

[89] A. Kangas and M. Maltamo, *Forest inventory: methodology and applications*, vol. 10. Springer Science & Business Media, 2006.

[90] Z. Feng, Y. Chen, T. Hakala, and J. Hyyppä, "Range calibration of airborne profiling radar used in forest inventory," in *2016 IEEE International Geoscience and Remote Sensing Symposium (IGARSS)*, pp. 6672–6675, IEEE, 2016.

[91] Y. Su, Q. Guo, B. Xue, T. Hu, O. Alvarez, S. Tao, and J. Fang, "Spatial distribution of forest aboveground biomass in china: Estimation through combination of spaceborne lidar, optical imagery, and forest inventory data," *Remote Sensing of Environment*, vol. 173, pp. 187–199, 2016.

[92] J. Rahlf, J. Breidenbach, S. Solberg, E. Næsset, and R. Astrup, "Digital aerial photogrammetry can efficiently support large-area forest inventories in norway," *Forestry: An International Journal of Forest Research*, vol. 90, no. 5, pp. 710–718, 2017.

[93] G. D. Pearse, J. P. Dash, H. J. Persson, and M. S. Watt, "Comparison of high-density lidar and satellite photogrammetry for forest inventory," *ISPRS journal of photogrammetry and remote sensing*, vol. 142, pp. 257–267, 2018.

[94] C. Torresan, A. Berton, F. Carotenuto, S. F. Di Gennaro, B. Gioli, A. Matese, F. Miglietta, C. Vagnoli, A. Zaldei, and L. Wallace, "Forestry applications of uavs in europe: A review," *International Journal of Remote Sensing*, vol. 38, no. 8-10, pp. 2427–2447, 2017.

[95] N. Guimarães, L. Pádua, P. Marques, N. Silva, E. Peres, and J. J. Sousa, "Forestry remote sensing from unmanned aerial vehicles: A review focusing on the data, processing and potentialities," *Remote Sensing*, vol. 12, no. 6, p. 1046, 2020.

[96] J. Tomaštík, M. Mokroš, Š. Saloň, F. Chudỳ, and D. Tunák, "Accuracy of photogrammetric uav-based point clouds under conditions of partially-open forest canopy," *Forests*, vol. 8, no. 5, p. 151, 2017.

[97] J. Tian, T. Dai, H. Li, C. Liao, W. Teng, Q. Hu, W. Ma, and Y. Xu, "A novel tree height extraction approach for individual trees by combining tls and uav image-based point cloud integration," *Forests*, vol. 10, no. 7, p. 537, 2019.

[98] M. Ehbrecht, P. Schall, C. Ammer, M. Fischer, and D. Seidel, "Effects of structural heterogeneity on the diurnal temperature range in temperate forest ecosystems," *Forest Ecology and Management*, vol. 432, pp. 860 – 867, 2019.

[99] D. Seidel, M. Ehbrecht, P. Annighöfer, and C. Ammer, "From tree to stand-level structural complexity — which properties make a forest stand complex?," *Agricultural and Forest Meteorology*, vol. 278, p. 107699, 2019.

[100] N. Chehata, N. David, and F. Bretar, "Lidar data classification using hierarchical k-means clustering," in *ISPRS Congress Beijing 2008*, vol. 37, pp. 325–330, Citeseer, 2008.

[101] S. Gupta, H. Weinacker, and B. Koch, "Comparative analysis of clustering-based approaches for 3-d single tree detection using airborne fullwave lidar data," *Remote Sensing*, vol. 2, no. 4, pp. 968–989, 2010.

[102] D. Yin and L. Wang, "Individual mangrove tree measurement using uav-based lidar data: Possibilities and challenges," *Remote sensing of environment*, vol. 223, pp. 34–49, 2019.

[103] W. Chen, X. Hu, W. Chen, Y. Hong, and M. Yang, "Airborne lidar remote sensing for individual tree forest inventory using trunk detection-aided mean shift clustering techniques," *Remote Sensing*, vol. 10, no. 7, p. 1078, 2018.

[104] M. Lu, B. Chen, X. Liao, T. Yue, H. Yue, S. Ren, X. Li, Z. Nie, and B. Xu, "Forest types classification based on multi-source data fusion," *Remote Sensing*, vol. 9, no. 11, p. 1153, 2017.

[105] K. Johansen, T. Raharjo, and M. F. McCabe, "Using multi-spectral uav imagery to extract tree crop structural properties and assess pruning effects," *Remote Sensing*, vol. 10, no. 6, p. 854, 2018.

[106] Y.-H. Tu, K. Johansen, S. Phinn, and A. Robson, "Measuring canopy structure and condition using multi-spectral uas imagery in a horticultural environment," *Remote Sensing*, vol. 11, no. 3, p. 269, 2019.

[107] M. Nikopensius, J. Pisek, and K. Raabe, "Spectral reflectance patterns and seasonal dynamics of common understory types in

three mature hemi-boreal forests," *International Journal of Applied Earth Observation and Geoinformation*, vol. 43, pp. 84 – 91, 2015.

[108] D. Seidel, N. Hoffmann, M. Ehbrecht, J. Juchheim, and C. Ammer, "How neighborhood affects tree diameter increment – new insights from terrestrial laser scanning and some methodical considerations," *Forest Ecology and Management*, vol. 336, no. Complete, pp. 119–128, 2015.

[109] C. Gallego Galán, P. Torralbo, M. José Pérez-Palazón, C. Galán, and M. José Polo, "Trend analysis of climatic variables and impacts in dehesa systems: a study case in sierra morena, southern spain," in *Proceedings of the 21st EGU General Assembly, EGU2019*, April 2019.

[110] P. M. Cristiano, N. Madanes, P. I. Campanello, D. Di Francescantonio, S. A. Rodríguez, Y.-J. Zhang, L. O. Carrasco, and G. Goldstein, "High ndvi and potential canopy photosynthesis of south american subtropical forests despite seasonal changes in leaf area index and air temperature," *Forests*, vol. 5, no. 2, pp. 287–308, 2014.

[111] R. B. Rusu and S. Cousins, "3d is here: Point cloud library (pcl)," in *2011 IEEE international conference on robotics and automation*, pp. 1–4, IEEE, 2011.

[112] G. Bradski and A. Kaehler, *Learning OpenCV: Computer vision with the OpenCV library*. " O'Reilly Media, Inc.", 2008.

[113] J. L. Carrivick, M. W. Smith, and D. J. Quincey, *Structure from Motion in the Geosciences*. John Wiley & Sons, 2016.

[114] V. F. Strîmbu and B. M. Strîmbu, "A graph-based segmentation algorithm for tree crown extraction using airborne lidar data," *ISPRS Journal of Photogrammetry and Remote Sensing*, vol. 104, pp. 30 – 43, 2015.

[115] Yun, Jiang, Hou, An, Chen, Jiang, Li, and Xue, "Rubber tree crown segmentation and property retrieval using ground-based mobile lidar after natural disturbances," *Remote Sensing*, vol. 11, p. 903, Apr 2019.

[116] T. Kanungo, D. M. Mount, N. S. Netanyahu, C. D. Piatko, R. Silverman, and A. Y. Wu, "An efficient k-means clustering algorithm: analysis and implementation," *IEEE Transactions on Pattern Analysis and Machine Intelligence*, vol. 24, no. 7, pp. 881–892, 2002.

[117] H. Edelsbrunner and E. P. Mücke, "Three-dimensional alpha shapes," *ACM Transactions on Graphics (TOG)*, vol. 13, no. 1, pp. 43–72, 1994.

[118] A.-V. Vo, L. Truong-Hong, D. F. Laefer, and M. Bertolotto, "Octree-based region growing for point cloud segmentation," *ISPRS Journal of Photogrammetry and Remote Sensing*, vol. 104, pp. 88–100, 2015.

[119] N. Amiri, W. Yao, M. Heurich, P. Krzystek, and A. Skidmore, "Estimation of regeneration coverage in a temperate forest by 3d segmentation using airborne laser scanning data," *International Journal of Applied Earth Observation and Geoinformation (JAG)*, vol. 52, pp. 252–262, 2016.

[120] A. Ferraz, S. Saatchi, C. Mallet, and V. Meyer, "Lidar detection of individual tree size in tropical forests," *Remote Sensing of Environment*, vol. 183, pp. 318 – 333, 2016.

[121] R. Gaulton and T. J. Malthus, "Lidar mapping of canopy gaps in continuous cover forests: A comparison of canopy height model and point cloud based techniques," *International Journal of Remote Sensing*, vol. 31, no. 5, pp. 1193–1211, 2010.

[122] G. R. Asrar, "Advances in quantitative earth remote sensing: Past, present and future," *Sensors*, vol. 19, no. 24, 2019.

[123] S. C. Steele-Dunne, H. McNairn, A. Monsivais-Huertero, J. Judge, P. Liu, and K. Papathanassiou, "Radar remote sensing of agricultural canopies: A review," *IEEE Journal of Selected Topics in Applied Earth Observations and Remote Sensing*, vol. 10, pp. 2249–2273, May 2017.

[124] H. Moreno, C. Valero, J. M. Bengochea-Guevara, A. Ribeiro, M. Garrido-Izard, and D. Andujar, "On-ground vineyard reconstruction using a lidar-based automated system," *Sensors*, vol. 20, no. 4, 2020.

[125] N. Snavely, S. M. Seitz, and R. Szeliski, "Modeling the world from internet photo collections," *International journal of computer vision*, vol. 80, no. 2, pp. 189–210, 2008.

[126] T. Luhmann, C. Fraser, and H.-G. Maas, "Sensor modelling and camera calibration for close-range photogrammetry," *ISPRS Journal of Photogrammetry and Remote Sensing*, vol. 115, pp. 37–46, 2016.

[127] M. Mokroš, X. Liang, P. Surovỳ, P. Valent, J. Čerňava, F. Chudỳ, D. Tunák, Š. Saloň, and J. Merganič, "Evaluation of close-range photogrammetry image collection methods for estimating tree diameters," *ISPRS International Journal of Geo-Information*, vol. 7, no. 3, p. 93, 2018.

[128] M. Favalli, A. Fornaciai, I. Isola, S. Tarquini, and L. Nannipieri, "Multiview 3d reconstruction in geosciences," *Computers & Geosciences*, vol. 44, pp. 168–176, 2012.

[129] B. Wu, L. Xie, H. Hu, Q. Zhu, and E. Yau, "Integration of aerial oblique imagery and terrestrial imagery for optimized 3d modeling in urban areas," *ISPRS Journal of Photogrammetry and Remote Sensing*, vol. 139, pp. 119 – 132, 2018.

[130] Y. Ninomiya and B. Fu, "Thermal infrared multispectral remote sensing of lithology and mineralogy based on spectral properties of materials," *Ore Geology Reviews*, 2018.

[131] C. Rother, M. Kiefel, L. Zhang, B. Schölkopf, and P. V. Gehler, "Recovering intrinsic images with a global sparsity prior on reflectance," in *Advances in Neural Information Processing Systems 24* (J. Shawe-Taylor, R. S. Zemel, P. L. Bartlett, F. Pereira, and K. Q. Weinberger, eds.), pp. 765–773, Curran Associates, Inc., 2011.

[132] H. Fu, T. Zhou, and C. Sun, "Object-based shadow index via illumination intensity from high resolution satellite images over urban areas," *Sensors*, vol. 20, no. 4, 2020.

[133] S. Bell, P. Upchurch, N. Snavely, and K. Bala, "Material recognition in the wild with the materials in context database," in *2015 IEEE Conference on Computer Vision and Pattern Recognition (CVPR)*, pp. 3479–3487, June 2015.

[134] M. Ángel Martínez-Domingo, E. M. Valero, J. Hernández-Andrés, S. Tominaga, T. Horiuchi, and K. Hirai, "Image processing pipeline for segmentation and material classification based on multispectral high dynamic range polarimetric images," *Opt. Express*, vol. 25, pp. 30073–30090, Nov 2017.

[135] J. P. Dandois and E. C. Ellis, "High spatial resolution three-dimensional mapping of vegetation spectral dynamics using computer vision," *Remote Sensing of Environment*, vol. 136, pp. 259 – 276, 2013.

[136] S. Del Pozo, R. Lindenbergh, P. Rodríguez-Gonzálvez, J. K. Blom, and D. González-Aguilera, "Discrimination between sedimentary

rocks from close-range visible and very-near-infrared images," *PloS one*, vol. 10, no. 7, 2015.

[137] H. Liu and J. S. Chahl, "A multispectral machine vision system for invertebrate detection on green leaves," *Computers and electronics in agriculture*, vol. 150, pp. 279–288, 2018.

[138] Q. Feng, D. Zhu, J. Yang, and B. Li, "Multisource hyperspectral and lidar data fusion for urban land-use mapping based on a modified two-branch convolutional neural network," *ISPRS International Journal of Geo-Information*, vol. 8, no. 1, p. 28, 2019.

[139] N. Audebert, B. Le Saux, and S. Lefèvrey, "Fusion of heterogeneous data in convolutional networks for urban semantic labeling," in *2017 Joint Urban Remote Sensing Event (JURSE)*, pp. 1–4, 03 2017.

[140] R. Alshehhi, P. R. Marpu, W. L. Woon, and M. Dalla Mura, "Simultaneous extraction of roads and buildings in remote sensing imagery with convolutional neural networks," *ISPRS Journal of Photogrammetry and Remote Sensing*, vol. 130, pp. 139–149, 2017.

[141] C. Wang, M. Ji, J. Wang, W. Wen, T. Li, and Y. Sun, "An improved dbscan method for lidar data segmentation with automatic eps estimation," *Sensors*, vol. 19, no. 1, p. 172, 2019.

[142] A. Romero, C. Gatta, and G. Camps-Valls, "Unsupervised deep feature extraction for remote sensing image classification," *IEEE Transactions on Geoscience and Remote Sensing*, vol. 54, no. 3, pp. 1349–1362, 2015.

[143] J. Nalepa, M. Myller, Y. Imai, K. Honda, T. Takeda, and M. Antoniak, "Unsupervised segmentation of hyperspectral images using 3-d convolutional autoencoders," *IEEE Geoscience and Remote Sensing Letters*, pp. 1–5, 2019.

[144] J. L. Schönberger and J. Frahm, "Structure-from-motion revisited," in *2016 IEEE Conference on Computer Vision and Pattern Recognition (CVPR)*, pp. 4104–4113, 06 2016.

[145] S. Jeong, S.-H. Park, and C.-H. Kim, "Simulation of morphology changes in drying leaves," *Computer Graphics Forum*, vol. 32, no. 1, pp. 204–215, 2013.

[146] Z. Jiang, A. R. Huete, J. Chen, Y. Chen, J. Li, G. Yan, and X. Zhang, "Analysis of ndvi and scaled difference vegetation index retrievals of vegetation fraction," *Remote sensing of environment*, vol. 101, no. 3, pp. 366–378, 2006.

[147] A. Guénoche, P. Hansen, and B. Jaumard, "Efficient algorithms for divisive hierarchical clustering with the diameter criterion," *Journal of classification*, vol. 8, no. 1, pp. 5–30, 1991.

[148] W. K. Härdle and L. Simar, "Cluster analysis," in *Applied Multivariate Statistical Analysis*, pp. 363–393, Springer, 2019.

[149] N. Brodu and D. Lague, "3d terrestrial lidar data classification of complex natural scenes using a multi-scale dimensionality criterion: Applications in geomorphology," *ISPRS Journal of Photogrammetry and Remote Sensing*, vol. 68, pp. 121–134, 2012.

[150] C. Zhang and J. M. Kovacs, "The application of small unmanned aerial systems for precision agriculture: a review," *Precision agriculture*, vol. 13, no. 6, pp. 693–712, 2012.

[151] U. R. Mogili and B. Deepak, "Review on application of drone systems in precision agriculture," *Procedia computer science*, vol. 133, pp. 502–509, 2018.

[152] M. F. F. Bernardes, M. Pazin, L. C. Pereira, and D. J. Dorta, "Impact of pesticides on environmental and human health," *Toxicology studies-cells, drugs and environment*, pp. 195–233, 2015.

[153] G. Scott and A. Rajabifard, "Sustainable development and geospatial information: a strategic framework for integrating a global policy agenda into national geospatial capabilities," *Geo-spatial information science*, vol. 20, no. 2, pp. 59–76, 2017.

[154] G. Ezenne, L. Jupp, S. Mantel, and J. Tanner, "Current and potential capabilities of uas for crop water productivity in precision agriculture," *Agricultural Water Management*, vol. 218, pp. 158–164, 2019.

[155] X. Shi, W. Han, T. Zhao, and J. Tang, "Decision support system for variable rate irrigation based on uav multispectral remote sensing," *Sensors*, vol. 19, no. 13, p. 2880, 2019.

[156] M. Zhang, J. Zhou, K. A. Sudduth, and N. R. Kitchen, "Estimation of maize yield and effects of variable-rate nitrogen application using uav-based rgb imagery," *Biosystems Engineering*, vol. 189, pp. 24–35, 2020.

[157] J. Mendes, T. M. Pinho, F. Neves dos Santos, J. J. Sousa, E. Peres, J. Boaventura-Cunha, M. Cunha, and R. Morais, "Smartphone applications targeting precision agriculture practices—a systematic review," *Agronomy*, vol. 10, no. 6, p. 855, 2020.

[158] A. Matese and S. F. Di Gennaro, "Technology in precision viticulture: A state of the art review," *International journal of wine research*, vol. 7, pp. 69–81, 2015.

[159] A. P. B. Proffitt, R. Bramley, D. Lamb, and E. Winter, *Precision viticulture: a new era in vineyard management and wine production.* Ashford, Winetitles, 2006.

[160] J. Campos, J. Llop, M. Gallart, F. García-Ruiz, A. Gras, R. Salcedo, and E. Gil, "Development of canopy vigour maps using uav for site-specific management during vineyard spraying process," *Precision Agriculture*, vol. 20, no. 6, pp. 1136–1156, 2019.

[161] L. Comba, P. Gay, J. Primicerio, and D. R. Aimonino, "Vineyard detection from unmanned aerial systems images," *Computers and Electronics in Agriculture*, vol. 114, pp. 78–87, 2015.

[162] A. J. Mathews and J. L. Jensen, "Visualizing and quantifying vineyard canopy lai using an unmanned aerial vehicle (uav) collected high density structure from motion point cloud," *Remote sensing*, vol. 5, no. 5, pp. 2164–2183, 2013.

[163] M. Weiss and F. Baret, "Using 3d point clouds derived from uav rgb imagery to describe vineyard 3d macro-structure," *Remote Sensing*, vol. 9, no. 2, p. 111, 2017.

[164] C. Poblete-Echeverría, G. F. Olmedo, B. Ingram, and M. Bardeen, "Detection and segmentation of vine canopy in ultra-high spatial resolution rgb imagery obtained from unmanned aerial vehicle (uav): A case study in a commercial vineyard," *Remote Sensing*, vol. 9, no. 3, p. 268, 2017.

[165] G. Caruso, L. Tozzini, G. Rallo, J. Primicerio, M. Moriondo, G. Palai, and R. Gucci, "Estimating biophysical and geometrical parameters of grapevine canopies ('sangiovese') by an unmanned aerial vehicle (uav) and vis-nir cameras," *Vitis*, vol. 56, no. 2, pp. 63–70, 2017.

[166] A. I. De Castro, F. M. Jimenez-Brenes, J. Torres-Sánchez, J. M. Peña, I. Borra-Serrano, and F. López-Granados, "3-d characterization of vineyards using a novel uav imagery-based obia procedure for precision viticulture applications," *Remote Sensing*, vol. 10, no. 4, p. 584, 2018.

[167] A. Matese and S. F. Di Gennaro, "Practical applications of a multisensor uav platform based on multispectral, thermal and rgb high resolution images in precision viticulture," *Agriculture*, vol. 8, no. 7, p. 116, 2018.

[168] J. Primicerio, G. Caruso, L. Comba, A. Crisci, P. Gay, S. Guidoni, L. Genesio, D. Ricauda Aimonino, and F. P. Vaccari, "Individual plant definition and missing plant characterization in vineyards from high-resolution uav imagery," *European Journal of Remote Sensing*, vol. 50, no. 1, pp. 179–186, 2017.

[169] L. Comba, A. Biglia, D. R. Aimonino, and P. Gay, "Unsupervised detection of vineyards by 3d point-cloud uav photogrammetry for precision agriculture," *Computers and Electronics in Agriculture*, vol. 155, pp. 84–95, 2018.

[170] L. Comba, A. Biglia, D. R. Aimonino, C. Tortia, E. Mania, S. Guidoni, and P. Gay, "Leaf area index evaluation in vineyards using 3d point clouds from uav imagery," *Precision Agriculture*, vol. 21, no. 4, pp. 881–896, 2020.

[171] F.-J. Mesas-Carrascosa, A. I. de Castro, J. Torres-Sánchez, P. Triviño-Tarradas, F. M. Jiménez-Brenes, A. García-Ferrer, and F. López-Granados, "Classification of 3d point clouds using color vegetation indices for precision viticulture and digitizing applications," *Remote Sensing*, vol. 12, no. 2, p. 317, 2020.

[172] M. Aboutalebi, A. F. Torres-Rua, M. McKee, W. P. Kustas, H. Nieto, M. M. Alsina, A. White, J. H. Prueger, L. McKee, J. Alfieri, *et al.*, "Incorporation of unmanned aerial vehicle (uav) point cloud products into remote sensing evapotranspiration models," *Remote sensing*, vol. 12, no. 1, p. 50, 2020.

[173] I. Colomina and P. Molina, "Unmanned aerial systems for photogrammetry and remote sensing: A review," *ISPRS Journal of photogrammetry and remote sensing*, vol. 92, pp. 79–97, 2014.

[174] X.-F. Han, J. S. Jin, M.-J. Wang, W. Jiang, L. Gao, and L. Xiao, "A review of algorithms for filtering the 3d point cloud," *Signal Processing: Image Communication*, vol. 57, pp. 103 – 112, 2017.

[175] A. D. Richardson, J. P. Jenkins, B. H. Braswell, D. Y. Hollinger, S. V. Ollinger, and M.-L. Smith, "Use of digital webcam images to track spring green-up in a deciduous broadleaf forest," *Oecologia*, vol. 152, no. 2, pp. 323–334, 2007.

[176] N. Otsu, "A threshold selection method from gray-level histograms," *IEEE transactions on systems, man, and cybernetics*, vol. 9, no. 1, pp. 62–66, 1979.

[177] S. Chen, G. J. McDermid, G. Castilla, and J. Linke, "Measuring vegetation height in linear disturbances in the boreal forest with uav photogrammetry," *Remote Sensing*, vol. 9, no. 12, p. 1257, 2017.

[178] J. Lisein, M. Pierrot-Deseilligny, S. Bonnet, and P. Lejeune, "A photogrammetric workflow for the creation of a forest canopy height model from small unmanned aerial system imagery," *Forests*, vol. 4, no. 4, pp. 922–944, 2013.

[179] M. Dalponte, L. Bruzzone, and D. Gianelle, "Fusion of hyperspectral and lidar remote sensing data for classification of complex forest areas," *IEEE Transactions on Geoscience and Remote Sensing*, vol. 46, no. 5, pp. 1416–1427, 2008.

[180] D. Panagiotidis, A. Abdollahnejad, P. Surovỳ, and V. Chiteculo, "Determining tree height and crown diameter from high-resolution uav imagery," *International journal of remote sensing*, vol. 38, no. 8-10, pp. 2392–2410, 2017.

[181] L. Cao, H. Liu, X. Fu, Z. Zhang, X. Shen, and H. Ruan, "Comparison of uav lidar and digital aerial photogrammetry point clouds for estimating forest structural attributes in subtropical planted forests," *Forests*, vol. 10, no. 2, p. 145, 2019.

[182] L. Comba, S. Zaman, A. Biglia, A. D. Ricauda, F. Dabbene, and P. Gay, "Semantic interpretation and complexity reduction of 3d point clouds of vineyards," *biosystems engineering*, vol. 197, pp. 216–230, 2020.

[183] N. Magalhães, "Tratado de viticultura. a videira, a vinha e o terroir," *Publicações Chaves Ferreira, Lisboa*, vol. 605, 2008.

[184] S. F. Di Gennaro and A. Matese, "Evaluation of novel precision viticulture tool for canopy biomass estimation and missing plant detection based on 2.5 d and 3d approaches using rgb images acquired by uav platform," *Plant Methods*, vol. 16, no. 1, pp. 1–12, 2020.

[185] M. H. Siebers, E. J. Edwards, J. A. Jimenez-Berni, M. R. Thomas, M. Salim, and R. R. Walker, "Fast phenomics in vineyards: development of grover, the grapevine rover, and lidar for assessing grapevine traits in the field," *Sensors*, vol. 18, no. 9, p. 2924, 2018.

[186] A. Milella, R. Marani, A. Petitti, and G. Reina, "In-field high throughput grapevine phenotyping with a consumer-grade depth camera," *Computers and electronics in agriculture*, vol. 156, pp. 293–306, 2019.

[187] J. Mendes, F. N. Dos Santos, N. Ferraz, P. Couto, and R. Morais, "Vine trunk detector for a reliable robot localization system," in *2016 International Conference on Autonomous Robot Systems and Competitions (ICARSC)*, pp. 1–6, IEEE, 2016.